

<https://www.mdc-berlin.de/de/veroeffentlichungstypen/clinical-journal-club>

The weekly Clinical Journal Club by Dr. Friedrich C. Luft

Usually every Wednesday 17:00 - 18:00

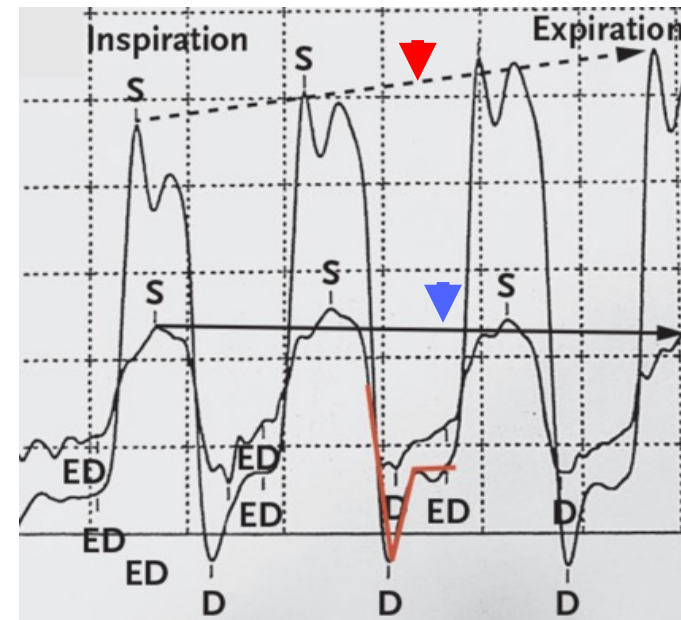


Klinische Forschung

Experimental and Clinical Research Center (ECRC) von MDC und Charité

Als gemeinsame Einrichtung von MDC und Charité fördert das Experimental and Clinical Research Center die Zusammenarbeit zwischen Grundlagenwissenschaftlern und klinischen Forschern. Hier werden neue Ansätze für Diagnose, Prävention und Therapie von Herz-Kreislauf- und Stoffwechselerkrankungen, Krebs sowie neurologischen Erkrankungen entwickelt und zeitnah am Patienten eingesetzt. Sie sind eingeladen, um uns beizutreten. [Bewerben Sie sich!](#)

A 69-year-old woman with a history of asbestos exposure presented to the emergency department with a 3-year history of dyspnea on exertion. Physical examination showed signs of volume overload. A chest radiograph showed circumferential calcification of the pericardium and pleural effusions. Simultaneous left and right heart catheterization showed ventricular interdependence and discordance of the pressure tracings (right ventricular pressure, solid blue arrow; left ventricular pressure, dotted red arrow). What is the diagnosis?



Cardiac Tamponade

Constrictive Pericarditis

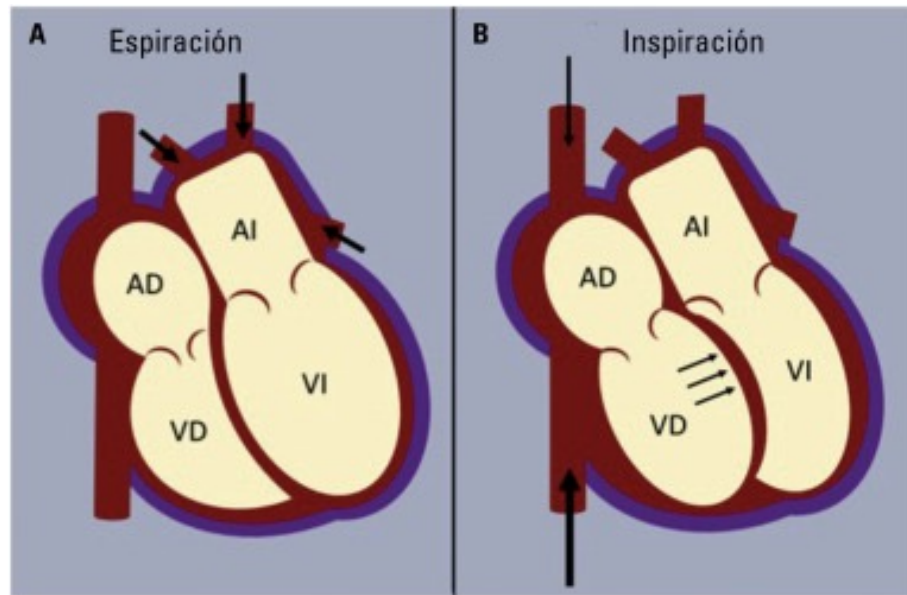
Effusive-Constrictive Pericarditis

Primary Pericardial Mesothelioma

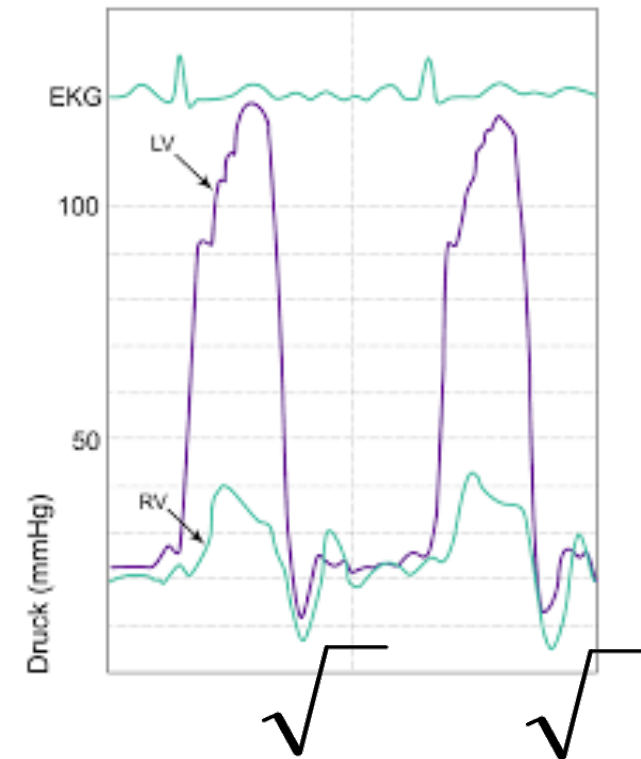
Restrictive Cardiomyopathy

Correct!

The correct answer is constrictive pericarditis, in this case owing to asbestosis. A transthoracic echocardiogram showed a preserved ejection fraction with a septal bounce in early diastole as well as expiratory diastolic reversal in the hepatic vein. The simultaneous left and right heart catheterization tracing was characteristic of constrictive pericarditis. During inspiration, when pressures in the right ventricle were at their highest, left ventricular pressures were at their lowest; this pattern reversed during expiration. A “square root” sign (also called a dip-and-plateau pattern; red line), which represents rapid ventricular filling in early diastole before abrupt cessation in late diastole, was also seen.



Ventricular interdependence is that property of the normal heart such that distension of one ventricle alters the distensibility and filling pressure of the other.



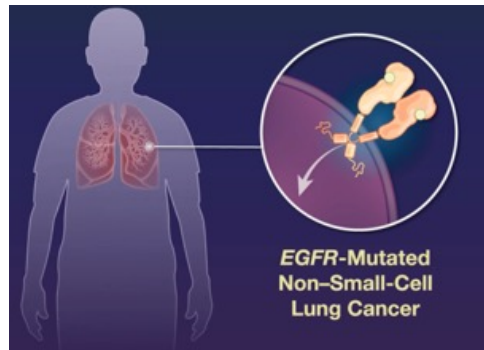
Der **EGF-Rezeptor** ist eine membranständige Rezeptorproteinkinase, die zur Familie der ErbB-Membranrezeptoren gehört, und zunächst in den achtziger Jahren durch Mendelsohn beschrieben wurde.

Durch Assoziation mit einem von mehreren Liganden bildet der Rezeptor ein Homodimer bzw. ein Heterodimer mit anderen ErbB(2-4)-Rezeptoren. Dabei werden durch Autophosphorylierungsprozesse an Tyrosinresten auf der zytosolischen Seite eine Reihe von Signalkaskaden initiiert. Bisher sind mehrere Liganden mit einer Bindungsfähigkeit an den EGF-Rezeptor beschrieben:

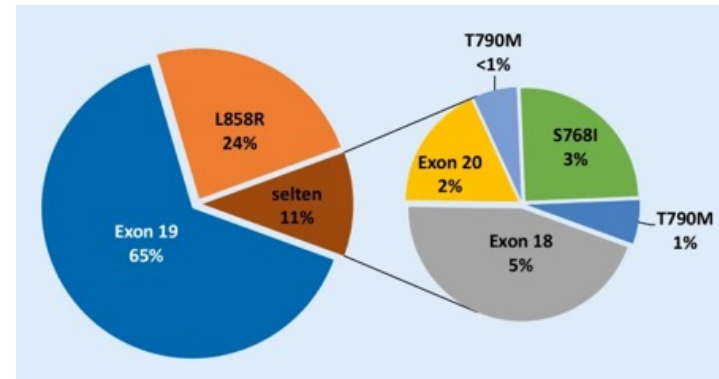
- **Epidermal Growth Factor (EGF)**
- **Transformierender Wachstumsfaktor α (TGF- α)**
- **Amphiregulin**
- **Betacellulin**
- **Epiregulin**
- **HB-EGF**



Man findet eine deutliche Überexpression des Rezeptors in vielen nicht-kleinzelligen Bronchialkarzinomen, Glioblastomen, Nierenzellkarzinomen, Ovarialtumoren sowie Col onkarzinomen und anderen Tumorentitäten. Mutationen sind in vielen der insgesamt 28 Exons, sowie in den Intronregionen beschrieben.

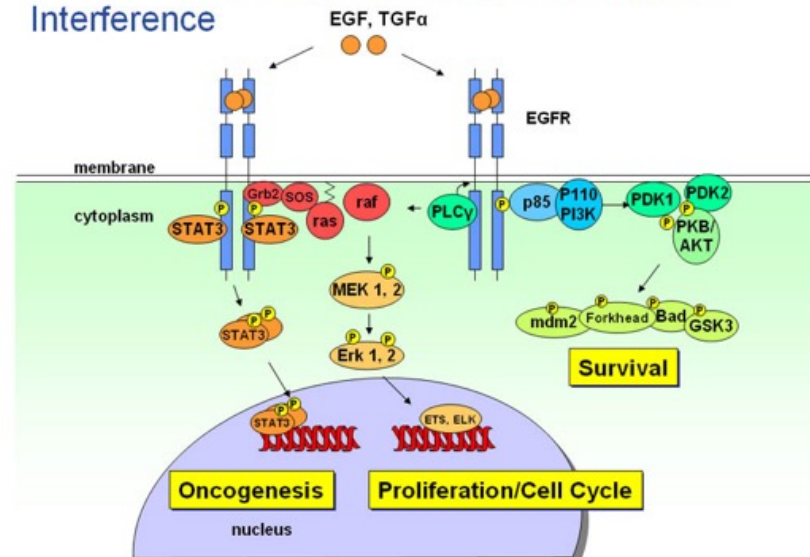


Del 19 und L858R sind die häufigsten EGFR-Treibermutationen



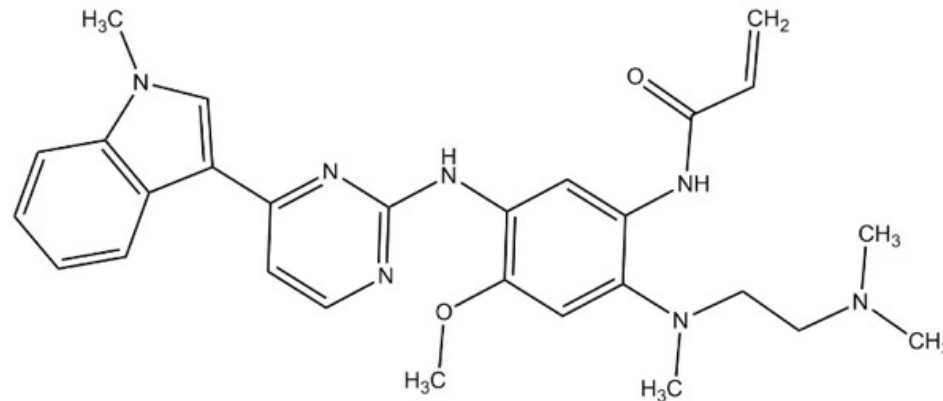
Häufigkeiten ausgewählter aktivierender *EGFR*-Mutationen (Epidermal-Growth-Factor-Rezeptor) in Europa.

The EGFR Pathway as Example for targeted Interference



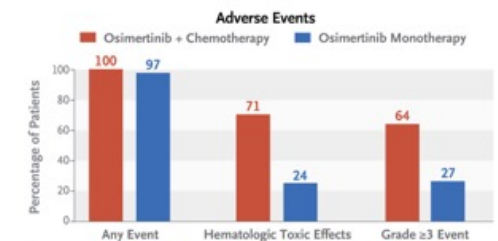
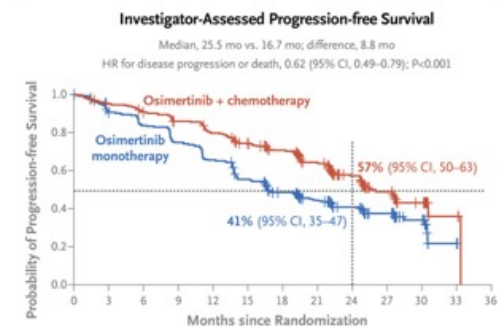
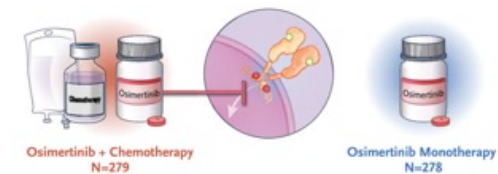
Wirkmechanismus

Osimertinib ist ein Tyrosinkinase-Inhibitor (TKI) des epidermalen Wachstumsfaktorrezeptors (EGFR). Osimertinib bindet an bestimmte mutierte Formen von EGFR (T790M, L858R und Exon 19-Deletion) bindet, die nach der Behandlung mit Erstlinien-EGFR-TKIs bei NSCLC vorherrschen. Als Tyrosinkinase-Inhibitor der dritten Generation ist Osimertinib spezifisch für die Gate-Keeper-T790M-Mutation, die die ATP-Bindungsaktivität an EGFR erhöht und für eine schlechten Prognose im Spätstadium der Erkrankung verantwortlich ist. Darüber hinaus hat sich gezeigt, dass Osimertinib den Wildtyp-EGFR während der Therapie verschont, wodurch die unspezifische Bindung reduziert und die Toxizität begrenzt wird.



Osimertinib with or without Chemotherapy in EGFR-Mutated Advanced NSCLC

Osimertinib is a third-generation epidermal growth factor receptor–tyrosine kinase inhibitor (EGFR-TKI) that is selective for EGFR-TKI–sensitizing and *EGFR* T790M resistance mutations. Evidence suggests that the addition of chemotherapy may extend the benefits of EGFR-TKI therapy. In this phase 3, international, open-label trial, we randomly assigned in a 1:1 ratio patients with *EGFR*-mutated (exon 19 deletion or L858R mutation) advanced non–small-cell lung cancer (NSCLC) who had not previously received treatment for advanced disease to receive osimertinib (80 mg once daily) with chemotherapy (pemetrexed [500 mg per square meter of body-surface area] plus either cisplatin [75 mg per square meter] or carboplatin [pharmacologically guided dose]) or to receive osimertinib monotherapy (80 mg once daily). The primary end point was investigator-assessed progression-free survival. Response and safety were also assessed. Here, we report efficacy and safety data for first-line osimertinib plus platinum–pemetrexed as compared with osimertinib alone.



CONCLUSIONS

Among patients with advanced *EGFR*-mutated NSCLC, first-line treatment with osimertinib plus platinum–pemetrexed led to significantly longer progression-free survival than osimertinib monotherapy.

Osimertinib is a third-generation, irreversible, oral epidermal growth factor receptor–tyrosine kinase inhibitor (EGFR-TKI) that potently and selectively inhibits both EGFR-TKI–sensitizing and *EGFR* p.Thr790Met (T790M) resistance mutations, with demonstrated efficacy in *EGFR*-mutated non–small-cell lung cancer (NSCLC), including in central nervous system (CNS) metastases. Osimertinib is the preferred first-line treatment for patients with *EGFR*-mutated advanced NSCLC, on the basis of results from the phase 3 FLAURA trial, which showed superior progression-free survival and overall survival benefits with first-line osimertinib treatment as compared with first-generation EGFR-TKIs.

Trial Population

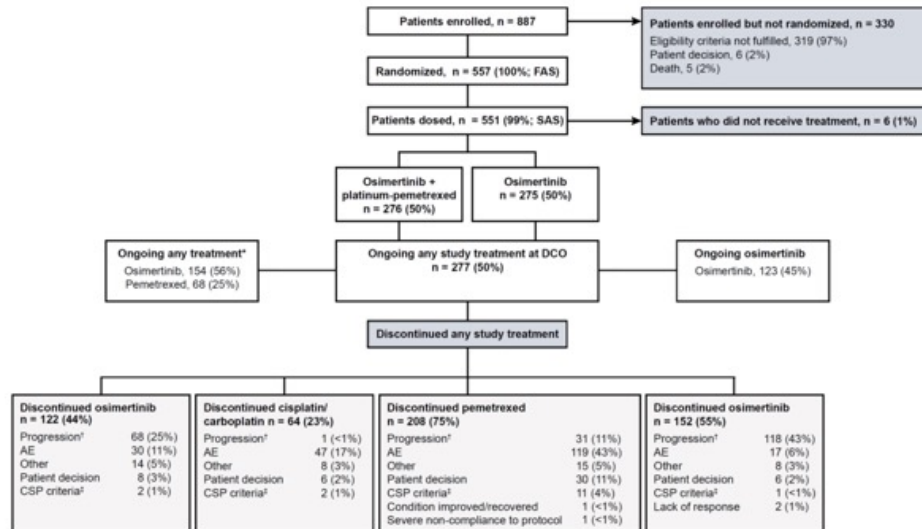
In this trial, we enrolled eligible patients who were 18 years of age or older (or ≥ 20 years of age in Japan), had locally advanced or metastatic NSCLC, and had not previously received systemic treatment for advanced disease.

Nonsquamous NSCLC was pathologically confirmed, with local or central confirmation of the *EGFR* exon 19 deletion or p.Leu858Arg (L858R) mutation, either alone or in combination with other *EGFR* mutations. Patients had a World Health Organization (WHO) performance-status score of 0 or 1 (scores range from 0 to 5, with higher numbers indicating greater disability). Patients with CNS metastases whose condition was neurologically stable were eligible.

Trial Design and Treatment

Results from a nonrandomized safety run-in phase supported continuation to the randomization phase of this trial. Patients were randomly assigned in a 1:1 ratio to receive osimertinib plus chemotherapy (with pemetrexed and a platinum-based agent) or osimertinib monotherapy. For the combination, patients received osimertinib (80 mg once daily) and intravenous pemetrexed (500 mg per square meter of body-surface area) plus either cisplatin (75 mg per square meter) or carboplatin (a pharmacologically guided dose defined as an area under the concentration–time curve of 5 mg per milliliter per minute), administered intravenously on day 1 of 21-day cycles for four cycles; the chemotherapy regimen was chosen by the investigator before randomization. This treatment was followed by osimertinib (80 mg once daily) plus pemetrexed maintenance therapy (500 mg per square meter) every 3 weeks. Patients in the monotherapy group received osimertinib at a dose of 80 mg once daily.

Figure S1. Patient Disposition.



* Platinum treatment was capped at 4 cycles per CSP.

† Includes both RECIST 1.1 objective PD and subjective PD.

‡ Development of study specific discontinuation criteria.

AE denotes adverse event, CSP clinical study protocol, DCO data cut-off, FAS full analysis set, PD progressive disease, RECIST Response Evaluation Criteria in Solid Tumors, SAS safety analysis set.

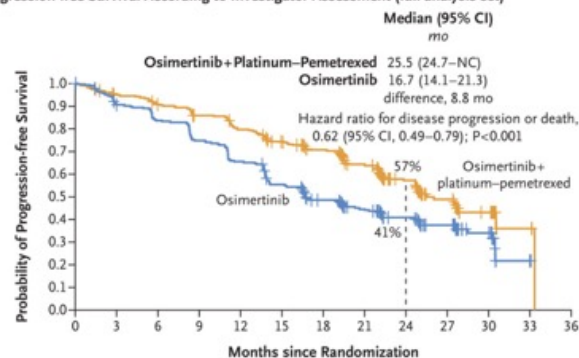
Characteristic	Osimertinib + Platinum–Pemetrexed (N = 279)	Osimertinib Monotherapy (N = 278)
Median age (range) — yr	61 (26–83)	62 (30–85)
Sex — no. (%)		
Male	106 (38)	109 (39)
Female	173 (62)	169 (61)
Race or ethnic group — no. (%)†		
Asian	179 (64)	176 (63)
White	74 (27)	83 (30)
American Indian or Alaska Native	11 (4)	6 (2)
Black	2 (1)	3 (1)
Other	13 (5)	10 (4)
WHO performance-status score — no. (%)‡		
0	104 (37)	102 (37)
1	174 (62)	176 (63)
2	1 (<1)	0
Histologic characteristics — no. (%)		
Adenocarcinoma	275 (99)	275 (99)
Adenosquamous carcinoma	2 (1)	0
Other	2 (1)	3 (1)
EGFR mutation at randomization — no. (%)§		
Exon 19 deletion	169 (61)	168 (60)
L858R mutation	106 (38)	107 (38)
Both exon 19 deletion and L858R mutation	3 (1)	1 (<1)
Unknown	1 (<1)	2 (1)
Disease extent at trial entry — no. (%)		
Locally advanced	14 (5)	7 (3)
Metastatic	265 (95)	271 (97)
CNS metastases — no. (%)¶		
Yes	116 (42)	110 (40)
No	163 (58)	168 (60)
Extrathoracic metastases — no. (%)**		
Yes	147 (53)	149 (54)
No	132 (47)	129 (46)
Liver metastases — no. (%)**		
Yes	43 (15)	66 (24)
No	236 (85)	212 (76)
Bone and locomotor-system metastases — no. (%)		
Yes	132 (47)	142 (51)
No	147 (53)	136 (49)
Median baseline tumor size (range) — mm††	57 (10–284)	57 (11–221)



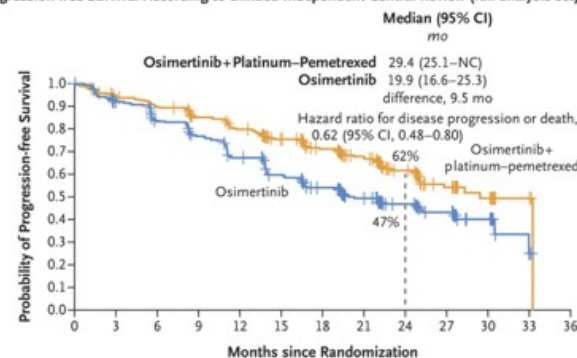
Der Folsäureanalogon Pemetrexed (Handelsname: Alimta®) vom Hersteller Lilly ist ein Zytostatikum aus der Gruppe der Antimetaboliten, dessen Hauptindikation die palliative Chemotherapie bei bestimmten, fortgeschrittenen Formen von Lungenkrebs darstellt.

Progression-free Survival.

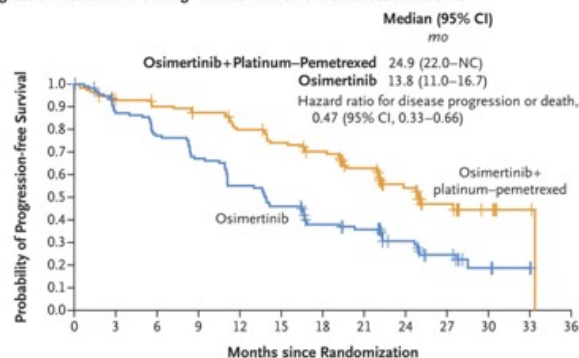
A Progression-free Survival According to Investigator Assessment (full analysis set)



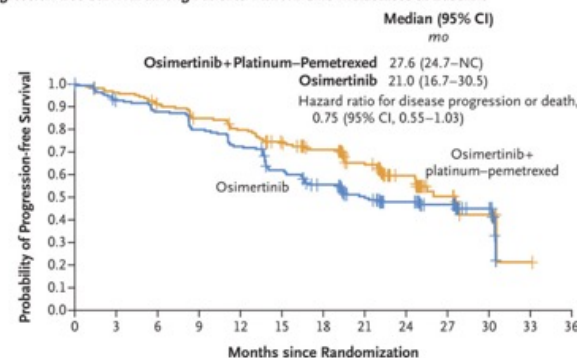
B Progression-free Survival According to Blinded Independent Central Review (full analysis set)



C Progression-free Survival among Patients with CNS Metastases at Baseline



D Progression-free Survival among Patients without CNS Metastases at Baseline

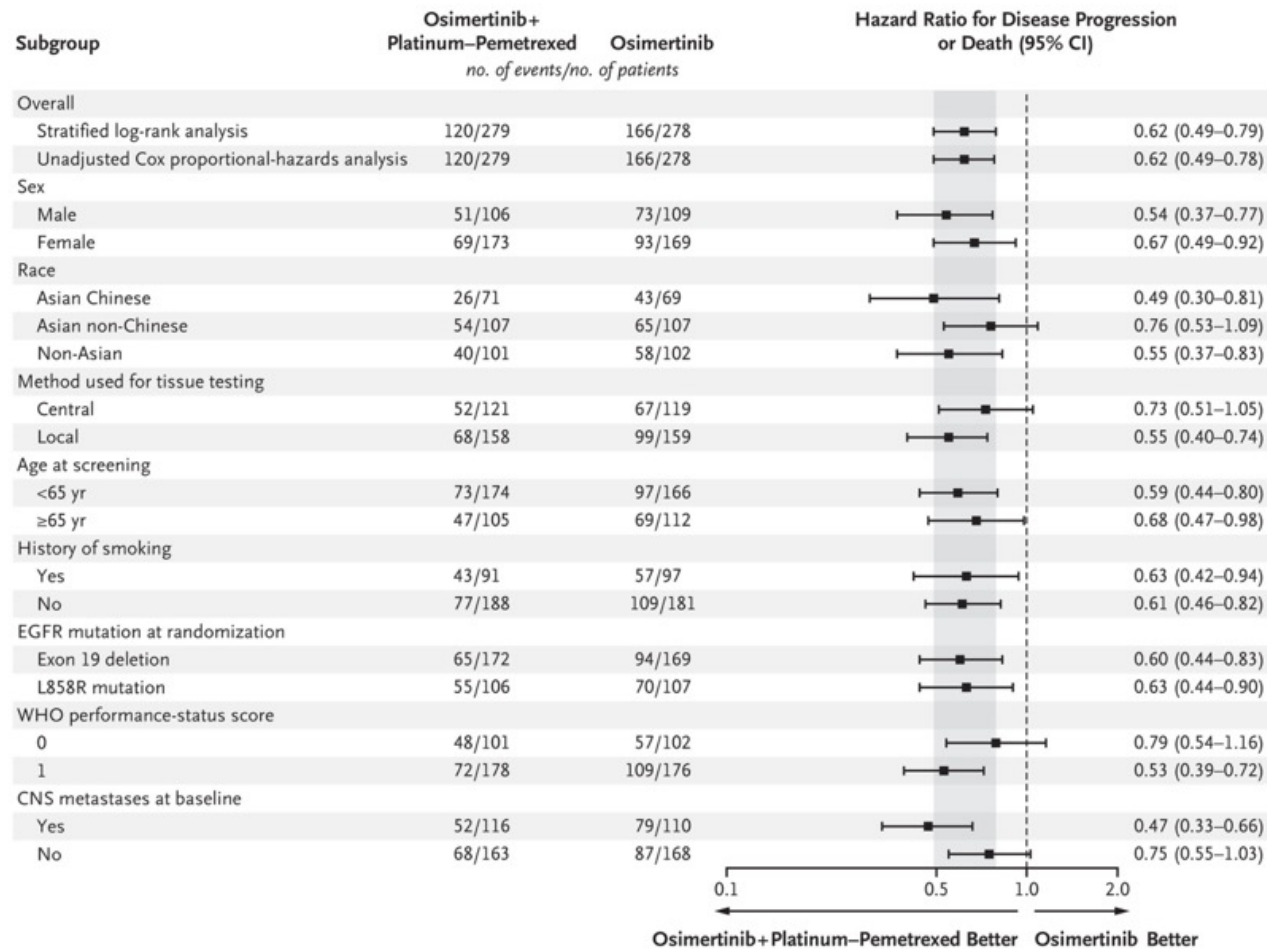


Shown are Kaplan–Meier estimates of progression-free survival in the full analysis set, as assessed by the investigators (Panel A), as assessed on the basis of blinded independent central review (Panel B), among patients with central nervous system (CNS) metastases at baseline (Panel C), and among those without CNS metastases at baseline (Panel D). Patients had been randomly assigned to receive osimertinib plus chemotherapy with pemetrexed and either cisplatin or carboplatin or to receive osimertinib monotherapy. The subgroups that were defined according to the presence or absence of CNS metastases at baseline were made according to investigator assessment on the basis of data in the electronic case-report form regarding the CNS lesion site at baseline, medical history, previous surgery, or a history of radiotherapy for CNS metastases. Tick marks indicate censored data. Patients who had not had disease progression or died at the time of analysis had their data censored at the time of the latest date of assessment from their last evaluable Response Evaluation Criteria in Solid Tumors, version 1.1, assessment. Disease progression events or death that did not occur within two scheduled visits after the last assessment (or randomization) were censored. The median follow-up among all the patients was 19.5 months (range, 0 to 33.3) in the osimertinib–chemotherapy group and 16.5 months (range, 0 to 33.1) in the osimertinib group; the median follow-up among all the patients with censored data was 22.2 months (range, 0 to 33.1) and 23.7 months (range, 0 to 33.1), respectively. The widths of the confidence intervals for progression free-survival according to investigator assessment (Panel A) have been adjusted for multiplicity; for all other analyses, the widths of the confidence intervals have not been adjusted for multiplicity. NC denotes not calculable.

Efficacy End Points (Full Analysis Set).

	Analysis according to the Investigator		Analysis according to Central Review	
	Osimertinib + Platinum–Pemetrexed (N = 279)	Osimertinib Monotherapy (N = 278)	Osimertinib + Platinum–Pemetrexed (N = 279)	Osimertinib Monotherapy (N = 278)
Median progression-free survival (95% CI) — mo	25.5 (24.7–NC)	16.7 (14.1–21.3)	29.4 (25.1–NC)	19.9 (16.6–25.3)
Hazard ratio for disease progression or death (95% CI)	0.62 (0.49–0.79) [†]	—	0.62 (0.48–0.80)	—
Progression-free survival (95% CI) — %				
At 12 mo	80 (74–84)	66 (60–71)	80 (75–84)	67 (61–73)
At 18 mo	71 (65–76)	49 (42–54)	71 (65–76)	54 (48–60)
At 24 mo	57 (50–63)	41 (35–47)	62 (55–68)	47 (40–53)
Objective response (95% CI) — %	83 (78–87)	76 (70–80)	92 (88–95)	83 (78–87)
Best objective response — no. (%) [‡]				
Complete response	1 (<1)	2 (1)	2 (1)	1 (<1)
Partial response	231 (83)	208 (75)	254 (91)	229 (82)
Stable disease for ≥35 days [§]	34 (12)	51 (18)	10 (4)	29 (10)
Disease progression	1 (<1)	9 (3)	3 (1)	12 (4)
Death [¶]	6 (2)	3 (1)	6 (2)	3 (1)
Could not be evaluated	6 (2)	5 (2)	4 (1)	4 (1)
Disease control (95% CI) — %	95 (92–98)	94 (90–96)	95 (92–98)	93 (90–96)
Median duration of response (95% CI) — mo ^{**}	24.0 (20.9–27.8)	15.3 (12.7–19.4)	28.3 (23.7–NC)	21.0 (17.8–NC)
Continued response (95% CI) — %				
At 12 mo	80 (74–84)	64 (57–70)	81 (76–86)	73 (66–78)
At 18 mo	69 (62–75)	44 (37–51)	70 (63–75)	56 (49–63)
At 24 mo	49 (41–57)	35 (27–42)	56 (48–64)	45 (36–52)

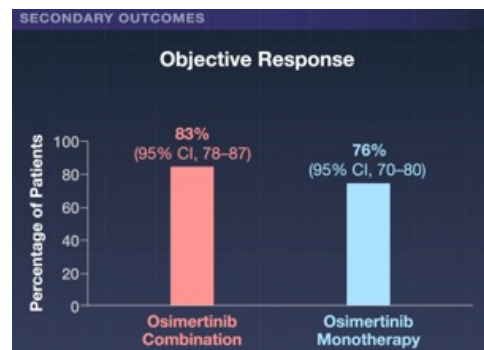
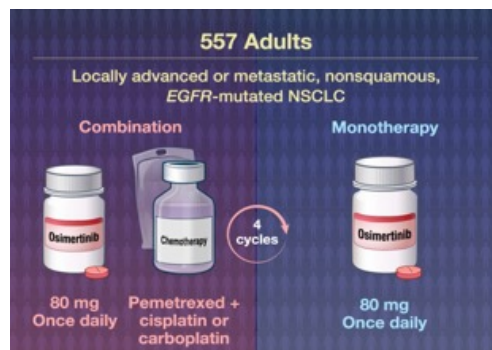
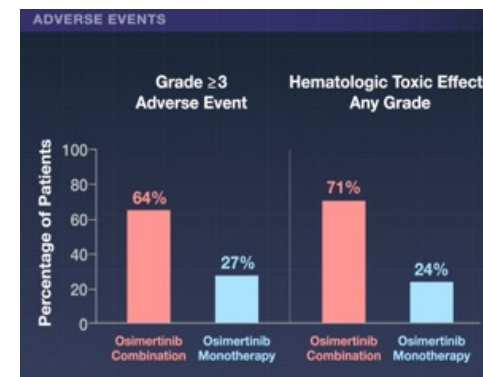
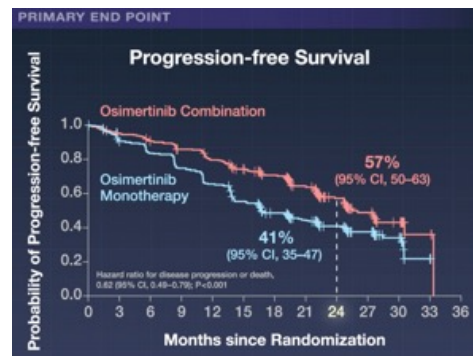
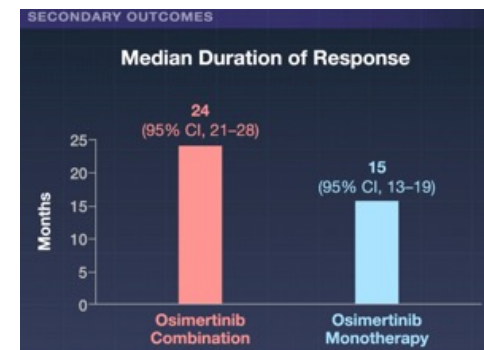
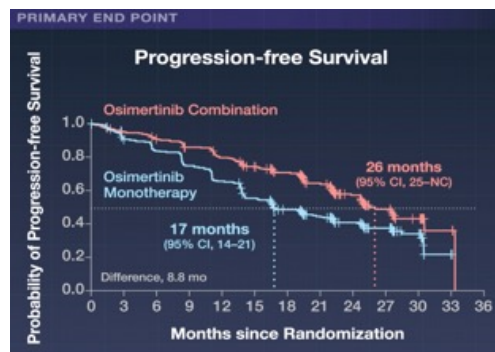
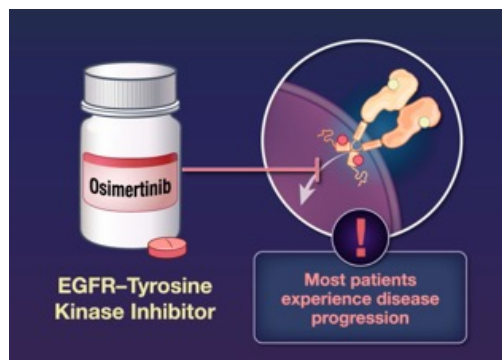
Subgroup Analysis of Progression-free Survival.

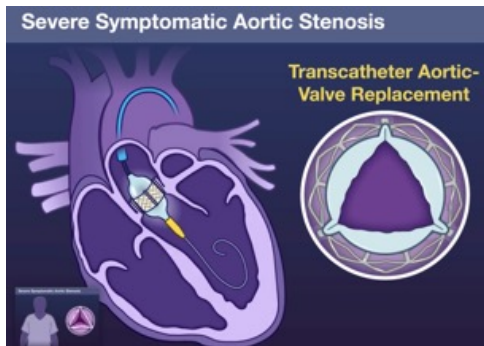
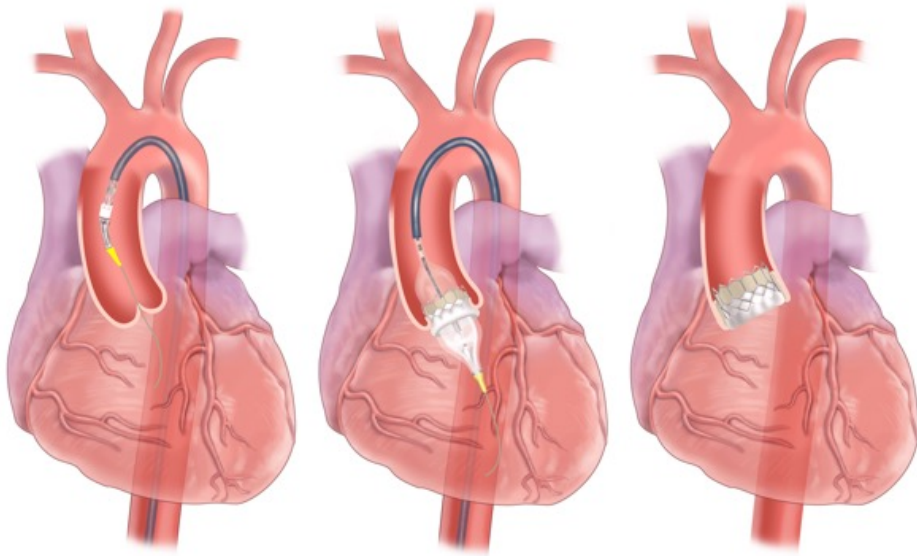


A hazard ratio of less than 1 indicates a lower risk of progression or death with osimertinib plus chemotherapy than with osimertinib monotherapy. The Cox proportional-hazards model includes randomized treatment, the subgroup covariate of interest, and the treatment according to subgroup interaction. Subgroups that were defined according to CNS metastases at baseline were made according to investigator assessment on the basis of data in the electronic case-report form regarding the CNS lesion site at baseline, medical history, previous surgery, or history of radiotherapy for CNS metastases. Race was reported by the patient; options were given on a drop-down list at randomization. World Health Organization (WHO) performance-status scores are assessed on a scale from 0 to 5, with higher scores indicating greater disability. A score of 0 indicates that the patient is fully active and able to carry out all predisease activities without restrictions, and a score of 1 indicates that the patient is restricted in physically strenuous activity but is ambulatory and able to carry out work of a light or sedentary nature, such as light housework or office work. Two additional subgroups that were analyzed to fulfill regulatory requirements for diagnostics are not included here: EGFR mutations as assessed by a central Cobas tissue test and EGFR mutations as assessed by a central Cobas circulating tumor DNA test. The shaded area indicates the 95% confidence interval for the overall hazard ratio (among all the patients). Other than in the analysis in the overall population, the widths of the confidence intervals have not been adjusted for multiplicity. Patients with co-occurring exon 19 deletion and L858R mutations were included in the subgroup for exon 19 deletion. EGFR denotes epidermal growth factor receptor, and L858R p.Leu858Arg.

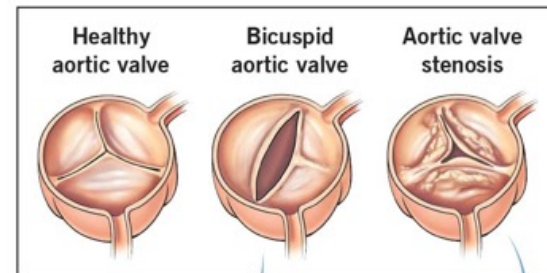
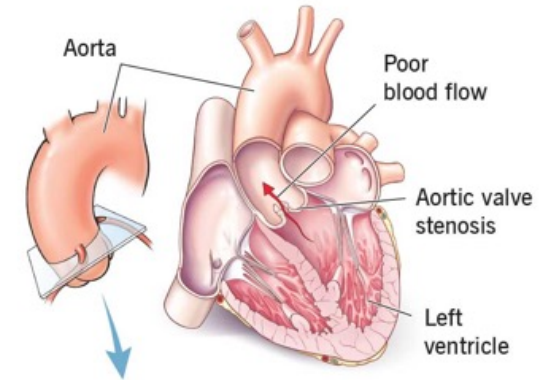
Adverse Events.

Event	Osimertinib + Platinum–Pemetrexed (N=276)					Osimertinib Monotherapy (N=275)				
	Any Grade	Grade 1	Grade 2	Grade 3	Grade 4	Any Grade	Grade 1	Grade 2	Grade 3	Grade 4
Anemia	128 (46)	30 (11)	43 (16)	55 (20)	0	22 (8)	15 (5)	6 (2)	1 (<1)	0
Diarrhea	120 (43)	83 (30)	29 (11)	8 (3)	0	112 (41)	89 (32)	22 (8)	1 (<1)	0
Nausea	119 (43)	81 (29)	34 (12)	4 (1)	0	28 (10)	22 (8)	6 (2)	0	0
Decreased appetite	85 (31)	49 (18)	28 (10)	8 (3)	0	26 (9)	18 (7)	6 (2)	2 (1)	0
Constipation	81 (29)	60 (22)	20 (7)	1 (<1)	0	28 (10)	23 (8)	5 (2)	0	0
Rash	77 (28)	55 (20)	21 (8)	1 (<1)	0	57 (21)	46 (17)	11 (4)	0	0
Fatigue	76 (28)	45 (16)	23 (8)	8 (3)	0	26 (9)	24 (9)	1 (<1)	1 (<1)	0
Vomiting	73 (26)	50 (18)	20 (7)	3 (1)	0	17 (6)	13 (5)	4 (1)	0	0
Stomatitis	68 (25)	40 (14)	27 (10)	1 (<1)	0	50 (18)	32 (12)	17 (6)	1 (<1)	0
Neutropenia	68 (25)	4 (1)	27 (10)	30 (11)	7 (3)	9 (3)	3 (1)	4 (1)	2 (1)	0
Paronychia	65 (24)	28 (10)	35 (13)	2 (1)	0	73 (27)	37 (13)	35 (13)	1 (<1)	0
Neutrophil count decrease	62 (22)	5 (2)	26 (9)	25 (9)	6 (2)	16 (6)	6 (2)	8 (3)	2 (1)	0
Covid-19†	57 (21)	23 (8)	31 (11)	2 (1)	0	39 (14)	18 (7)	21 (8)	0	0
ALT increase	56 (20)	36 (13)	16 (6)	4 (1)	0	21 (8)	17 (6)	3 (1)	1 (<1)	0
Platelet count decrease	51 (18)	19 (7)	11 (4)	18 (7)	3 (1)	19 (7)	18 (7)	1 (<1)	0	0
Thrombocytopenia	51 (18)	19 (7)	13 (5)	16 (6)	3 (1)	12 (4)	6 (2)	3 (1)	3 (1)	0
Dry skin	50 (18)	43 (16)	7 (3)	0	0	66 (24)	62 (23)	4 (1)	0	0
AST increase	48 (17)	42 (15)	5 (2)	1 (<1)	0	13 (5)	12 (4)	0	1 (<1)	0
Blood creatinine increase	46 (17)	33 (12)	13 (5)	0	0	12 (4)	10 (4)	2 (1)	0	0
White-cell count decrease	44 (16)	7 (3)	28 (10)	8 (3)	1 (<1)	18 (7)	9 (3)	8 (3)	1 (<1)	0
Peripheral edema	42 (15)	33 (12)	9 (3)	0	0	12 (4)	9 (3)	3 (1)	0	0



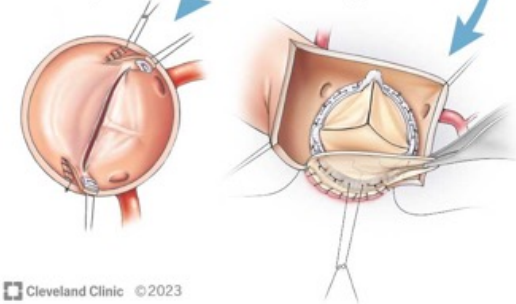


Aortic valve surgery



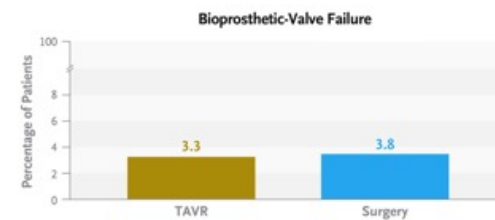
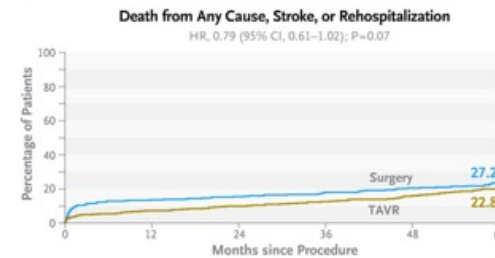
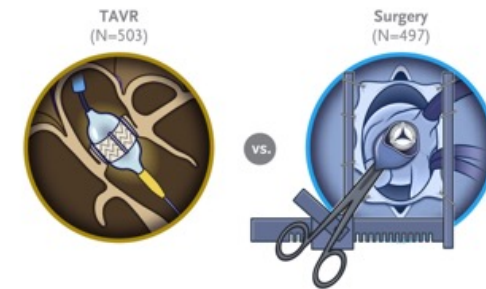
Aortic valve repair

Surgical aortic valve replacement



Transcatheter Aortic-Valve Replacement in Low-Risk Patients at Five Years

A previous analysis in this trial showed that among patients with severe, symptomatic aortic stenosis who were at low surgical risk, the rate of the composite end point of death, stroke, or rehospitalization at 1 year was significantly lower with transcatheter aortic-valve replacement (TAVR) than with surgical aortic-valve replacement. Longer-term outcomes are unknown. We randomly assigned patients with severe, symptomatic aortic stenosis and low surgical risk to undergo either TAVR or surgery. The first primary end point was a composite of death, stroke, or rehospitalization related to the valve, the procedure, or heart failure. The second primary end point was a hierarchical composite that included death, disabling stroke, nondisabling stroke, and the number of rehospitalization days, analyzed with the use of a win ratio analysis. Clinical, echocardiographic, and health-status outcomes were assessed through 5 years.



CONCLUSIONS

Among patients with severe, symptomatic aortic stenosis and low surgical risk who underwent TAVR or surgical aortic-valve replacement, the frequency of adverse cardiovascular events appeared to be similar in the two groups at 5 years of follow-up.

Transcatheter aortic-valve replacement (TAVR) has been increasingly used as an alternative to surgery for treating patients with severe, symptomatic aortic stenosis. Randomized trials of both balloon-expandable and self-expanding TAVR valves have shown that in patients at intermediate or high risk for death by 30 days after surgery, TAVR was either noninferior or superior to surgical aortic-valve replacement at 5 years of follow-up. In two randomized trials involving younger patients who were at low surgical risk, TAVR was either noninferior or superior to surgery at 2 or 3 years. The Placement of Aortic Transcatheter Valves (PARTNER) 3 trial showed that the rate of the composite end point of death, stroke, or rehospitalization at 1 and 2 years was significantly lower with TAVR than with surgery. Here, we report the 5-year outcomes in this trial.

Patients

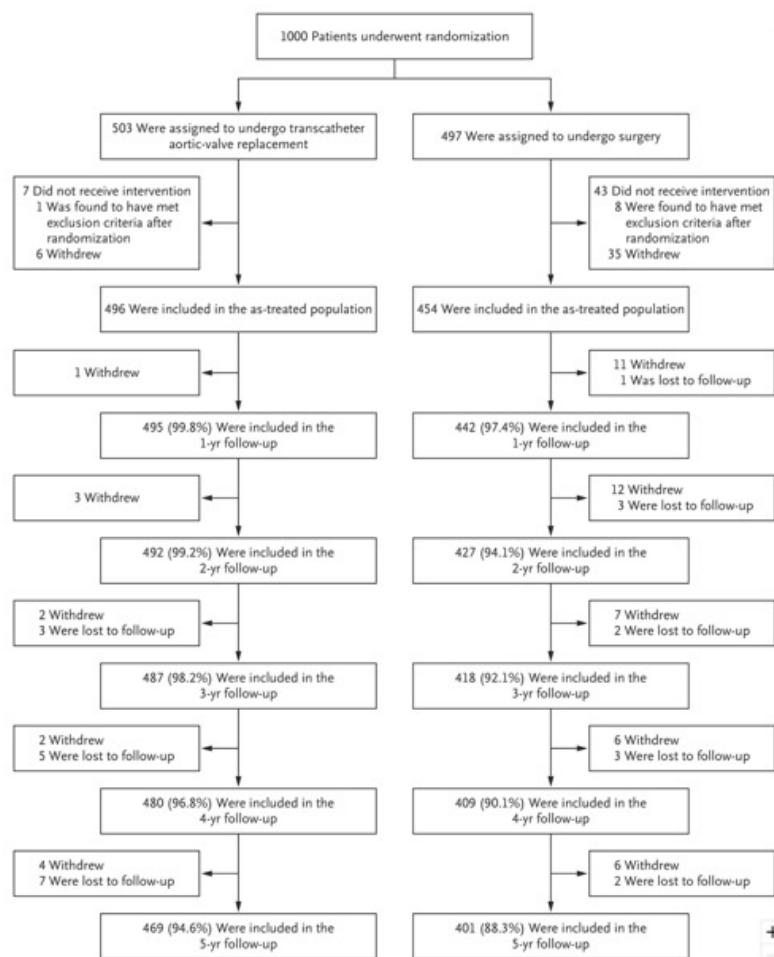
Patients were eligible for inclusion if they had severe, symptomatic aortic stenosis and were considered to be at low surgical risk on the basis of clinical and anatomical assessment, including a Society of Thoracic Surgeons Predicted Risk of Mortality (STS-PROM) score of less than 4% (with scores ranging from 0 to 100% and higher scores indicating a greater risk of death within 30 days after the procedure) and on the basis of assessment by the heart team. Patients also had to be eligible for TAVR through transfemoral access. The eligibility of all the patients was reviewed and approved by a case review board.

Randomization, Procedures, and Follow-up

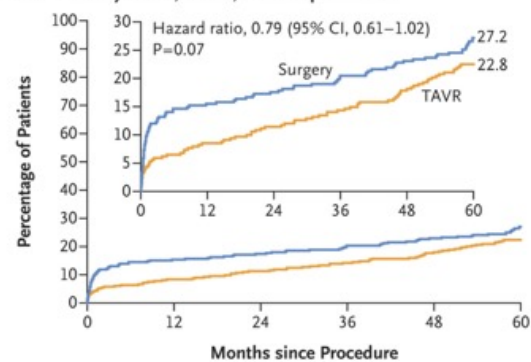
Patients were assigned in a 1:1 ratio to undergo either TAVR with a SAPIEN 3 valve or surgical aortic-valve replacement with a commercially available bioprosthetic valve. The SAPIEN 3 system and the procedures for TAVR and surgery have been described previously. Clinical outcomes and transthoracic echocardiography data were assessed at baseline, after the implantation procedure, at hospital discharge, 30 days, 6 months, 1 year, and then annually to 5 years.

End Points

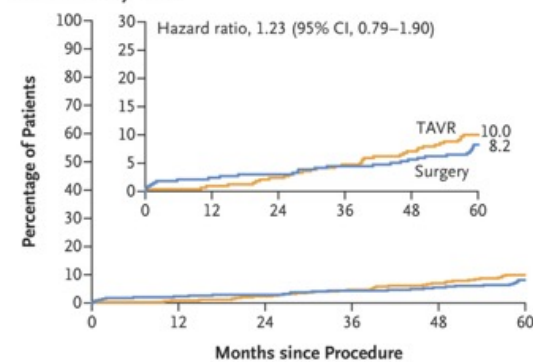
The original primary end point, assessed at 1 year, was a nonhierarchical composite of death from any cause, stroke, or rehospitalization related to the procedure, the valve, or heart failure.



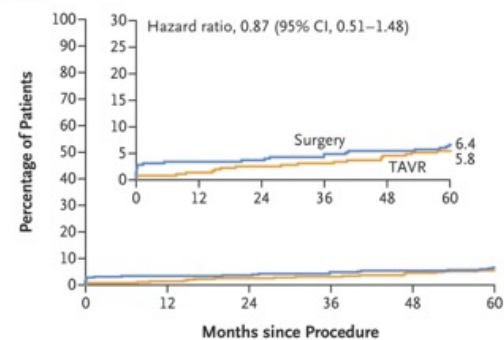
A Death from Any Cause, Stroke, or Rehospitalization



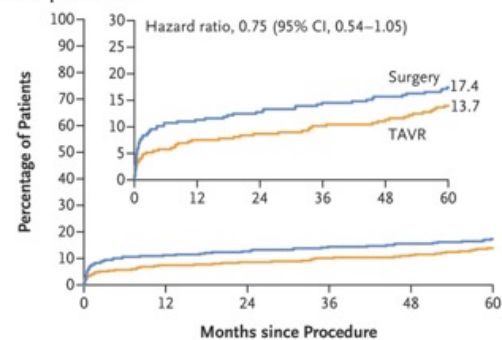
B Death from Any Cause



C Stroke



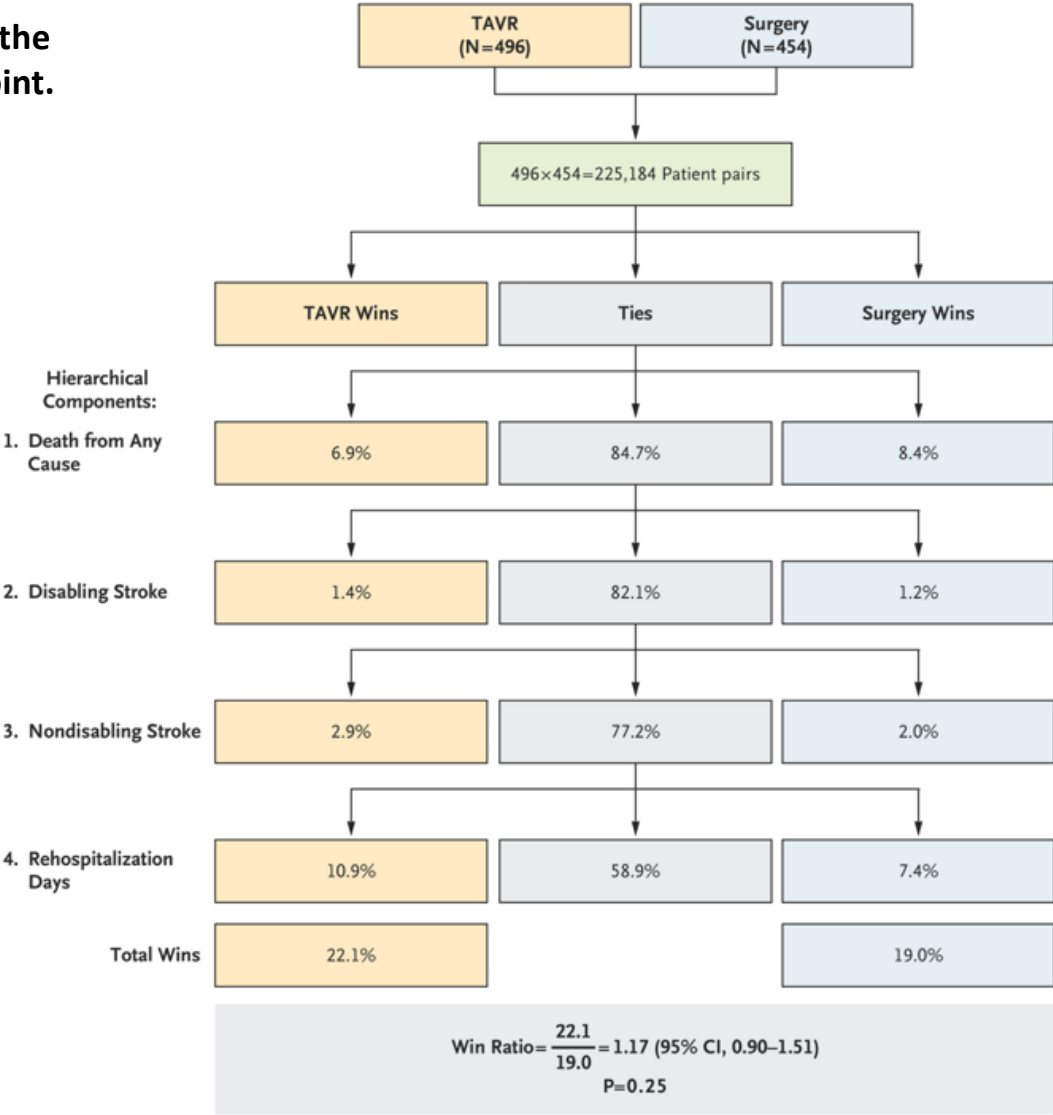
D Rehospitalization



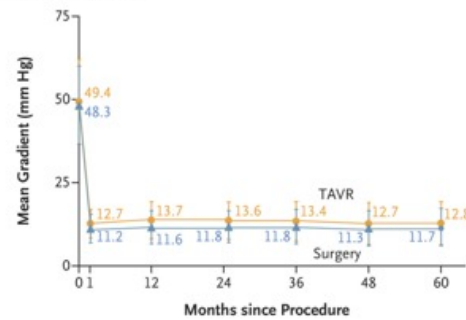
Key Clinical End Points.

End Point	Baseline to 5 Years			1 Year to 5 Years		
	TAVR (N=496)	Surgery (N=454)	Hazard Ratio (95% CI)	TAVR (N=490)	Surgery (N=427)	Hazard Ratio (95% CI)
	<i>no. of patients with event (Kaplan–Meier estimate, %)</i>			<i>no. of patients with event (Kaplan–Meier estimate, %)</i>		
Death, stroke, or rehospitalization†	111 (22.8)	117 (27.2)	0.79 (0.61–1.02)‡	69 (15.7)	47 (13.7)	1.17 (0.81–1.70)
Death from any cause	48 (10.0)	34 (8.2)	1.23 (0.79–1.90)§	43 (9.1)	23 (5.9)	1.61 (0.97–2.67)
Death from cardiovascular causes	26 (5.5)	21 (5.1)	1.08 (0.61–1.92)§	22 (4.7)	12 (3.1)	1.58 (0.78–3.19)
Death from noncardiovascular causes	22 (4.8)	13 (3.3)	1.46 (0.74–2.90)§	21 (4.6)	11 (2.8)	1.64 (0.79–3.41)
Stroke	27 (5.8)	27 (6.4)	0.87 (0.51–1.48)	21 (4.6)	12 (3.2)	1.49 (0.73–3.02)
Disabling stroke	13 (2.9)	11 (2.7)	1.03 (0.46–2.30)	12 (2.7)	6 (1.6)	1.73 (0.65–4.61)
Nondisabling stroke	15 (3.2)	16 (3.7)	0.82 (0.40–1.65)	10 (2.2)	6 (1.5)	1.41 (0.51–3.89)
Death or disabling stroke	55 (11.5)	41 (9.8)	1.17 (0.78–1.75)§	50 (10.6)	27 (6.9)	1.60 (1.00–2.55)
Rehospitalization†	65 (13.7)	74 (17.4)	0.75 (0.54–1.05)	29 (6.9)	24 (6.9)	0.98 (0.57–1.69)
Aortic-valve reintervention	12 (2.6)	12 (3.0)	0.86 (0.39–1.92)	9 (2.0)	10 (2.6)	0.77 (0.31–1.90)
Endocarditis	6 (1.3)	8 (2.0)	0.65 (0.23–1.87)	5 (1.1)	6 (1.5)	0.72 (0.22–2.35)
Valve thrombosis¶	12 (2.5)	1 (0.2)	10.52 (1.37–80.93)	10 (2.1)	1 (0.2)	8.72 (1.12–68.12)
New-onset atrial fibrillation**	55 (13.7)	155 (42.4)	0.25 (0.19–0.34)	21 (6.0)	5 (2.6)	2.30 (0.87–6.10)
New pacemaker**	63 (13.5)	43 (10.4)	1.33 (0.90–1.96)	25 (6.1)	18 (4.9)	1.22 (0.67–2.24)
Serious bleeding	49 (10.2)	64 (14.8)	0.65 (0.45–0.95)	25 (5.6)	18 (5.1)	1.15 (0.63–2.11)
Myocardial infarction	10 (2.1)	18 (4.4)	0.48 (0.22–1.05)	6 (1.3)	10 (2.6)	0.51 (0.19–1.41)
Revascularization	17 (3.7)	25 (6.0)	0.59 (0.32–1.09)	12 (2.7)	12 (3.2)	0.85 (0.38–1.88)
Percutaneous coronary intervention	16 (3.5)	20 (4.9)	0.69 (0.36–1.34)	11 (2.5)	12 (3.2)	0.78 (0.35–1.78)
Coronary-artery bypass grafting	2 (0.5)	5 (1.1)	0.36 (0.07–1.85)	1 (0.2)	0	—

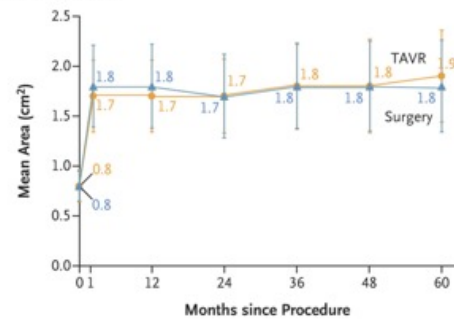
Win Ratio Diagram for the
Second Primary End Point.



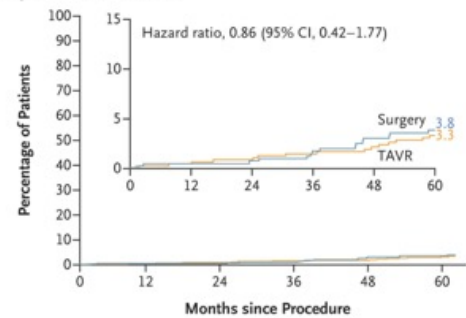
A Aortic-Valve Gradient



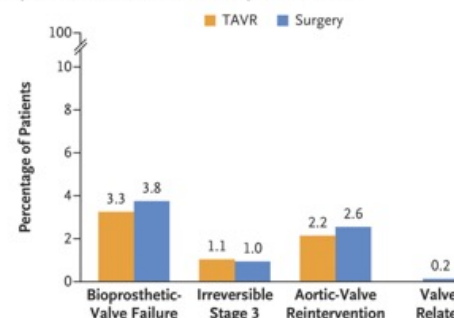
B Aortic-Valve Area



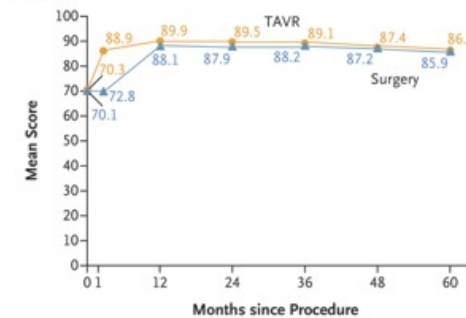
C Bioprosthetic-Valve Failure



D Bioprosthetic-Valve Failure and Components at 5 Yr

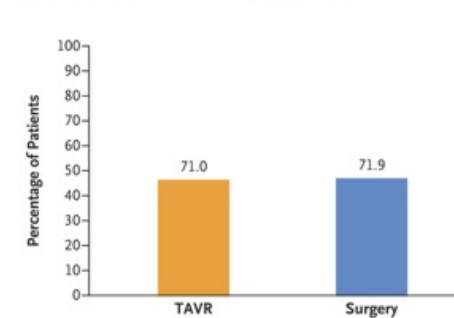


E KCCQ-OS Scores



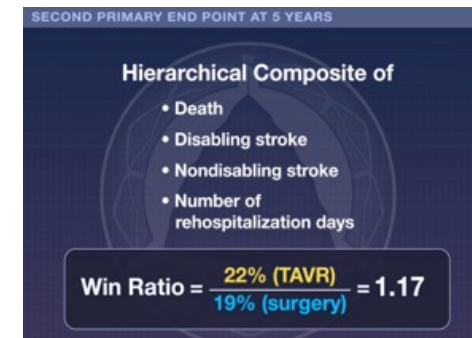
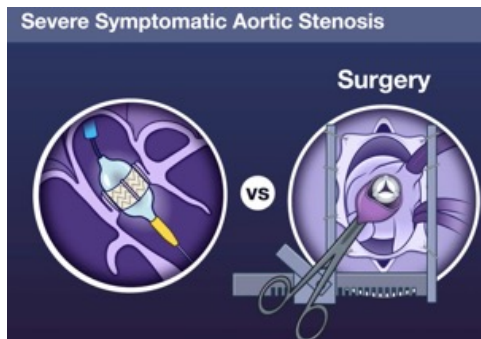
No. at Risk

F Patients Who Were Alive with KCCQ-OS Score ≥ 75



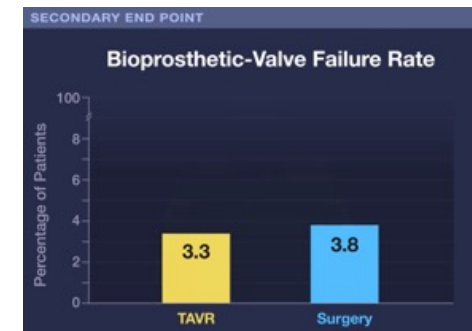
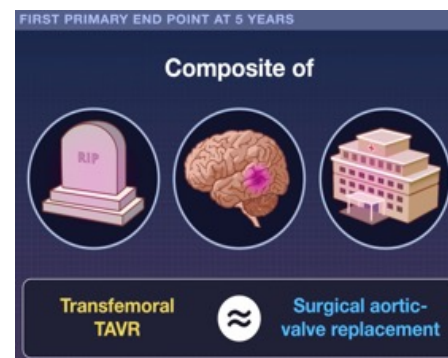
Echocardiographic Outcomes, Bioprosthetic-Valve Failure, and Quality-of-Life Outcomes.

The mean aortic-valve gradients, shown in Panel A, and the mean aortic-valve areas, shown in Panel B, were assessed by an echocardiography core laboratory. I bars indicate standard deviations. Kaplan–Meier estimates for bioprosthetic-valve failure, adjudicated according to Valve Academic Research Consortium 3 criteria, are shown in Panel C. The inset in Panel C shows the same data on an enlarged y axis. The components of bioprosthetic-valve failure at 5 years are shown in Panel D. The mean Kansas City Cardiomyopathy Questionnaire–Overall Summary (KCCQ–OS) scores are shown in Panel E, and the percentage of patients who were alive with a KCCQ–OS score of 75 or higher are shown in Panel F. KCCQ–OS scores range from 0 to 100, with higher scores indicating better health status.



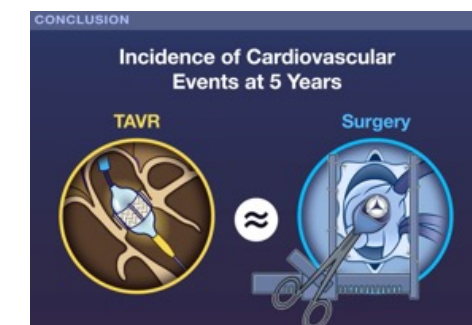
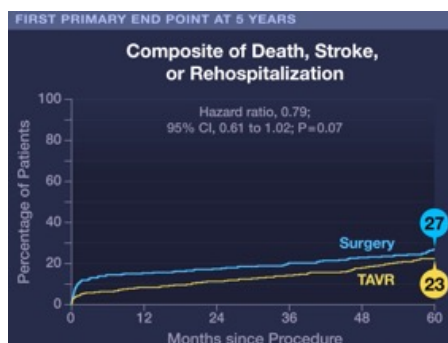
PARTNER 3 Trial

- Enrolled patients at low surgical risk
- Found TAVR to be superior to surgical valve replacement with respect to adverse cardiovascular events at 1 and 2 years



PARTNER 3 Trial

5-Year Outcomes?



Urothelkarzinom: Erdafitinib erfolgreich in Phase-II



Forscher publizierten Ergebnisse einer Phase-II-Studie mit Patienten mit einem metastasierten und vorbehandelten Urothelkarzinom mit FGFR-2- oder FGFR-3-Mutation. Auch nach Chemo- und Immuntherapie zeigte Erdafitinib eine vielversprechende Antitumoraktivität.

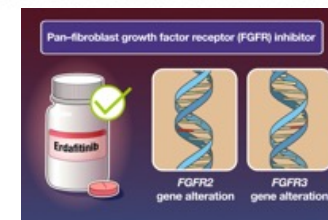
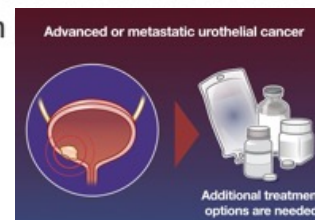


Hintergrund

Veränderungen des für den Fibroblasten-Wachstumsfaktor-Rezeptor (fibroblast growth factor receptor [FGFR]) kodierenden Gens sind beim Urothelkarzinom häufig und können mit einer geringeren Empfindlichkeit gegenüber Immuninterventionen verbunden sein. Erdafitinib, ein Tyrosinkinaseinhibitor von FGFR1–4, zeigte in präklinischen Modellen und in einer Phase-I-Studie mit Patienten mit FGFR-Veränderungen Antitumoraktivität.

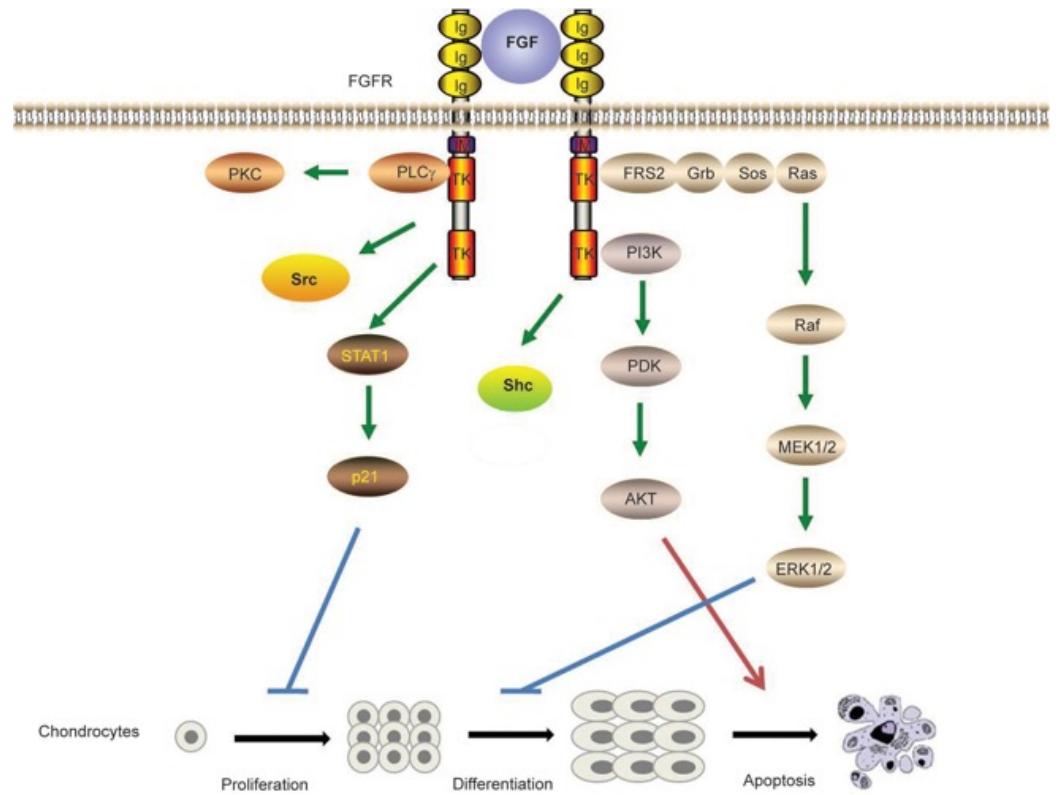
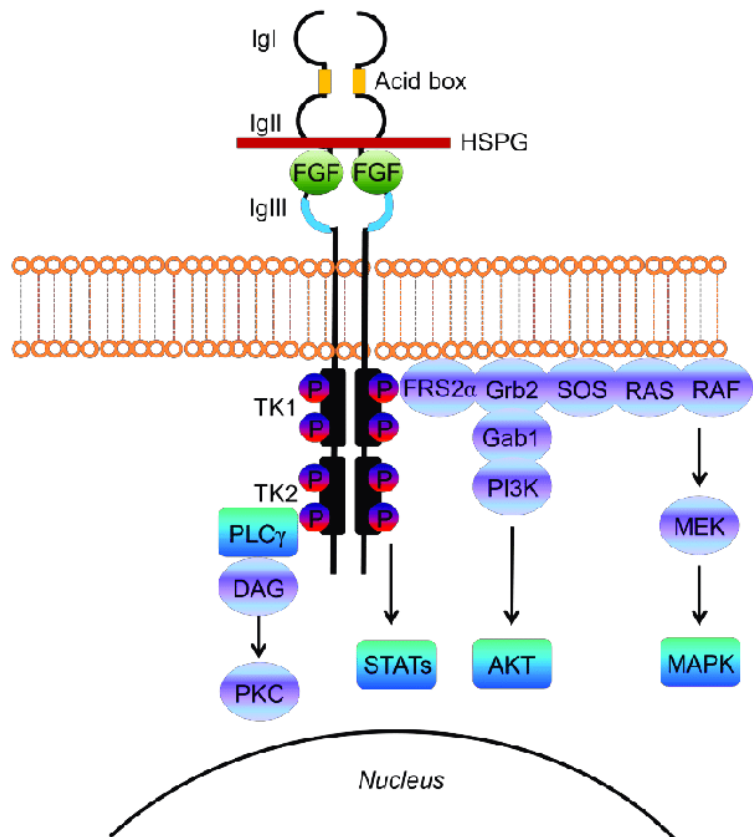
Zielsetzung

Ein wissenschaftliches Team um Dr. Yohann Loriot vom Institut Gustave Roussy und der Université Paris-Saclay in Villejuif, Frankreich, untersuchte im Rahmen einer offenen, multizentrischen Phase-II-Studie die Wirksamkeit und Sicherheit von Erdafitinib bei Patienten mit Urothelkarzinom



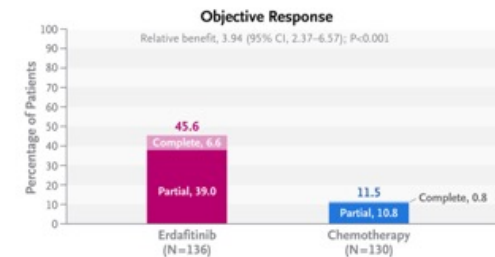
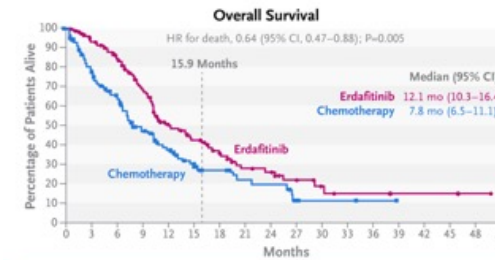
Der Fibroblasten-Wachstumsfaktor-Rezeptor, kurz FGFR, ist eine Gruppe von zellulären Rezeptoren, die verschiedene Fibroblasten-Wachstumsfaktoren (FGF) binden. Sie gehören zu den Rezeptortyrosinkinasen. Der FGFR besteht aus einer extrazellulären Liganden-Domäne, einer singulären transmembranen Helix-Domäne und einer intrazellulären Domäne mit Tyrosinkinaseaktivität. Es sind mehr als 48 verschiedene Isoformen des FGFR bekannt, die durch alternatives mRNA-Splicing aus vier Genen (FGFR1-4) hervorgehen. Diese Isoformen unterscheiden sich in der Ligandenbindung und ihrer Kinasedomäne. Gleich ist allen Isoformen die extrazelluläre Domäne, die aus drei Immunglobulin-ähnlichen (IG-like) Domänen aufgebaut ist. Somit gehört der Rezeptor zur Immunglobulin-Superfamilie. In Säugetieren konnten bisher sechs FGFR identifiziert werden. Vier der Rezeptoren besitzen eine hohe Sequenzhomologie von 55 bis 72%:

- FGFR1
 - FGFR2
 - FGFR3
 - FGFR4
- Bei vielen Tumoren, wie zum Beispiel bei Plattenepithelkarzinomen des Kopf-Hals-Bereichs (HNSCC), bei Schilddrüsenkarzinomen, beim Cholangiokarzinom oder beim Urothelkarzinom, liegt eine Dysregulation FGFR-gesteuerter Signalwege vor. Zu den relevanten Veränderungen der FGFR-Signalwege bei malignen Erkrankungen gehören Genamplifikationen, Mutationen oder Translokationen



Erdafitinib or Chemotherapy in Advanced or Metastatic Urothelial Carcinoma

Erdafitinib is a pan–fibroblast growth factor receptor (FGFR) inhibitor approved for the treatment of locally advanced or metastatic urothelial carcinoma in adults with susceptible *FGFR3/2* alterations who have progression after platinum-containing chemotherapy. The effects of erdafitinib in patients with *FGFR*-altered metastatic urothelial carcinoma who have progression during or after treatment with checkpoint inhibitors (anti–programmed cell death protein 1 [PD-1] or anti–programmed death ligand 1 [PD-L1] agents) are unclear. We conducted a global phase 3 trial of erdafitinib as compared with chemotherapy in patients with metastatic urothelial carcinoma with susceptible *FGFR3/2* alterations who had progression after one or two previous treatments that included an anti–PD-1 or anti–PD-L1. Patients were randomly assigned in a 1:1 ratio to receive erdafitinib or the investigator’s choice of chemotherapy (docetaxel or vinflunine). The primary end point was overall survival.



CONCLUSIONS

In patients with advanced or metastatic urothelial carcinoma with *FGFR* alterations and previous treatment with PD-1 or PD-L1 inhibitors, erdafitinib resulted in significantly longer overall survival than standard chemotherapy.

Cisplatin-based chemotherapy is the standard treatment for newly diagnosed advanced and metastatic urothelial cancer. However, more than 50% of patients with metastatic urothelial carcinoma are ineligible for cisplatin treatment, and those who receive chemotherapy typically have progression within a few months.

Inhibitors of programmed cell death protein 1 (PD-1) and programmed death ligand 1 (PD-L1) are often used in patients who are ineligible for cisplatin, as maintenance therapy after platinum-based chemotherapy, or as second-line therapy for relapsed or refractory disease. However, only approximately 30% of patients with metastatic urothelial cancer have a response to PD-1 or PD-L1 inhibitors. Enfortumab vedotin is a standard drug that is given after platinum treatment and after PD-1 or PD-L1 inhibitor treatment; other options are sacituzumab govitecan and single-agent chemotherapy.

Alterations in the gene encoding fibroblast growth factor receptor (*FGFR*) are observed in approximately 20% of advanced or metastatic urothelial cancers (and in approximately 36% of upper tract urothelial cancers) and may function as oncogenic drivers. Erdafitinib is an oral selective pan-FGFR tyrosine kinase inhibitor. In a phase 2, single-group study (BLC2001) involving patients with locally advanced or metastatic urothelial cancer with susceptible *FGFR3/2* alterations who had progression after platinum-containing chemotherapy.

Patients

Eligible patients were 18 years of age or older with metastatic or surgically unresectable urothelial cancer and select *FGFR3/2* alterations (mutations or fusions); an Eastern Cooperative Oncology Group (ECOG) performance-status score of 0, 1, or 2 (on a 5-point scale in which higher scores reflect greater disability); adequate organ function; and progression during or after previous systemic therapy that included an anti-PD-1 or anti-PD-L1 agent; patients had received no more than two previous lines of therapy.

Treatment

Patients were randomly assigned in a 1:1 ratio to receive 21-day cycles of oral erdafitinib (8 mg per day with a pharmacodynamically guided increase in the dose to 9 mg on day 14) or the investigator's choice of chemotherapy (docetaxel at a dose of 75 mg per square meter of body-surface area intravenously over a 1-hour period or vinflunine at a dose of 320 mg per square meter intravenously over a 20-minute period) every 3 weeks until the occurrence of disease progression or unacceptable toxic effects. Randomization was stratified according to the ECOG performance-status score (0 or 1 vs. 2), disease distribution (presence vs. absence of visceral [lung, liver, or bone] metastases), and geographic region (North America vs. Europe vs. the rest of the world).

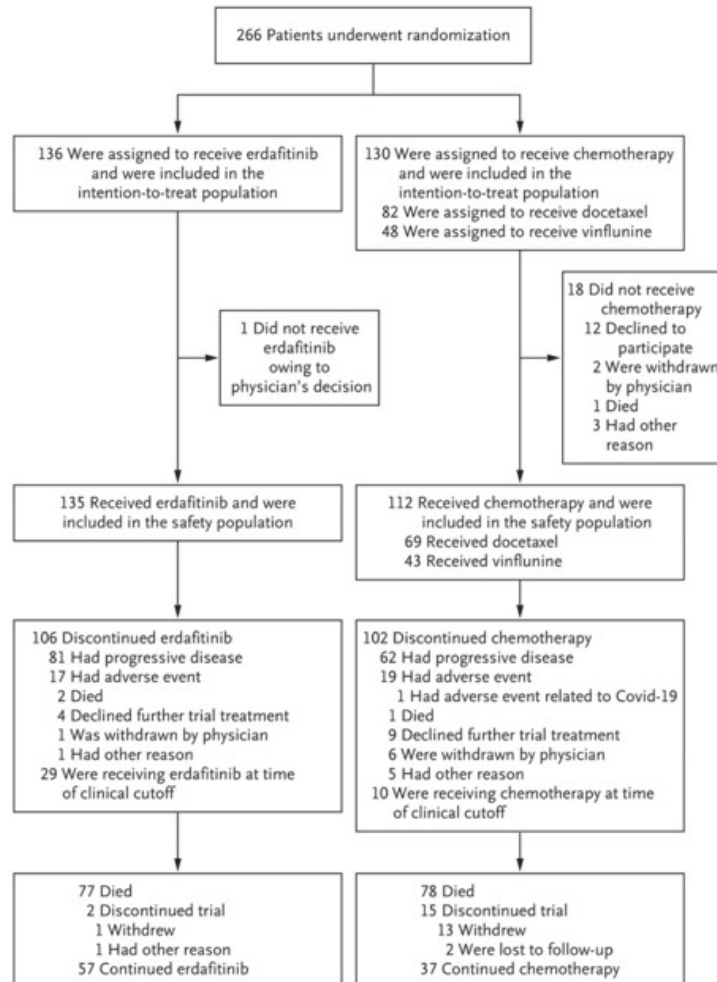
End Points

The primary end point was overall survival, defined as the time from randomization to death from any cause. Secondary end points included investigator-assessed progression-free survival (time from randomization to investigator-assessed disease progression according to Response Evaluation Criteria in Solid Tumors [RECIST], version 1.1, or death), objective response (complete or partial response according to RECIST, version 1.1, as assessed by the investigator), response duration (duration from the date of initial documentation of a response to first documented evidence of progressive disease or death), and safety.

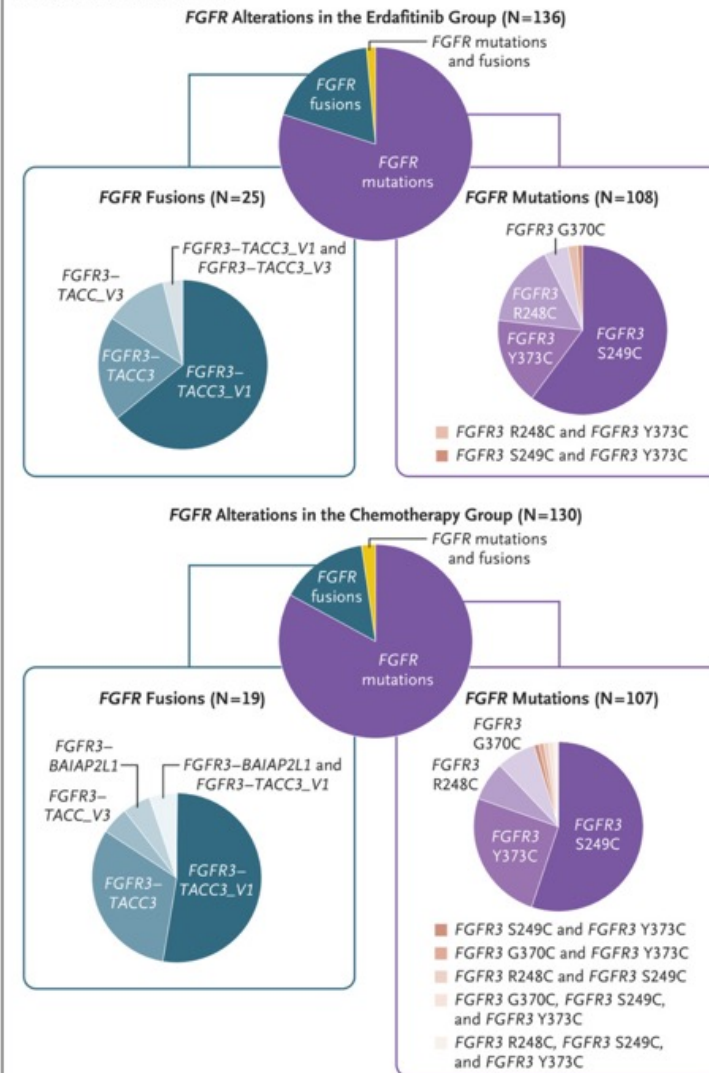
Assessments

Responses for solid tumors were assessed by the investigator according to RECIST, version 1.1, every 6 weeks for the first 6 months and every 12 weeks for the next 6 months and beyond. Adverse events were graded according to the National Cancer Institute Common Terminology Criteria for Adverse Events, version 4.03.

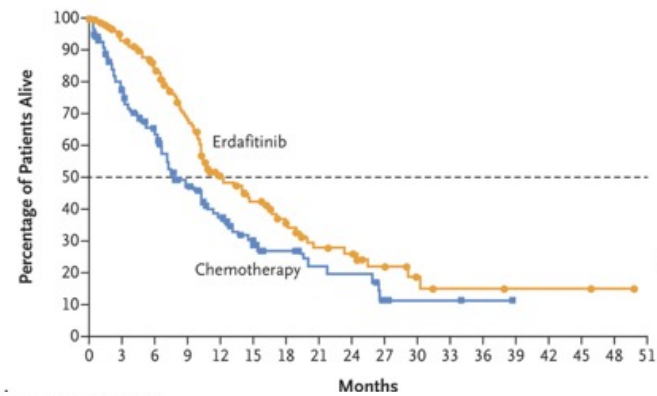
A Patient Flow in THOR Cohort 1



B Baseline FGFR Alterations

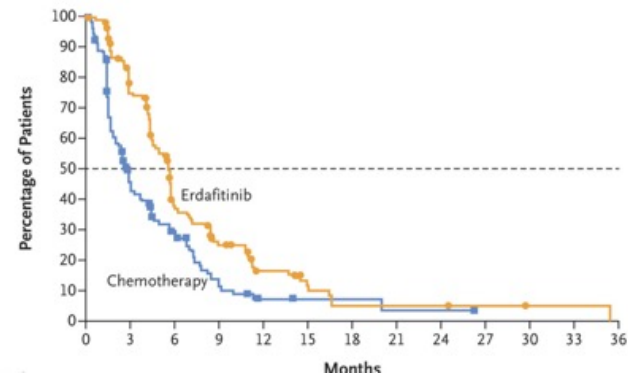


Characteristic	Erdaftinib (N=136)	Chemotherapy (N=130)
Median age (range) — yr	66 (32–85)	69 (35–86)
Age group — no. (%)		
<65 yr	59 (43.4)	45 (34.6)
≥65 yr	77 (56.6)	85 (65.4)
Sex — no. (%)		
Male	96 (70.6)	94 (72.3)
Female	40 (29.4)	36 (27.7)
Race — no. (%)†		
White	81 (59.6)	63 (48.5)
Asian	37 (27.2)	40 (30.8)
Black	0	1 (0.8)
Multiple	0	1 (0.8)
Not reported	18 (13.2)	25 (19.2)
Geographic region — no. (%)		
North America	8 (5.9)	5 (3.8)
Europe	82 (60.3)	80 (61.5)
Rest of the world	46 (33.8)	45 (34.6)
Visceral metastasis — no. (%)		
Present‡	101 (74.3)	97 (74.6)
Absent	35 (25.7)	33 (25.4)
ECOG performance-status score§		
0	63 (46.3)	51 (39.2)
1	61 (44.9)	66 (50.8)
2	12 (8.8)	13 (10.0)
Primary tumor location — no. (%)		
Upper tract	41 (30.1)	48 (36.9)
Lower tract	95 (69.9)	82 (63.1)
PD-L1 or PD-L1 status — no./total no. (%)¶		
CPS <10	89/96 (93)	68/79 (86)
CPS ≥10	7/96 (7)	11/79 (14)
FGFR alterations — no. (%)		
Mutation	108 (79.4)	107 (82.3)
Fusion	25 (18.4)	19 (14.6)
Mutation and fusion	2 (1.5)	3 (2.3)
False positive result	1 (0.7)	1 (0.8)
Previous lines of systemic therapy — no. (%)		
1	45 (33.1)	33 (25.4)
2	90 (66.2)	97 (74.6)
3	1 (0.7)	0



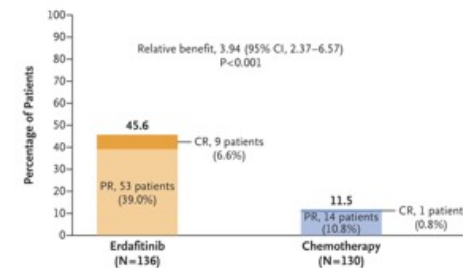
	No. of Deaths/ No. of Patients	Median Overall Survival (95% CI) mo
Erdaftinib	77/136	12.1 (10.3–16.4)
Chemotherapy	78/130	7.8 (6.5–11.1)
	Hazard ratio for death, 0.64 (95% CI, 0.47–0.88) P=0.005	

A Progression-free Survival



	No. of Progressions or Deaths/ No. of Patients	Median Progression-free Survival (95% CI) mo
Erdaftinib	101/136	5.6 (4.4–5.7)
Chemotherapy	90/130	2.7 (1.8–3.7)
	Hazard ratio for disease progression or death, 0.58 (95% CI, 0.44–0.78) P<0.001	

B Objective Response

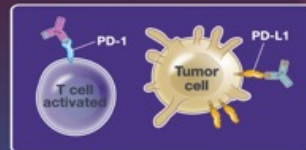


Adverse Events in the Safety Population.

Event	Erdafitinib (N = 135)				Chemotherapy (N = 112)			
	Any Grade	Grade 1	Grade 2	Grade ≥3	Any Grade	Grade 1	Grade 2	Grade ≥3
	number (percent)							
Hyperphosphatemia	108 (80.0)	70 (51.9)	31 (23.0)	7 (5.2)	0	0	0	0
Diarrhea	84 (62.2)	49 (36.3)	31 (23.0)	4 (3.0)	19 (17.0)	7 (6.2)	9 (8.0)	3 (2.7)
Stomatitis	65 (48.1)	22 (16.3)	32 (23.7)	11 (8.1)	14 (12.5)	4 (3.6)	8 (7.1)	2 (1.8)
Dry mouth	53 (39.3)	45 (33.3)	8 (5.9)	0	4 (3.6)	4 (3.6)	0	0
Palmar–plantar erythrodysesthesia syndrome	41 (30.4)	6 (4.4)	22 (16.3)	13 (9.6)	1 (0.9)	0	1 (0.9)	0
Dysgeusia	37 (27.4)	28 (20.7)	8 (5.9)	1 (0.7)	8 (7.1)	5 (4.5)	3 (2.7)	0
Alanine aminotransferase increased	37 (27.4)	24 (17.8)	9 (6.7)	4 (3.0)	4 (3.6)	2 (1.8)	1 (0.9)	1 (0.9)
Constipation	36 (26.7)	24 (17.8)	12 (8.9)	0	31 (27.7)	13 (11.6)	16 (14.3)	2 (1.8)
Decreased appetite	36 (26.7)	18 (13.3)	14 (10.4)	4 (3.0)	23 (20.5)	10 (8.9)	10 (8.9)	3 (2.7)
Anemia	35 (25.9)	10 (7.4)	15 (11.1)	10 (7.4)	36 (32.1)	8 (7.1)	19 (17.0)	9 (8.0)
Alopecia	34 (25.2)	29 (21.5)	4 (3.0)	1 (0.7)	27 (24.1)	16 (14.3)	11 (9.8)	0
Dry skin	31 (23.0)	23 (17.0)	6 (4.4)	2 (1.5)	5 (4.5)	4 (3.6)	1 (0.9)	0
Onycholysis	31 (23.0)	9 (6.7)	14 (10.4)	8 (5.9)	1 (0.9)	0	1 (0.9)	0
Weight decreased	30 (22.2)	12 (8.9)	15 (11.1)	3 (2.2)	3 (2.7)	3 (2.7)	0	0
Aspartate aminotransferase increased	29 (21.5)	21 (15.6)	5 (3.7)	3 (2.2)	3 (2.7)	2 (1.8)	1 (0.9)	0
Onychomadesis	28 (20.7)	9 (6.7)	17 (12.6)	2 (1.5)	2 (1.8)	1 (0.9)	1 (0.9)	0
Nail discoloration	24 (17.8)	16 (11.9)	7 (5.2)	1 (0.7)	2 (1.8)	1 (0.9)	1 (0.9)	0
Dry eye	23 (17.0)	20 (14.8)	3 (2.2)	0	2 (1.8)	1 (0.9)	1 (0.9)	0
Asthenia	20 (14.8)	6 (4.4)	12 (8.9)	2 (1.5)	28 (25.0)	9 (8.0)	15 (13.4)	4 (3.6)
Nausea	20 (14.8)	10 (7.4)	8 (5.9)	2 (1.5)	27 (24.1)	15 (13.4)	10 (8.9)	2 (1.8)
Neutropenia	0	0	0	0	22 (19.6)	1 (0.9)	5 (4.5)	16 (14.3)
Fatigue	20 (14.8)	12 (8.9)	8 (5.9)	0	21 (18.8)	13 (11.6)	4 (3.6)	4 (3.6)

Survival benefit?

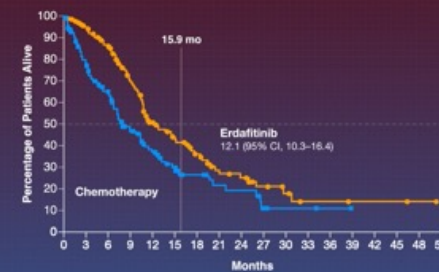
Patients with progression after treatment with inhibitors of PD-1 or PD-L1



Primary End Point

Overall Survival

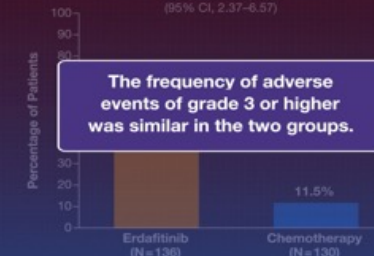
Hazard ratio for death, 0.64 (95% CI, 0.47–0.88)



Secondary End Points

Objective Response

Relative benefit, 3.94 (95% CI, 2.37–6.57)



The frequency of adverse events of grade 3 or higher was similar in the two groups.

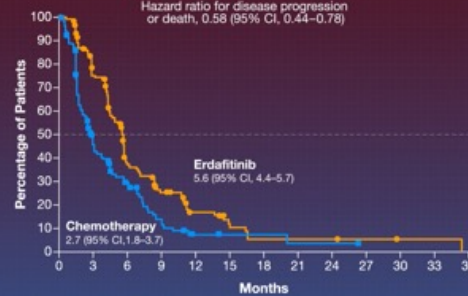
266 Adults



Secondary End Points

Progression-free Survival

Hazard ratio for disease progression or death, 0.58 (95% CI, 0.44–0.78)



Conclusion



- Patients with advanced or metastatic urothelial carcinoma
- *FGFR* alterations
- Progression after PD-1 or PD-L1 inhibitors

Treatment

21-Day Cycles

	SUN	MON	TUE	WED	THU	FRI	SAT
1							
2							
3							
4							
5							
6							
7							
8							
9							
10							
11							
12							
13							
14							
15							
16							
17							
18							
19							
20							
21							

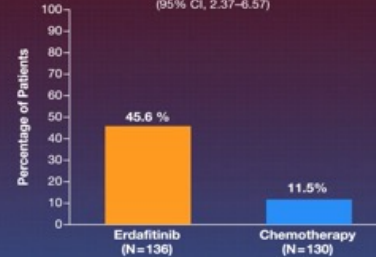


- Disease progression
- Unacceptable toxic effects

Secondary End Points

Objective Response

Relative benefit, 3.94 (95% CI, 2.37–6.57)



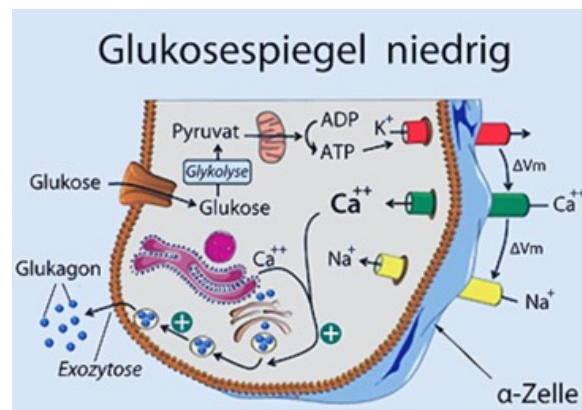
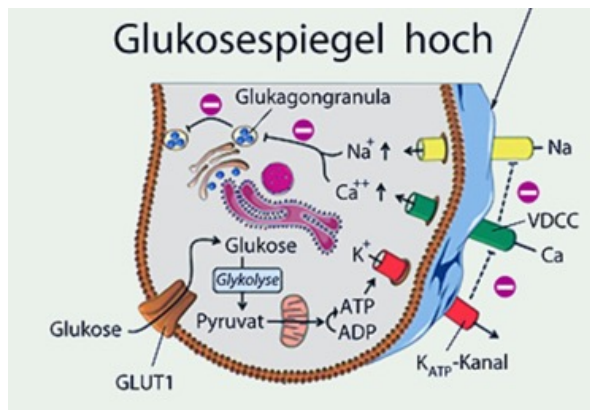
Conclusion

Overall survival was significantly longer with erdafitinib

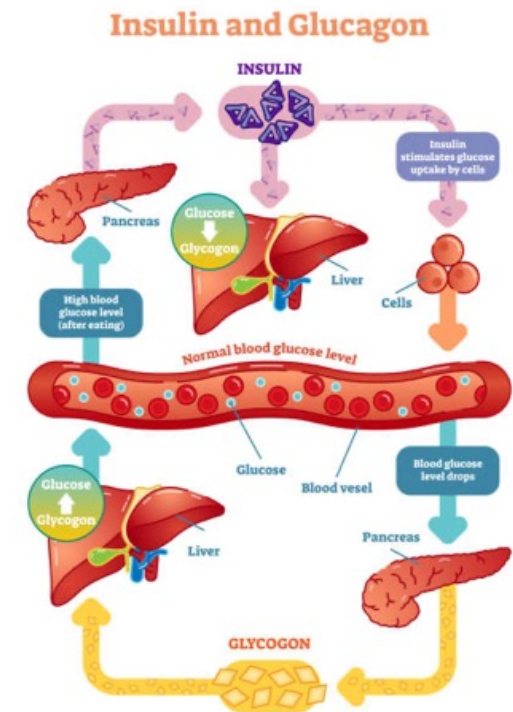


Glucagon (auch Glukagon) ist ein Peptidhormon, dessen Hauptwirkung die Erhöhung des Blutzuckerspiegels durch Anregung der Bildung von energiereicher Glucose aus Glykogen in der Leber ist. Es ist bedeutsam für die Glukosehomöostase. Es wird aus den Präkursoren Präglucagon und Präproglucagon in den Langerhans-Inseln der Bauchspeicheldrüse (α -Inseldellen) gebildet. Bei Blutzuckerabfall, aber auch nach einer proteinreichen Mahlzeit wird Glucagon von der Bauchspeicheldrüse in die Blutbahn abgegeben und dort frei transportiert. Dieses Hormon ist in seiner Wirkung auf den Glucose-, Protein- und Fettsäurestoffwechsel ein Gegenspieler des Insulins. Glucagon wird von der Leber aufgenommen und durch Spaltung inaktiviert.

Alpha Zelle



Alpha Zelle

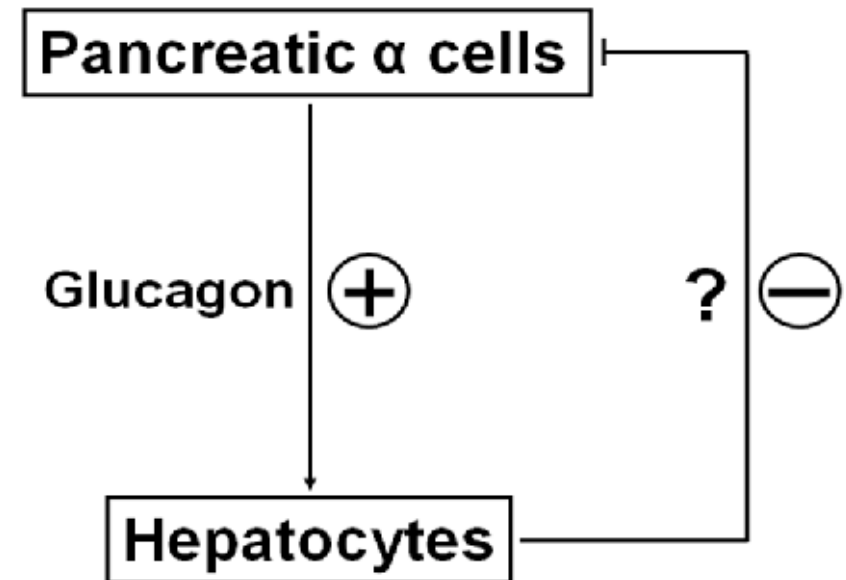
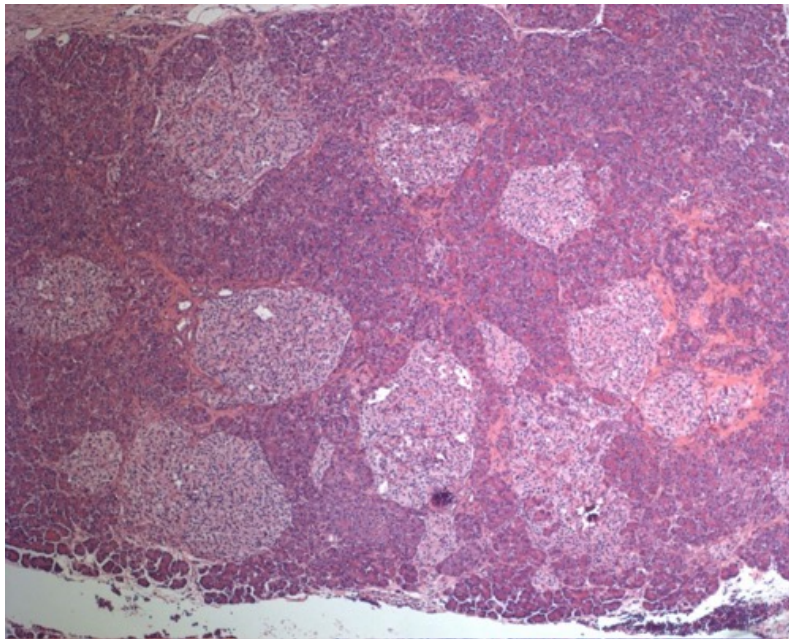


Mahvash (the index patient's first name) disease is an autosomal recessive, hereditary pancreatic neuroendocrine tumor syndrome. The genetic defect that causes Mahvash disease is biallelic inactivating mutations of the glucagon receptor gene (GCGR). Mahvash disease was discovered by American physician Run Yu and his colleagues in 2008. Mahvash disease is very rare. There have been over 10 cases of Mahvash disease described by the end of 2018. Mahvash disease occurs in both females and males. Mahvash disease is also called "glucagon cell hyperplasia and neoplasia" or "glucagon cell adenomatosis" by some authors but Mahvash disease is a distinct disease entity while the two alternative terms are mostly histological descriptions. Some patients with "glucagon cell hyperplasia and neoplasia" do not have glucagon receptor mutations.

Most patients with Mahvash disease are diagnosed in adulthood. Patients with Mahvash disease usually present with vague abdominal discomfort. Imaging with CT or MRI identifies a very large pancreas with one or more tumors. Biochemical testing shows marked hyperglucagonemia (hundreds-fold elevated). If the tumors are resected, they are found to be neuroendocrine tumors that usually express glucagon. In the tumor margin, pancreatic alpha cell hyperplasia is pervasive, numerous large islets composed of mostly alpha cells are evident, and multiple microadenomas and small neuroendocrine tumors often are present. The pancreatic neuroendocrine tumors are the main health concern for patients with Mahvash disease. Although the tumors commonly are indolent, death due to liver metastasis has been reported.

ALPHA-CELL HYPERPLASIA WITH GLUCAGONEMIA

Biallelic inactivating mutations of the glucagon receptor gene (GCGR).



Lucas et al. J Mol Genet Med 2013

In Mahvash disease, hepatocytes are rendered unresponsive to glucagon, which results in disruption of the feedback loop between the liver and the pancreas that helps regulate glucose and amino-acid metabolism. This disruption stimulates pancreatic α-cell hyperproliferation and causes pancreaticomegaly, overproduction of glucagon, and ultimately development of pancreatic neuroendocrine tumors.

Liver Transplantation in a Woman with Mahvash Disease

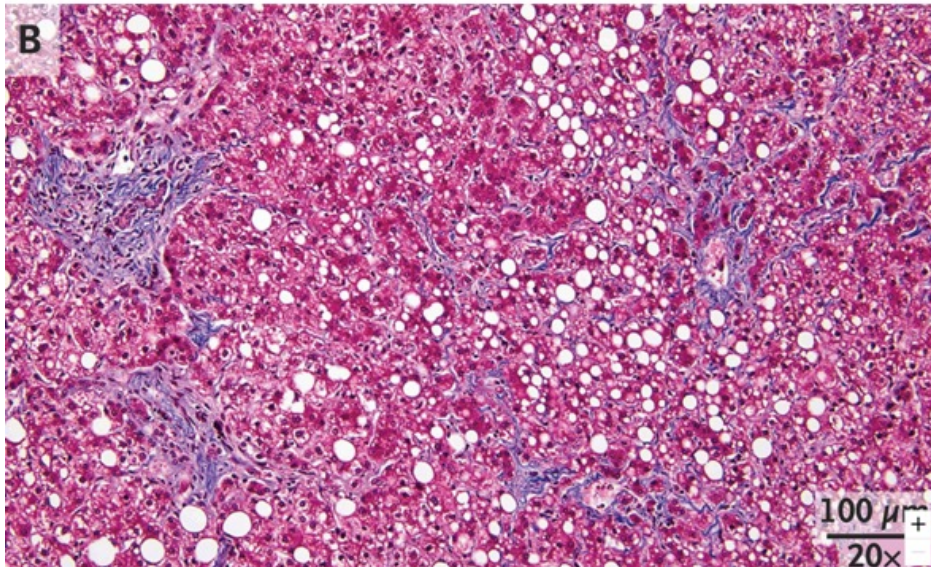
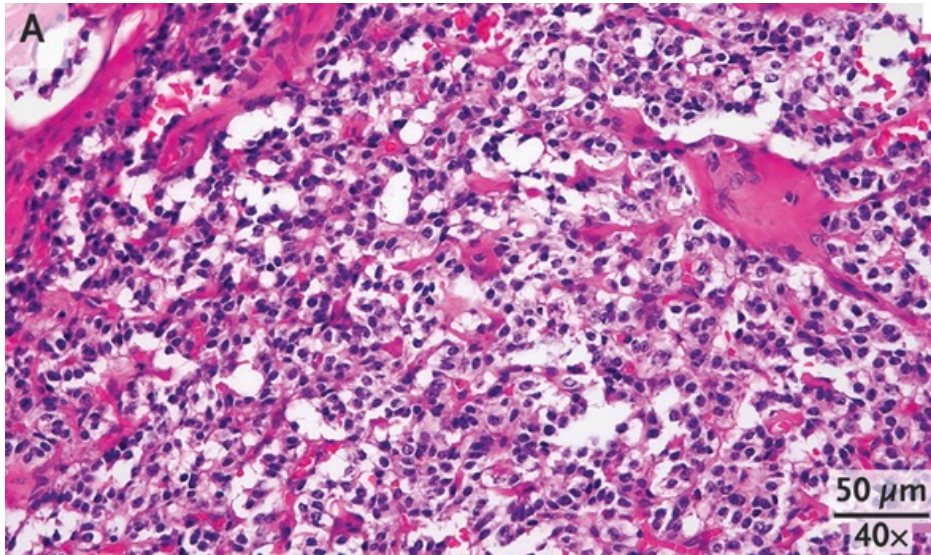
Summary

Mahvash disease is an exceedingly rare genetic disorder of glucagon signaling characterized by hyperglucagonemia, hyperaminoacidemia, and pancreatic α -cell hyperplasia. Although there is no known definitive treatment, octreotide has been used to decrease systemic glucagon levels. We describe a woman who presented to our medical center after three episodes of small-volume hematemesis. She was found to have hyperglucagonemia and pancreatic hypertrophy with genetically confirmed Mahvash disease and also **had evidence of portal hypertension** (recurrent portosystemic encephalopathy and variceal hemorrhage) in the absence of cirrhosis. These findings established a diagnosis of **portosinusoidal vascular disease**, a **presinusoidal** type of portal hypertension previously known as noncirrhotic portal hypertension. Liver transplantation was followed by normalization of serum glucagon and ammonia levels, reversal of pancreatic hypertrophy, and resolution of recurrent encephalopathy and bleeding varices.

Under normal physiologic conditions, glucagon is secreted by pancreatic α -cells in response to hypoglycemia and hyperaminoacidemia. This process establishes a catabolic state by stimulating gluconeogenesis and glycogen degradation while also inhibiting glycolysis and further glycogen synthesis, ultimately increasing blood glucose. Mahvash disease is an exceedingly rare disease characterized by pathogenic variants in the glucagon receptor gene (*GCGR*) that render hepatocytes unresponsive to glucagon. The loss of this feedback mechanism results in reactive pancreatic α -cell hyperplasia, which often leads to pancreatic neuroendocrine tumors and hyperaminoacidemia. Mahvash disease has traditionally been characterized by symptoms driven by pancreatic stimulation. However, here we describe a woman with Mahvash disease who was found to have portosinusoidal vascular disease (previously termed noncirrhotic portal hypertension) with variceal hemorrhage and portosystemic shunting leading to recurrent portosystemic encephalopathy. These findings indicate that portosinusoidal vascular disease may be an underlying feature of Mahvash disease. Liver transplantation resolved the patient's hyperglucagonemia by replacing defective hepatic glucagon receptors and instilling glucagon sensitivity. Replacing the liver, the site of increased portal-vein resistance, also resolved her intractable recurrent portosystemic encephalopathy and variceal hemorrhage.

Case Report

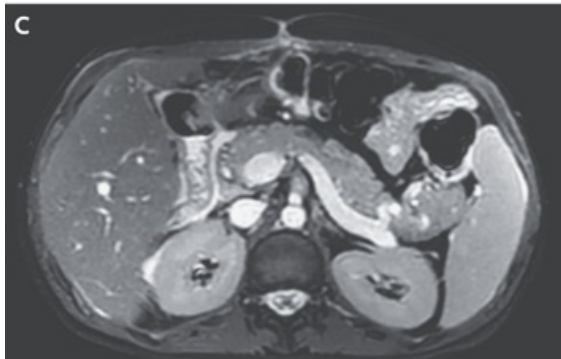
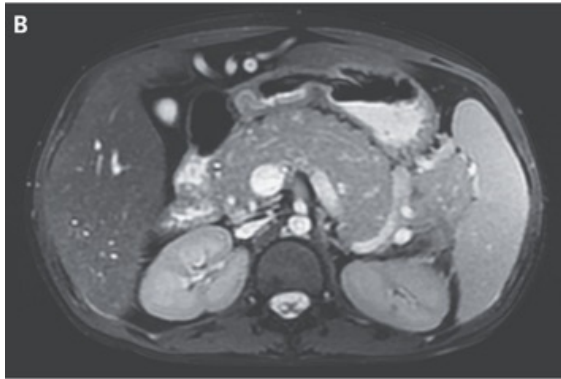
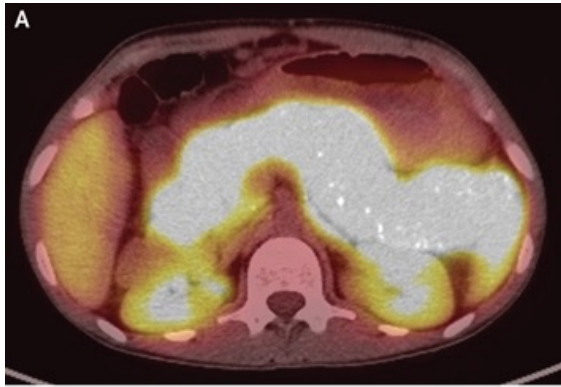
A 27-year-old woman without a substantial contributory medical history presented to our medical center after three episodes of small-volume hematemesis. She was found to have mild elevations in aminotransferase levels, with imaging showing chronic pancreatitis and possible hepatic cirrhosis without splenomegaly, as suggested by nodularity along the right hepatic lobe. She had no notable history of alcohol use. Findings on esophagogastroduodenoscopy were significant for small esophageal varices and portal hypertensive gastropathy. Endoscopic ultrasonography with needle biopsy of the pancreas was performed, preliminarily revealing a hyperplastic pancreas with multiple subcentimeter cysts and calcifications but no masses. Nadolol was prescribed as secondary prophylaxis to prevent recurrent variceal hemorrhage, and the patient was discharged home.



Pathological Findings.

Hematoxylin and eosin staining of a pancreatic-tissue sample obtained by needle biopsy showed uniform-appearing solid nests of neuroendocrine cells (Panel A). Trichrome staining of the liver explant showed perisinusoidal and mild periportal fibrosis with background moderate steatosis (Panel B).

The patient underwent genetic testing to confirm the diagnosis of Mahvash disease, and germline sequencing of *GCGR* revealed two variants (NM_000160.5:c.247del and NM_000160.5:c.463del) that predict truncation of the GCGR protein (p.Trp83GlyfsTer61, p.Ala155ProfsTer32).

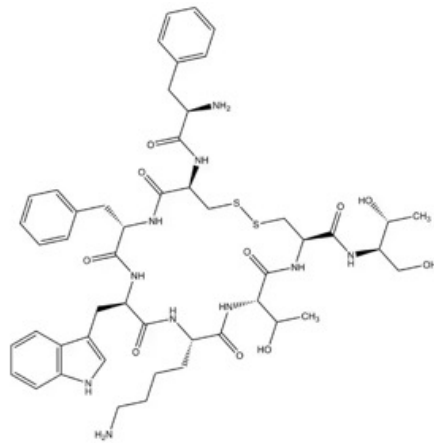


Radiographic Evaluation throughout the Clinical Course.

Initial combined positron-emission tomography with gallium-68-dotatate (Panel A) showed considerable and uniform uptake within the entire pancreas. Magnetic resonance imaging (MRI) of the abdomen performed before transplantation (Panel B) revealed an enlarged pancreas, with the neck measuring approximately 3.4 cm. An MRI of the abdomen obtained 6 months after transplantation (Panel C) showed a reduction in the size of the pancreas, with the neck measuring approximately 1.5 cm.

Laboratory Data.

Variable	Reference Range	Initial Presentation 28 mo before Transplantation	Hospital Admissions before Transplantation			Office Visit 2 wk before Transplantation	After Transplantation		
			21 mo before	12 mo before	3 mo before		2 days after	30 days after	270 days after
Creatinine (mg/dl)	0.7–1.4	0.59	0.61	0.56	0.44	0.49	0.34	0.45	0.74
Hemoglobin (g/dl)	12.5–15.0	5.9	9.4	13.4	13.2	8.8	9.1	8.4	7.6
Platelet count ($\times 10^9$ /liter)	140–400	417	360	290	335	230	154	155	133
International normalized ratio	0.83–1.14	1.29	2.49	1.29	1.34	1.1	1.15	—	—
Albumin (g/dl)	3.2–4.9	3.5	4	4.9	4.6	4.1	3.2	4.1	3.9
Total bilirubin (mg/dl)	0.1–0.9	0.4	0.5	0.7	1.0	0.7	0.4	0.3	0.2
Aspartate aminotransferase (U/liter)	7–35	169	71	158	123	130	77	13	14
Alanine aminotransferase (U/liter)	<30	84	39	86	56	52	148	16	14
Alkaline phosphatase (U/liter)	29–92	188	252	177	119	105	89	81	65
Glucagon (pg/ml)	—	—	>8000†	—	—	—	1576	401	75
Ammonia (μ mol/liter)	—	—	354	189	144	123	—	14	11
Lipase (U/liter)	13–60	464	111	114	94	—	—	—	—
Glutamine (μ mol/liter)	428–747	—	3007	866	—	798	769	—	—
Ornithine (μ mol/liter)	27–83	—	316	246	—	243	220	—	—
Citrulline (μ mol/liter)	16–51	—	177	121	—	103	106	—	—
Arginine (μ mol/liter)	43–107	—	203	400	—	372	377	—	—



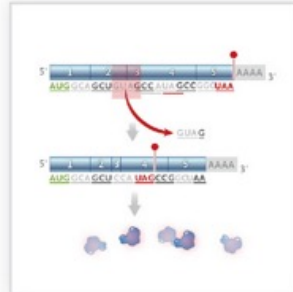
Wirkmechanismus

Octreotid ist ein synthetisches Analogon des natürlichen Hormons **Somatostatin**. Es bindet selektiv an Somatostatin-Rezeptoren, insbesondere an Subtypen 2, 3 und 5. Durch diese Bindung hemmt Octreotid die Freisetzung verschiedener Hormone, einschließlich Wachstumshormon (GH), Glukagon, Insulin, Gastrin, VIP (Vasoaktives intestinales Peptid) und Sekretin.

Octreotide is used in the treatment of Mahvash disease, but because the use of octreotide in this patient led to recurrent hospitalizations, alternative treatments were considered. Unlike previously described persons with Mahvash disease, this patient showed evidence of portal hypertension without cirrhosis — meeting criteria for portosinusoidal vascular disease — accompanied by intractable recurrent portosystemic encephalopathy. Therefore, she was placed on a waiting list for liver transplantation, with Model for End-stage Liver Disease (MELD) exception points because of her genetic diagnosis. (MELD scores determine a patient's ranking on the waiting list for a liver transplant.) The decision to pursue transplantation was based on previous evidence of the efficacy of liver transplantation in other metabolic disorders.

While awaiting transplant, the patient was hospitalized multiple times owing to sequelae of portal hypertension, including episodes of hyperammonemic encephalopathy and hematemesis due to gastric varices. On June 11, 2022 (28 months after the initial presentation), she underwent orthotopic liver transplantation (with a liver from a donor after brain death).

In Mahvash disease, hepatocytes are rendered unresponsive to glucagon, which results in disruption of the feedback loop between the liver and the pancreas that helps regulate glucose and amino-acid metabolism. This disruption stimulates pancreatic α -cell hyperproliferation and causes pancreaticomegaly, overproduction of glucagon, and ultimately development of pancreatic neuroendocrine tumors. As a result, the complications of the disease are primarily pancreatic in nature, and the focus of management of the disease has been the pancreas. Although pancreatectomy has been considered, there remain no firm criteria to indicate the conditions under which to pursue this treatment. In addition, somatostatin analogues have been used to suppress hyperglucagonemia, but the efficacy of this approach is not well known. The benefits of sunitinib, everolimus, and peptide-receptor radionuclide therapy in the treatment of patients with Mahvash-related pancreatic neuroendocrine tumors have not yet been established, although their benefits have been shown in the treatment of other syndromes associated with pancreatic neuroendocrine tumors. Our study underscores the importance of an underlying hepatic pathophysiology in the context of a traditional focus on the pancreatic complications of Mahvash disease. Blocking glucagon signaling results in the downregulation of genes involved in the metabolism of amino acids, leading to hyperaminoacidemia. We hypothesized that an impaired ability of amino acids to enter the liver and undergo ureagenesis results in the secondary impairment of the urea cycle. This leads to an increased nitrogen load and hyperammonemia — to a level beyond that caused by the primary effect of portosystemic shunting — because the extrahepatic metabolism of high levels of circulating glutamine, mediated by glutaminase, generates glutamic acid and ammonia. There was no evidence of a primary urea-cycle defect, since the ratios among ureagenic amino acids (ornithine, citrulline, and arginine) were normal and the pattern of this patient's amino-acid profile is similar to that of a pediatric patient with biallelic *GCGR* mutations.



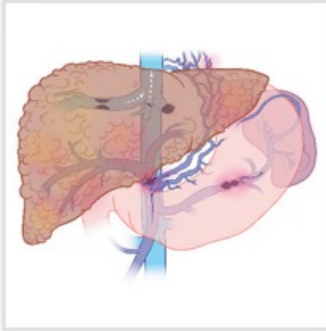
Frameshift mutation

An insertion or a deletion of a number of nucleotides in a gene that is not divisible by three, forcing a shift in the codon reading frame of the gene and transcribed messenger RNA. Frameshift mutations usually result in a premature stop codon and loss of function of the encoded protein product.



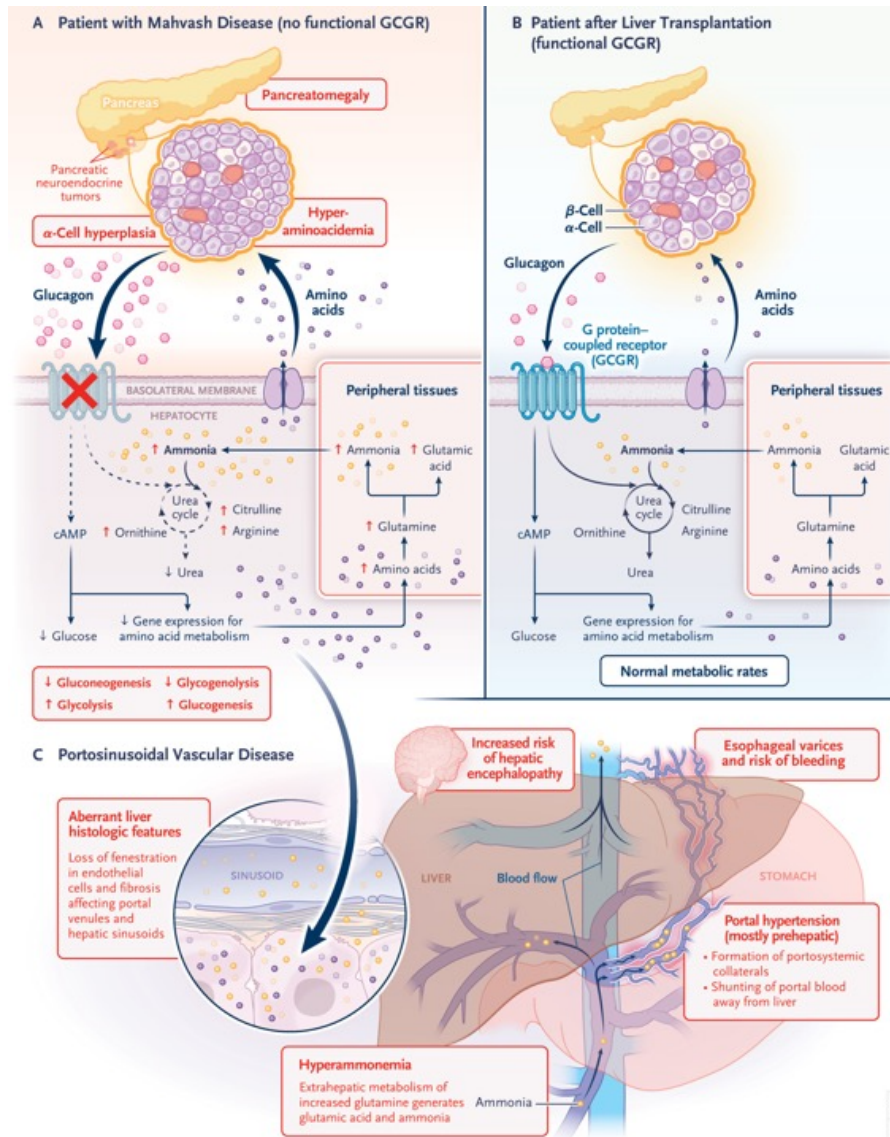
Pancreatic α -cell

An endocrine cell that produces glucagon, the counter-regulatory hormone to insulin for maintenance of glucose homeostasis. Pancreatic α -cells are found in the islets of Langerhans of the pancreas and secrete glucagon in response to hypoglycemia. Glucagon induces release of glucose into the bloodstream from glycogen stores in the liver by activating glycogenolysis and gluconeogenesis. The hepatic–pancreatic α -cell homeostatic axis is disrupted in type 2 diabetes mellitus and liver disease and in ultrarare Mahvash disease due to biallelic variants in the glucagon receptor gene, *GCGR*.



Portal hypertension

An increase in pressure gradient in any segment of the portal venous system. It is classified on the basis of the site of increased vascular resistance: extrahepatic or intrahepatic. Extrahepatic portal hypertension is classified as prehepatic (e.g., portal or splenic vein thrombosis) or posthepatic (e.g., Budd–Chiari syndrome). Intrahepatic portal hypertension is classified as presinusoidal (affecting mainly hepatic portal tracts, as in portal sinusoidal vascular disease), sinusoidal (affecting hepatic sinusoids, as occurs in cirrhosis, the most common cause of portal hypertension), or postsinusoidal (sinusoidal obstruction syndrome). Complications of portal hypertension include varices, variceal hemorrhage, ascites, and encephalopathy, and their development depends on the site of increased resistance, the degree of portal hypertension and portosystemic shunting, and the presence or absence of liver dysfunction.



Therapeutic Transplantation.

A patient with Mahvash disease described by Robbins et al.² had biallelic null variants in GCGR, encoding the glucagon receptor. The defect led to a lack of glucagon receptors in hepatocytes, which triggered hyperaminoacidemia and pancreatic α -cell hyperplasia. Portosinusoidal vascular disease (PSVD) developed, resulting in presinusoidal portal hypertension with formation of varices and recurrent variceal hemorrhage. In addition, the patient had hyperammonemia that was due to the acquired urea-cycle defect caused by lack of GCGR signaling and increased substrate load. Hyperammonemia, combined with portosystemic shunting (as the result of portal hypertension), led to intractable portosystemic encephalopathy. Transplantation of a liver with functional glucagon receptors and healthy vasculature restored glucagon homeostasis and relieved portal hypertension. Glucagon levels decreased, and pancreatic α -cell hyperplasia reversed. The pathologic drivers of PSVD (varices and shunting) were eliminated, and the patient remains free of varices and encephalopathy. The term cAMP denotes cyclic AMP.

Osteoporosis

High bone density

Healthy



Low bone density

Osteoporosis



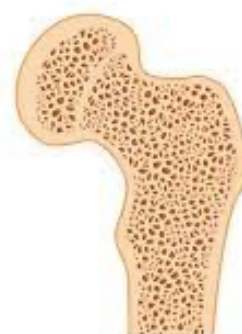
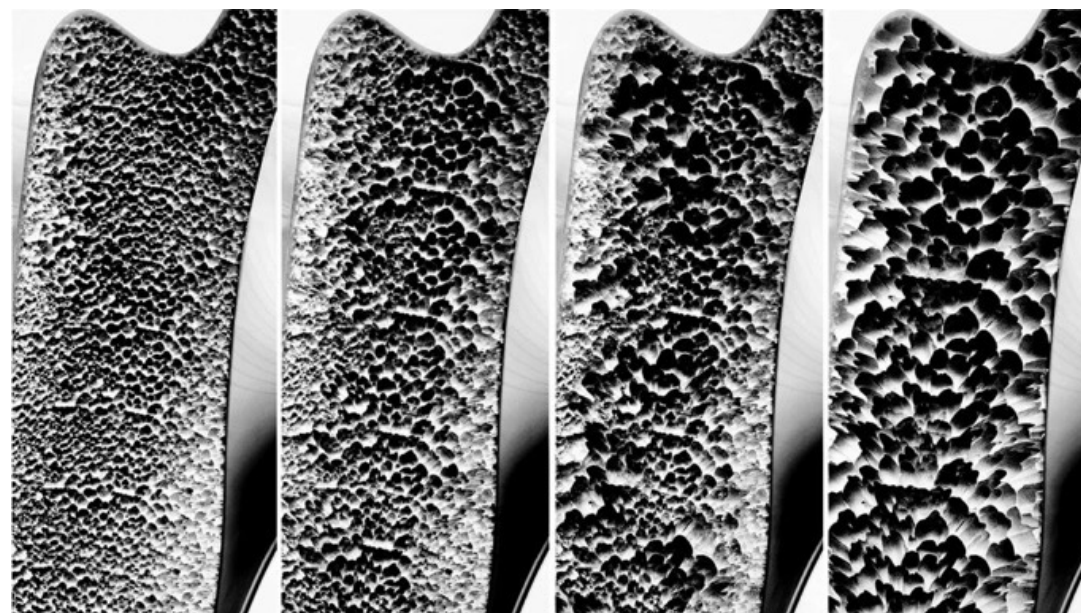
Healthy spine



Spine with
osteoporosis



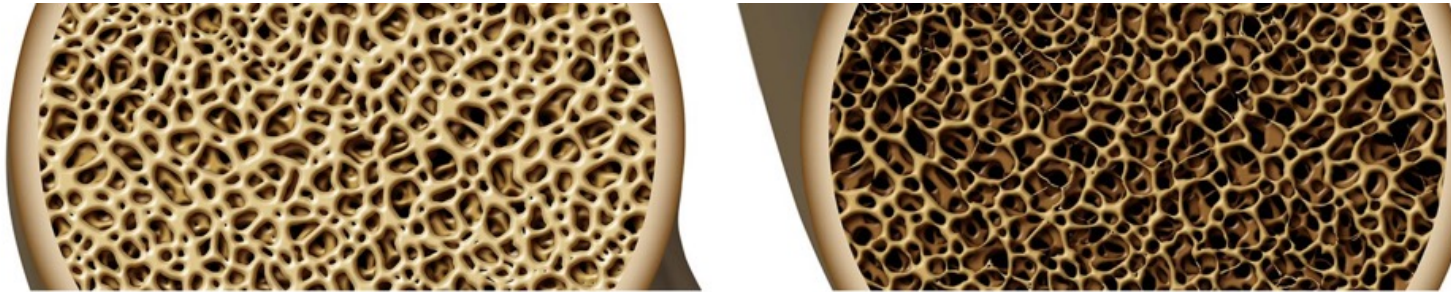
Compression fracture



Healthy bone



Osteoporosis



Die Dual-Röntgen-Absorptiometrie (DXA) ist ein röntgendiagnostisches Verfahren zur Bestimmung der Knochendichte und -masse sowie der Zusammensetzung des gesamten Körpers.

Der sogenannte T-Wert drückt das Meßergebnis in Standardabweichungen (SD) von der peak bone mass eines Referenzkollektivs aus. Demnach gelten Meßwerte, die innerhalb einer Standardabweichung um den Mittelwert streuen als normal; von Osteoporose spricht man bei einer Abweichung um mehr als -2,5 SD vom Mittelwert.

Knochendichte Messung

Früherkennung von Osteoporose

Die Knochendichtemessung ist ein medizinisch-technisches Verfahren, das zur Bestimmung der Dichte bzw. des Kalziumgehaltes des Knochens dient. Bei Menschen mit einem verminderten Kalziumgehalt des Knochens, besteht ein erhöhtes Risiko für einen Knochenbruch.

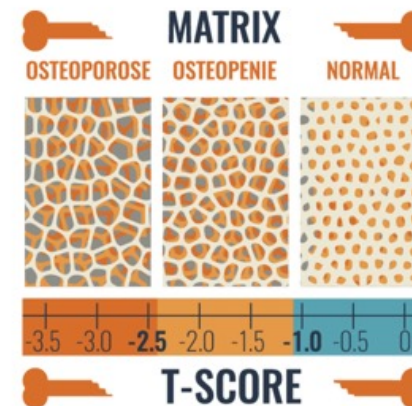
Risikogruppen sind vor allem:

- Frauen in der Postmenopause
- Frauen über 50 Jahre
- Raucher
- Alkoholiker
- Menschen mit Mangelernährung und daraus resultierendem Vitaminmangel
- Hyperthyreose
- Regelmäßige Cortisoneinnahme

Der anerkannte Goldstandard ist die DXA-Messung (Knochendichtemessung).

Hier wird mit einem modernen Spezialgerät ein Schenkelhals und die Lendenwirbelsäule geringer Röntgenstrahlung ausgesetzt und die durchtretende Strahlenmenge gemessen.

Die Messwerte werden anhand von Tabellen mit den Normalwerten der Altersgruppe verglichen und so eine Beurteilung ermöglicht. Eine weitere Untersuchungsmöglichkeit der Knochendichte ist die quantitative Computertomographie. Bei dieser Untersuchung wird, ebenfalls mit einer in diesem Fall allerdings höheren Strahlung gemessen, allerdings lediglich an einem einzelnen Wirbelkörper. Diese Methode eignet sich vor allem zum Screening, also für eine grobe Voruntersuchung, da sie nicht sehr genau ist und vor allem nicht die bei der Osteoporose wichtigen Regionen untersucht (Wirbelsäule und Schenkelhals).



Postmenopausal Osteoporosis

A 69-year-old woman presents to review the results of her first dual-energy x-ray absorptiometry (DXA) scan. Her T scores are -2.6 at the lumbar spine and -2.3 at the total hip. She fell while walking 18 months ago and fractured her left humerus. Imaging of the spine, performed to investigate 5 cm (2 in.) of height loss and moderate thoracic kyphosis, reveals two vertebral fractures. How should this patient be evaluated and treated?

Postmenopausal osteoporosis is caused by estrogen deficiency, which leads to increased osteoclast differentiation and activation, accelerated bone resorption that outpaces formation, and rapid bone loss, particularly in the years immediately before and after menopause. This results in low bone mineral density, deteriorated bone microarchitecture, decreased bone strength, and increased risk of fragility fractures. Postmenopausal osteoporosis is diagnosed on the basis of the occurrence of a fragility fracture (with no associated trauma or with trauma equivalent to falling from a standing height or less) or bone mineral density at the spine, total hip, or femoral neck that is at least 2.5 standard deviations below the mean of that in a young adult reference population (T score of -2.5 or less), as measured with the use of DXA. In the United States, approximately 20% of women over 50 years of age and 30% of women 65 years of age or older meet DXA criteria for osteoporosis. In the United States, osteoporosis is more common among White, Asian, and Hispanic women than among non-Hispanic Black women. An additional 40% of postmenopausal women have low bone mass (osteopenia; defined as a T score between -1.0 and -2.49). Approximately 50% of postmenopausal women will have fragility fractures, which cause pain, disability, and decreased quality of life. After a hip fracture, many women never regain independence, 20% are institutionalized, and the risk of death within 1 year doubles.

KEY CLINICAL POINTS

Postmenopausal Osteoporosis

- Fragility fractures are very common among postmenopausal women and are associated with increased morbidity, mortality, and health care expenditures.
- Dual-energy x-ray absorptiometry (DXA) is recommended in postmenopausal women 65 years of age or older and postmenopausal women younger than 65 years of age who have risk factors.
- Osteoporosis is diagnosed on the basis of a fragility fracture or a DXA T score of -2.5 or less.
- Treatment of postmenopausal osteoporosis is recommended for patients who have any of the following findings: a fragility fracture (or fractures), particularly of the hip or spine, regardless of the patient's bone mineral density; a T score of -2.5 or less at the lumbar spine, total hip, or femoral neck; or a high 10-year fracture risk (hip fracture risk of $\geq 3\%$ or major osteoporotic fracture risk of $\geq 20\%$) according to the fracture risk assessment tool (FRAX).
- Evaluation should include risk stratification (based on the T score, presence of fractures, and FRAX score) to categorize candidates who meet treatment thresholds as “high risk” or “very high risk.”
- The selection of therapy must include consideration of coexisting conditions and contraindications, but anabolic agents are the preferred first line of treatment in women at very high risk.

Risk Factors for Postmenopausal Osteoporosis and Fracture.

Older age

Low weight (<127 lb [<58 kg])

Previous fracture during adulthood (particularly hip, spine, or wrist); recent fracture indicates a higher risk than remote or unclear history

Parental history of hip fracture

Current or past glucocorticoid treatment (>5 mg prednisolone daily or equivalent for 3 mo or more)

Other medications that cause bone loss*

Current smoking

Excess alcohol intake

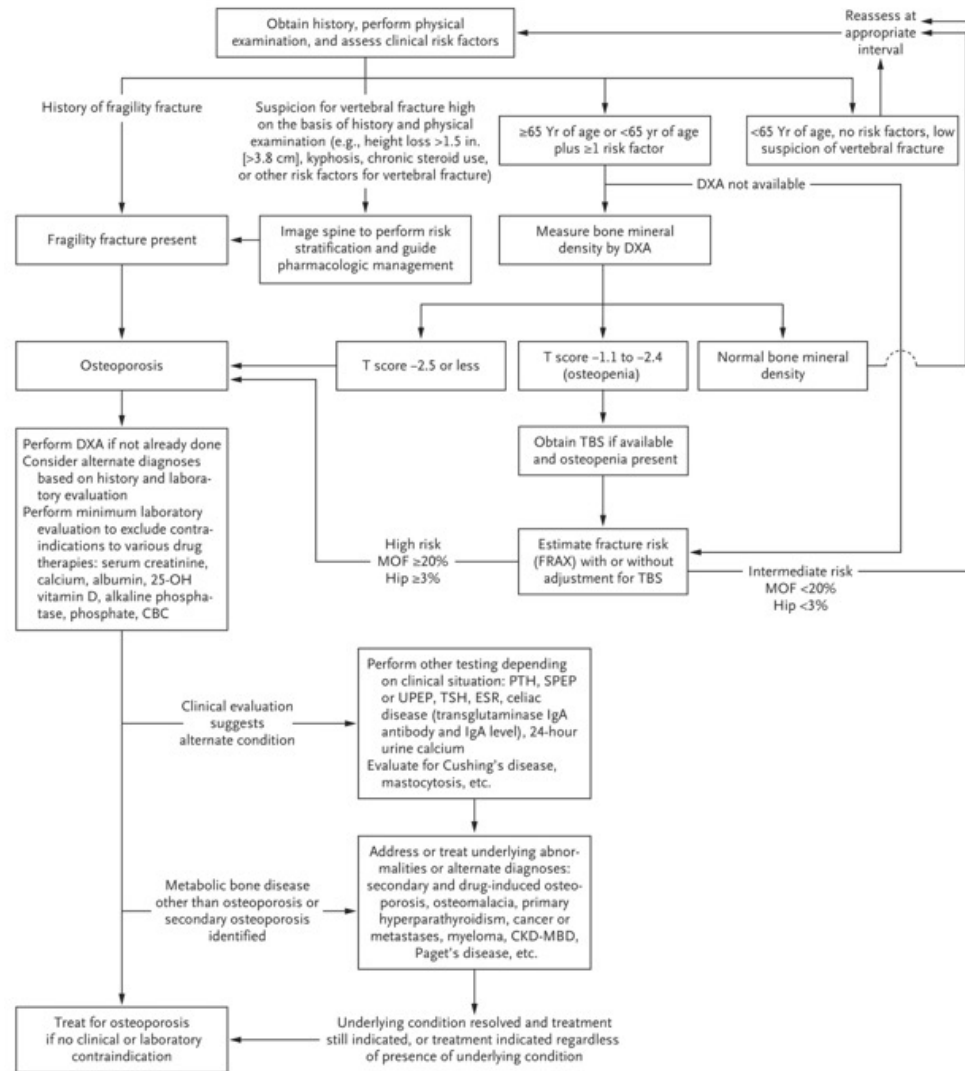
Causes of secondary osteoporosis†

Rheumatoid arthritis

Premature menopause (<40 yr of age) or hypogonadism

Frequent falls

Diagnostic Algorithm for the Evaluation of Postmenopausal Osteoporosis.



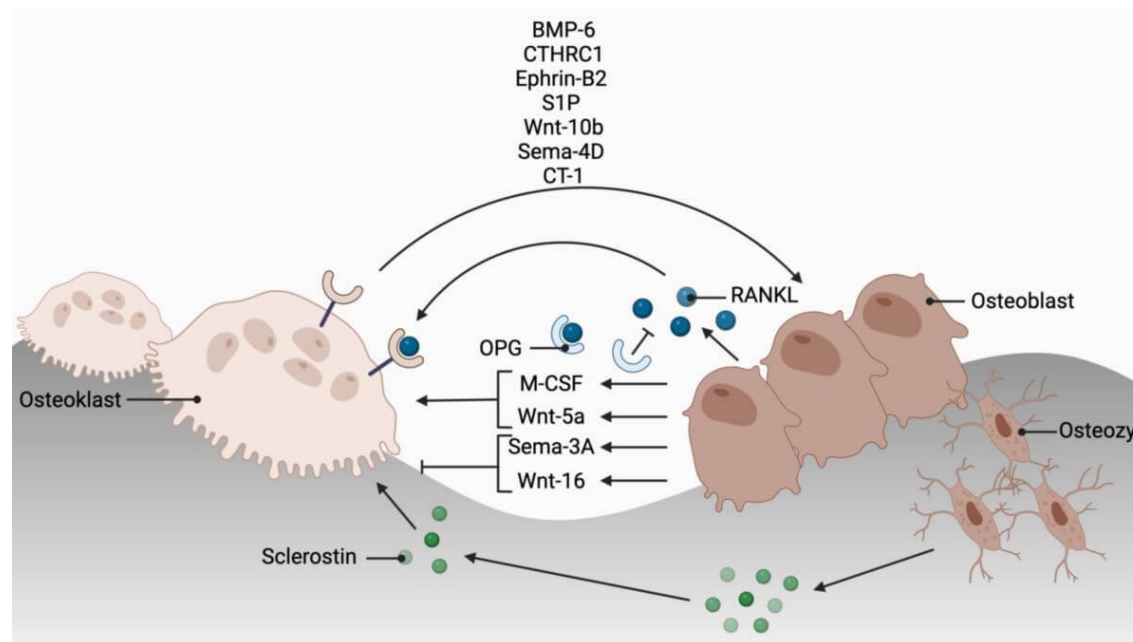
The evaluation of skeletal health in postmenopausal women starts with a history focusing on previous fractures and clinical risk factors for osteoporosis and fractures. A physical examination should evaluate for significant kyphosis and height loss, which if present should prompt imaging of the spine. A fragility fracture (particularly of the spine, hip, wrist, humerus, or pelvis) is diagnostic of osteoporosis. Women 65 years of age or older, regardless of other risk factors, and women younger than 65 years of age who have risk factors for bone loss or fractures should undergo dual-energy x-ray absorptiometry (DXA) screening. The timing of spine imaging may occur before, coincident with, or after DXA. If software is available to assess a trabecular bone score (TBS), the score can be obtained with a measurement of bone mineral density for fracture risk stratification in women with low bone mass (osteopenia). A T score of -2.5 or less is consistent with osteoporosis. T scores of -1.0 to -2.49 are consistent with osteopenia or low bone mass. The fracture risk assessment tool (FRAX) can be used with or without DXA and TBS to estimate a 10-year probability of major osteoporotic fracture (MOF) and hip fracture. MOF risk of 20% or more or hip fracture risk of 3% or more is consistent with osteoporosis in the absence of a fragility fracture even if the T score is above -2.5 . DXA can be obtained in women with a fragility fracture and used to monitor effectiveness of treatment but is not necessary for diagnosis. Laboratory evaluation should exclude contraindications to treatments. Additional laboratory evaluations and studies may be appropriate depending on the clinical situation; a complete blood count (CBC) should be performed to evaluate for myeloma, if results are not already available. Alternative diagnoses (e.g., drug-induced osteoporosis, osteomalacia, primary hyperparathyroidism, cancer, and chronic kidney disease—mineral and bone disorder [CKD-MBD]) should be considered and addressed on the basis of clinical and laboratory information. Treatment of postmenopausal osteoporosis should be initiated if there are no contraindications. 25 OH vitamin D denotes 25-hydroxyvitamin D, ESR erythrocyte sedimentation rate, PTH parathyroid hormone, SPEP serum protein electrophoresis, TSH thyrotropin, and UPEP urine protein electrophoresis.

Pharmacologic Therapies for Postmenopausal Osteoporosis.

Drug Class and Medication	Mechanism of Action	Treatment Dose	Fracture Risk Reduction ^{17,18†}			Adverse Effects	Contraindications and Warnings
			Vertebral	Hip	Non-vertebral		
			percent				
Antiresorptives							
Bisphosphonates	Bind to bone hydroxyapatite, engulfed by osteoclasts, and inhibit bone resorption						
Alendronate‡		10 mg once daily or 70 mg once weekly orally	44	40	17	GI irritation, MSK pain; rarely ONJ, AFF ^{19‡}	Esophageal varices or dysmotility, creatinine clearance <30–35 ml per min, hypocalcemia, bisphosphonate allergy
Risedronate‡		5 mg daily, 35 mg weekly, or 150 mg monthly orally	36	26	20	Same as for alendronate	Same as for alendronate
Ibandronate‡¶		2.5 mg daily or 150 mg monthly orally, or 3 mg every 3 mo IV	31	ND	ND	Same as for alendronate	Same as for alendronate
Zoledronic acid¶		5 mg per yr IV	56	42	18	Acute-phase reaction, renal impairment, hypocalcemia, atrial fibrillation, rarely ONJ and AFF ^{19¶}	Creatinine clearance <35 ml per min, AKI, hypocalcemia, bisphosphonate allergy; important to ensure vitamin D sufficiency
RANK ligand inhibitor — denosumab	Human monoclonal antibody that binds RANKL; inhibits osteoclast formation, function, and survival	60 mg every 6 mo subcutaneously	68	40	20	MSK pain, skin infections, rashes, hypocalcemia, rarely ONJ and AFF ¹⁹ ; rebound bone loss and fractures after stopping	Hypocalcemia, hypersensitivity; important to ensure vitamin D sufficiency
Estrogens — CEE‡	Decreases osteoclastic bone resorption	0.625 mg daily orally	34	29	21	CEE alone: stroke; CEE plus medroxyprogesterone: stroke, CHD, breast cancer, dementia, thromboembolic events	History of breast cancer, CHD, VTE, stroke, TIA; active liver disease; unexplained vaginal bleeding; increased risk of endometrial cancer
SERMs (e.g., raloxifene) ^{*,¶}	Weak estrogen agonist activity in bone, decreases osteoclastic bone resorption	Raloxifene 60 mg daily orally	40	ND	ND	VTE, hot flashes, night sweats, peripheral edema, leg cramps, increased risk of death from stroke	History of VTE, PE, retinal vein thrombosis
Anabolic agents, PTH receptor agonists							
PTH analogue — teriparatide (PTH 1-34)	Increases bone formation	20 µg daily subcutaneously	74	ND	39	Hypercalcemia, muscle cramps, nausea, headache, dizziness, hypotension	Bone metastases, skeletal cancers, history of skeletal radiation, increased risk of osteosarcoma, Paget's disease, hypercalcemic disorders, unexplained elevated alkaline phosphatase, hypersensitivity
PTH-rP analogue — abaloparatide (PTHrP 1-34)	Increases bone formation	80 µg daily subcutaneously	87	ND	46	Same as for teriparatide (PTH 1-34)	Same as for teriparatide (PTH 1-34)
Anabolic-antiresorptive agent							
Sclerostin inhibitor — romosozumab	Human monoclonal antibody against sclerostin; increases bone formation, decreases bone resorption	210 mg per mo subcutaneously	73	38††	19††	Arthralgia, headache, MSK pain, hypocalcemia, CV events; rarely ONJ, AFF	Recent stroke or MI; other CV risks, hypocalcemia, or hypersensitivity; important to ensure vitamin D sufficiency

Receptor Activator of NF- κ B Ligand - RANK-Ligand ist der wichtigste Faktor für die Bildung, Funktion und das **Überleben von Osteoklasten**, die für den kontinuierlichen Knochenumbau verantwortlich sind. Indem RANKL an RANK auf unreifen und reifen Osteoklasten bindet, fördert er die Osteoklastogenese und die Aktivität der reifen Zellen.

Sclerostin ist ein Glykoprotein, das **die Osteogenese hemmt** und in Abhängigkeit von der mechanischen Belastung des Knochens sezerniert wird. Je geringer die Belastung, desto höher die Sclerostinsekretion. Dies erklärt den zunehmenden Schwund der Knochenmasse bei langer Inaktivität (z.B. bei Bettlägerigkeit).



Intervention and Treatment Guidelines.

Guideline	Intervention Threshold	Initial Treatment		Duration
		High Risk of Fracture	Very High Risk of Fracture†	
AACE–ACE 2020 ¹¹	T score of ≤ -2.5 or less at the spine, femoral neck, total hip, or 33% radius; osteopenia (T score, -1.00 to -2.49) and history of fragility fracture of the hip or spine; osteopenia and high probability of fracture as estimated with the use of FRAX	Alendronate, denosumab, risedronate, zoledronate‡; ibandronate or raloxifene are alternatives for spine-specific therapy only ²²	Abaloparatide, denosumab, romosozumab, teriparatide, zoledronate‡; alternate therapy is alendronate and risedronate	Oral bisphosphonates ²² — treat for 5 yr, then consider holiday if fracture risk is no longer high; if fracture risk remains high, continue treatment for up to an additional 5 yr; in patients at very high risk, consider holiday after 6–10 yr of stable BMD; zoledronic acid ²² — consider holiday after 3 yr of high risk or until fracture risk is no longer high, continue for 6 years in patients at very high risk; holiday not recommended for non-bisphosphonate antiresorptive therapies; abaloparatide or teriparatide — treat for 2 yr, then follow with antiresorptives; romosozumab — treat for 1 yr, then follow with antiresorptives ²²
American College of Physicians 2023 ¹⁰	T score of ≤ -2.5 or less; individualize in those >65 yr of age with osteopenia	Bisphosphonates; denosumab if contraindications to or adverse effects from bisphosphonates	Teriparatide or romosozumab followed by antiresorptives‡	Bisphosphonate use for >3 –5 yr reduces vertebral fracture but not other fractures, with increased risk of long-term harms; consider stopping after 5 yr unless strong indication to continue
Bone Health and Osteoporosis Foundation ⁴	T score of ≤ -2.5 or less at the femoral neck, total hip, lumbar spine, 33% radius¶; fracture of the hip or vertebra regardless of BMD by DXA; osteopenia at the femoral neck or total hip by DXA with 10-yr hip fracture risk $\geq 3\%$ or MOF risk $\geq 20\%$ by FRAX; osteopenia with fracture of proximal humerus, pelvis, or distal forearm; individualized approach for those with proximal humerus, pelvis, or distal forearm fractures without osteopenia	Generally follows Endocrine Society algorithm	Generally follows Endocrine Society algorithm	Oral and IV bisphosphonates — treat for 5 yr and 3 yr respectively; with modest risk of fracture (e.g., T score greater than -2.5 and no recent fracture), consider holiday; for patients who remain at high fracture risk (e.g., T score of ≤ -2.5 or less or recent fracture or both), consider alternative treatment or continued treatment with a bisphosphonate for ≤ 10 yr (oral) or ≤ 6 yr (annual IV zoledronic acid) ²²
Endocrine Society 2019–2020 ^{23,24}	Postmenopausal women at high risk of fractures, especially those with a recent fracture	Bisphosphonates‡; alternative therapy is denosumab; SERMs, ET, and calcitonin recommended in specific groups only ^{24*}	Teriparatide or abaloparatide; romosozumab if not at high CV risk	Bisphosphonates — reassess fracture risk in 3 yr (IV) or 5 yr (oral); if high risk, continue therapy or begin alternative therapy; if low to moderate risk, consider holiday up to 5 yr but reassess every 2–4 yr ^{23††} ; denosumab — reassess fracture risk after 5–10 yr; women remaining at high risk should continue denosumab or be treated with other therapies; abaloparatide or teriparatide — treat for 2 yr, then follow with antiresorptives; romosozumab — treat for 1 yr, then follow with antiresorptives
ESCEO and IOF ⁹	Women >65 yr of age with a previous fragility fracture and those without a previous fracture who have an age-specific probability of fragility fracture that is equal to that of women with a previous fragility fracture‡‡	Oral bisphosphonates; IV bisphosphonates or denosumab are the most appropriate alternatives with contraindications to or adverse effects from oral bisphosphonates; raloxifene and HRT are also options	Teriparatide is preferentially recommended	Bisphosphonate treatment should be reviewed after 3–5 yr; bisphosphonates should be used after discontinuation of denosumab; little evidence to guide decision making beyond 10 yr; treatment decisions should be individualized

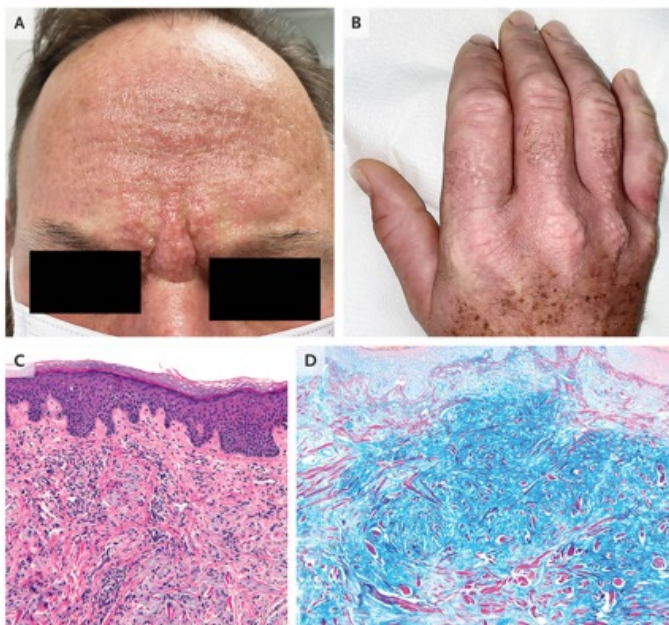
Guidelines

Guidelines for diagnosis and management of postmenopausal osteoporosis vary with respect to the threshold for starting therapy and the choice and duration of treatment. Our recommendations are generally consistent with the guidelines of the Endocrine Society and the Bone Health and Osteoporosis Foundation.

Conclusions and Recommendations

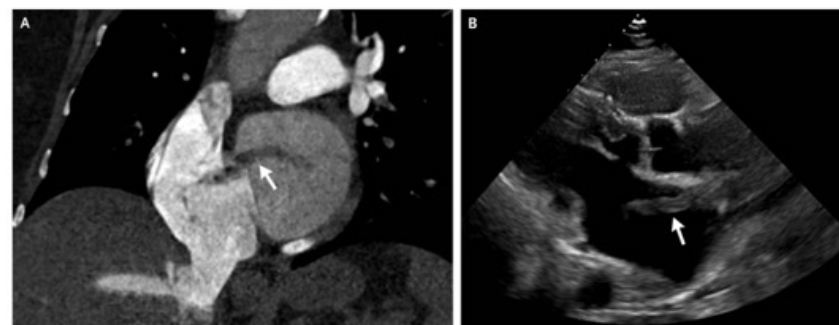
The presentation of the patient described in the vignette is typical of postmenopausal osteoporosis in that the initial humerus fracture was not recognized as indicating osteoporosis, which was later diagnosed by the T score of -2.6 and prevalent vertebral fractures. History and laboratory testing should identify modifiable risk factors, medications, and underlying conditions affecting fracture risk and therapy decisions. The patient's multiple fragility fractures indicate a very high risk of additional fractures. Therefore, we favor therapy with anabolic agents first with either a PTH receptor agonist or romosozumab followed by treatment with a bisphosphonate or denosumab. If anabolic therapy was declined, we would favor denosumab over bisphosphonates, given her severe osteoporosis and the greater effects of denosumab on bone mineral density. Despite the debated utility of repeat DXA, we would reevaluate clinically and reassess bone mineral density with DXA 1 or 2 years after initiating therapy.

Scleromyxedema



A 53-year-old man presented to the rheumatology clinic with a 3-year history of an itchy rash, Raynaud's phenomenon, dysphagia, and a burning sensation in his hands. Physical examination was notable for firm, greasy papules across his forehead that led to the formation of glabellar grooves (Panel A). There were waxy papules on his hands, with associated skin thickening and finger flexion contractures (Panel B). Similar skin changes were seen on his nose, lips, ears, trunk, and feet. There was no telangiectasia or calcinosis. Sensory neuropathy was present in his hands, arms, and face. Tests of thyroid function were normal. Serum protein electrophoresis with immunofixation identified an IgG- λ monoclonal gammopathy, and a bone marrow biopsy was normal. A subsequent skin-biopsy sample obtained from the right side of the neck showed dermal spindle-cell proliferation, thickened collagen fibers, fibrosis, and perivascular inflammation (Panel C, hematoxylin and eosin stain), as well as increased dermal mucin deposition (Panel D, colloidal iron stain). A diagnosis of scleromyxedema was made. Scleromyxedema is a primary cutaneous mucinosis typically associated with a paraproteinemia. This type of sclerosing skin disorder may cause extracutaneous symptoms, as was seen in this patient. Although infusions of intravenous immune globulin provided minimal relief initially, treatment with lenalidomide resulted in abatement of symptoms and reduction in paraproteinemia after 4 months.

Thrombus in Transit across a Patent Foramen Ovale



Hypoxemia and shock developed suddenly in a 67-year-old woman with atrial fibrillation who had been admitted to the hospital for management of an acute ischemic stroke. She had stopped taking apixaban 2 days before a colon polypectomy that had been performed 3 days before the current admission. At the

current presentation, her heart rate was 118 beats per minute, blood pressure 70/36 mm Hg, and oxygen saturation 72% while she was breathing ambient air. After her condition was stabilized, a computed tomographic pulmonary angiogram was obtained. It showed pulmonary emboli in the main pulmonary arteries, right ventricular dilatation, and a large thrombus in transit through a previously unknown patent foramen ovale (PFO; Panel A, arrow). A subsequent transthoracic echocardiogram showed a thrombus crossing through the PFO into the left atrium (Panel B, arrow, and [Video 1](#) [parasternal long-axis view] and [Video 2](#) [parasternal short-axis view]). Advanced interventional therapies were deemed by a multidisciplinary team to be too high risk. Treatment with heparin was initiated. Four days later, new cerebellar infarcts (thought to be cardioembolic from the thrombus) developed, along with hemorrhagic transformation of the left middle cerebral artery infarct that had been present on admission. Therapeutic anticoagulation was stopped to allow for stabilization of the intracranial hemorrhage. On hospital day 20, therapeutic anticoagulation was restarted, and the patient was discharged to a stroke rehabilitation facility 15 weeks after admission.

Video



Transthoracic Echocardiography. (00:22)

A 19-Year-Old Man with Diabetes and Kidney Cysts

A 19-year-old man was evaluated in the nephrology clinic of this hospital because of kidney cysts. The patient had been well until 3 years before the current presentation, when diffuse abdominal pain, nausea, vomiting, and increased urinary frequency developed. The patient's mother brought him to the emergency department of this hospital for evaluation. In the emergency department, the patient reported that he woke up 3 or 4 times each night to urinate. He also had weight loss, decreased appetite, and increased thirst. The temporal temperature was 36.9°C, the blood pressure 123/70 mm Hg, and the heart rate 65 beats per minute. The weight was 51.3 kg, the height 165 cm, and the body-mass index (BMI; the weight in kilograms divided by the square of the height in meters) 18.8. The patient had dry skin; the remainder of the examination was normal. The blood glucose level was 780 mg per deciliter (43.3 mmol per liter; reference range, 70 to 110 mg per deciliter [3.9 to 6.1 mmol per liter]), and the glycated hemoglobin level was 12.9% (reference range, 4.3 to 5.6). The blood creatinine level was 1.45 mg per deciliter (128 μmol per liter; reference range, 0.60 to 1.50 mg per deciliter [53 to 133 μmol per liter]).

Variable	Reference Range, This Hospital†	3 Yr before This Evaluation, Emergency Department	1 Yr before This Evaluation, Gastroenterology Clinic	1 Wk before This Evaluation, Gastroenterology Clinic
White-cell count (per μl)	4500–13,000	—	4280	5030
Hemoglobin (g/dl)	13.0–16.0	—	12.8	13.9
Hematocrit (%)	37.0–49.0	—	39.3	42.7
Platelet count (per μl)	150,000–400,000	—	144,000	161,000
Sodium (mmol/liter)	135–145	126	135	135
Potassium (mmol/liter)	3.4–5.0	4.1	3.8	4.0
Chloride (mmol/liter)	98–108	79	97	93
Carbon dioxide (mmol/liter)	23–32	31	28	28
Urea nitrogen (mg/dl)	8–25	28	13	21
Creatinine (mg/dl)	0.60–1.50	1.45	1.11	1.26
Estimated glomerular filtration rate (ml/min/1.73 m ²)	>59	—	—	84
Glucose (mg/dl)	70–110	780	338	345
Magnesium (mg/dl)	1.7–2.4	1.9	—	1.6
Phosphorus (mg/dl)	3.0–4.5	3.8	—	—
Calcium (mg/dl)	8.5–10.5	10.9	10.1	10.5
Aspartate aminotransferase (U/liter)	10–40	—	87	118
Alanine aminotransferase (U/liter)	10–55	—	158	158
Alkaline phosphatase (U/liter)	55–149	—	468	484
Total bilirubin (mg/dl)	0.0–1.0	—	0.7	1.0
γ-Glutamyltransferase (U/liter)	8–61	—	1158	1912
Albumin (g/dl)	3.3–5.0	—	4.2	4.4
Osmolality (mOsm/kg)	280–296	313	—	—
β-Hydroxybutyrate (mmol/liter)	0.0–0.4	2.1	—	—
C peptide (ng/ml)	1.1–4.4	1.3	—	—
Glycated hemoglobin (%)	4.3–5.6	12.9	—	12.7
Venous blood gases				
pH	7.30–7.40	7.40	—	—
Partial pressure of carbon dioxide (mm Hg)	38–50	54	—	—
Partial pressure of oxygen (mm Hg)	35–50	70	—	—

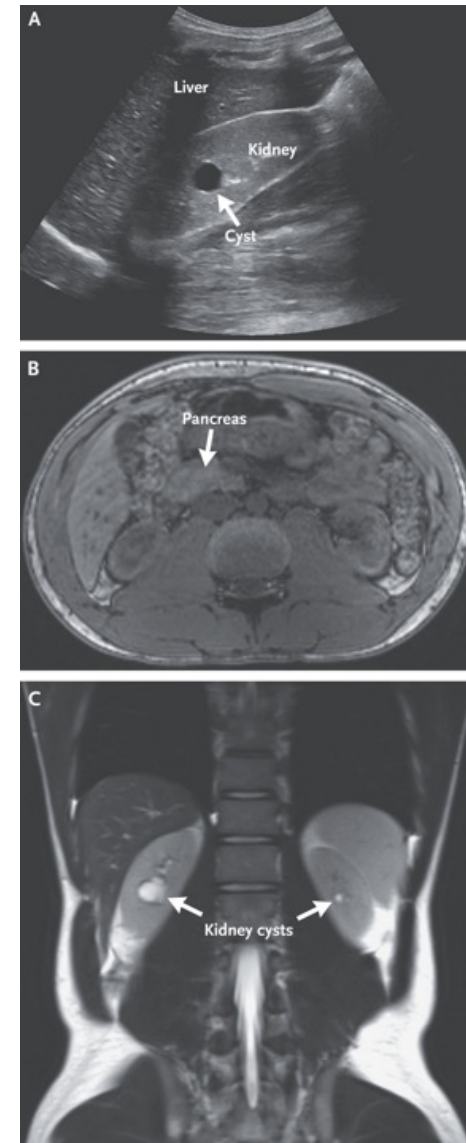
He received insulin and was sent home.

During the subsequent 2 years, the patient continued treatment with insulin. Tests for glutamic acid decarboxylase 65 (GAD65), islet antigen 2 (IA-2), and insulin autoantibodies were negative. One year before the current presentation, the patient was referred to the gastroenterology clinic of this hospital because of elevated levels of aspartate aminotransferase (AST), alanine aminotransferase (ALT), and alkaline phosphatase (ALP) obtained by his primary care provider as part of an annual physical examination.

In the gastroenterology clinic, the patient reported no symptoms, and the examination was normal. The blood AST level was 87 U per liter (reference range, 10 to 40), the ALT level 158 U per liter (reference range, 10 to 55), the ALP level 468 U per liter (reference range, 55 to 149), and the γ -glutamyltransferase (GGT) level 1158 U per liter (reference range, 8 to 61).

Imaging Studies.

An ultrasound image of the right upper quadrant (Panel A) shows a simple cyst (arrow) in the right kidney. An axial T1-weighted image from magnetic resonance cholangiopancreatography (MRCP) (Panel B) shows a small pancreatic head (arrow) and the absence of the pancreatic body and tail. A coronal T2-weighted MRCP image (Panel C) shows bilateral simple kidney cysts (arrows).



In the nephrology clinic, the patient reported that he felt well. He had had normal growth and development and had received all routine childhood vaccinations. Medications included insulin degludec and insulin lispro. There were no known drug allergies. He was a senior in high school and worked part-time at a restaurant. He lived in an apartment in a suburban area of New England with his mother and three siblings. He did not smoke cigarettes, drink alcohol, or use illicit drugs. His father had prediabetes, obesity, and hypertension; his mother and three siblings were healthy. His paternal grandfather, maternal grandfather, and maternal great-grandfather had diabetes. The blood pressure was 124/66 mm Hg and the heart rate 76 beats per minute. The weight was 65.5 kg, the height 176 cm, and the BMI 21.2. The examination was normal. Analysis of a freshly voided urine specimen revealed 1+ proteinuria, 2+ glucosuria, and trace ketonuria. Microscopic examination showed one mixed granular cast per low-power field and scattered squamous epithelial cells. Imaging studies were obtained.

Differential Diagnosis

Diabetes in Adolescence

When the patient was 16 years of age, he presented with symptomatic hyperglycemia and an elevated blood glycated hemoglobin level, findings that met the diagnostic criteria for diabetes mellitus. Diabetes classification depends on the patient's clinical and laboratory features at presentation, and such classification informs options for therapy.

Persistently Abnormal Results of Liver-Function Tests

Two years after the diagnosis of diabetes was established, abnormal results of liver-function tests were detected as part of a routine annual physical examination. The patient was asymptomatic, and MRCP showed a normal-appearing liver, biliary system, and spleen. One year later, the abnormal test results persisted, and MRCP findings were unchanged.

Autosomal Dominant Polycystic Kidney Disease

ADPKD is the most common genetic cause of chronic kidney disease in adults worldwide. In most cases, the disease is due to mutations in the gene encoding polycystin 1 or 2 (*PKD1* or *PKD2*). Patients typically have a family history of kidney disease, and kidney failure often develops during adulthood.

Autosomal Recessive Polycystic Kidney Disease

ARPKD is a severe pediatric cystic kidney disorder with hepatic involvement and marked phenotypic variability. It is most often caused by mutations in the gene encoding fibrocystin (*PKHD1*). Patients typically present during the neonatal period or early childhood with progressive, severe bilateral cystic kidney disease with kidney enlargement.

Nephronophthisis

Nephronophthisis is a genetically heterogeneous autosomal recessive disease and one of the most common genetic causes of chronic kidney disease in children, adolescents, and young adults. To date, approximately 90 single-gene disorders have been associated with this condition.

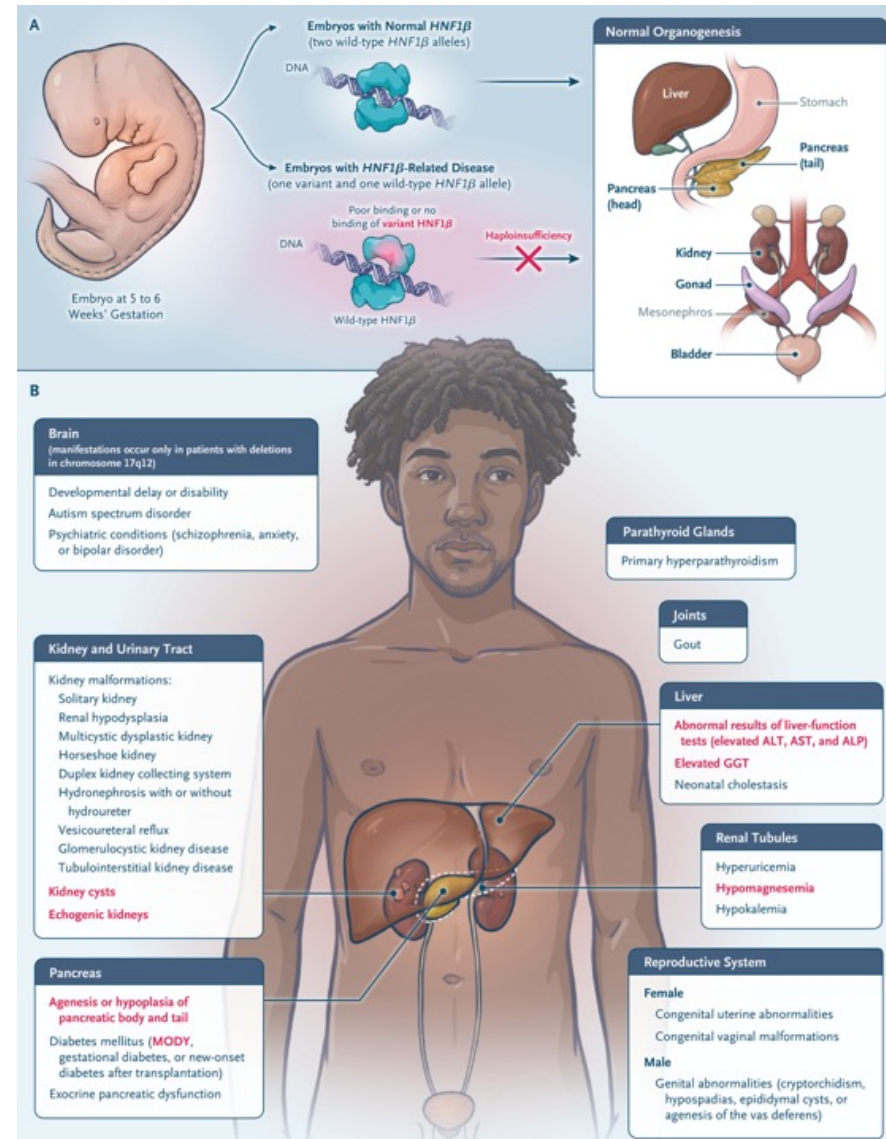
***HNF1B*-Related Disease**

The final systemic disease to consider in relation to cystic kidney disease is *HNF1B*-related disease consistent with RCAD spectrum disorder. This autosomal dominant disorder has substantial phenotypic heterogeneity. The renal cysts and diabetes phenotype can vary considerably among persons carrying the same *HNF1B* mutation, even among members of the same family. *HNF1B* is a transcription factor that plays a role in the development of multiple organ systems, including the kidneys, liver, and pancreas. Consequently, *HNF1B*-related disease can manifest as a multisystemic disease affecting multiple organs, or it can manifest as an isolated kidney or urinary tract malformation.

HNF1B mutations or deletions are the most common genetic cause of CAKUT.

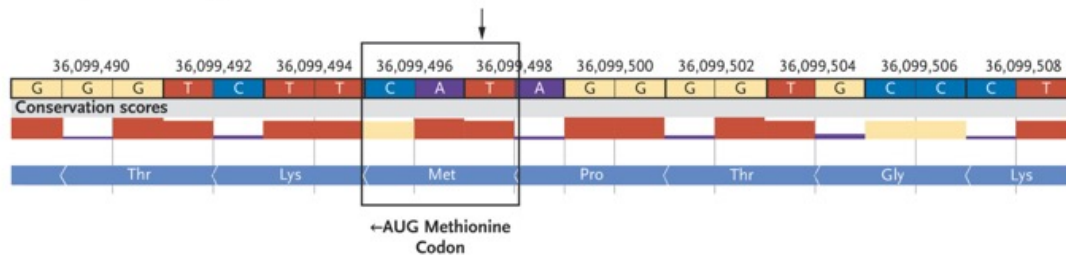
Manifestations of *HNF1B*-Related Disease.

Mutations in the gene encoding the transcription factor hepatocyte nuclear factor 1 β (*HNF1B*) are known to cause disease. *HNF1B* is a developmental gene expressed in utero that can alter the expression of other downstream targets, affecting the development of multiple organ systems, including the kidneys, liver, and pancreas (Panel A). *HNF1B*-related disease can manifest heterogeneously (Panel B). Features seen in this patient are shown in red. Not included in the figure is chromophobe renal-cell carcinoma; case reports have shown the occurrence of this disease in association with *HNF1B* loss. ALP denotes alkaline phosphatase, ALT alanine aminotransferase, AST aspartate aminotransferase, GGT γ -glutamyltransferase, and MODY maturity-onset diabetes of the young.



Genetics of *HNF1B*-Related Disease.

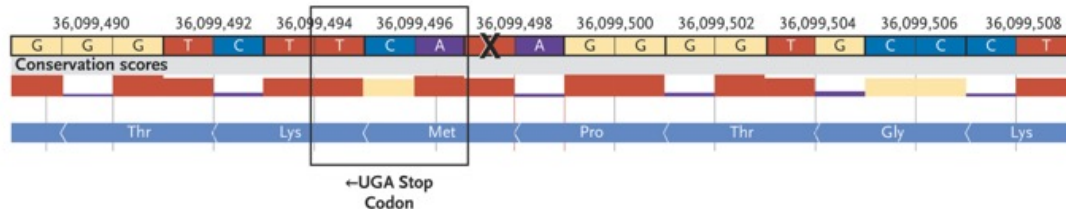
A *HNF1B* Sequence Containing the Patient's Variant



B Exon and Intron Structure of the *HNF1B* Sequence



C Replacement of the AUG Methionine Codon



D Truncation of the mRNA Message

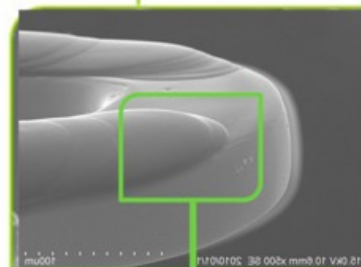


Shown is the reference sequence for the segment of *HNF1B* that contains the variant detected in this patient, as depicted in VarSome (Panel A). The reference thymine (T) nucleotide (arrow) is part of a CAT trinucleotide sequence that, when transcribed from the reverse mRNA strand, becomes an AUG codon encoding methionine in the reference sequence. The exon and intron structure of the *HNF1B* reference sequence for the *HNF1B* transcript NM_000458.4 is also shown (Panel B). The patient's variant — NM_000458.4:c.477del (p.Met160*) — results in the deletion of a single base (T) in the DNA that encodes the mRNA message encoding the *HNF1B* protein. This deletion results in a shift in the reading frame of the message encoding the *HNF1B* protein, causing the replacement of the AUG methionine codon at amino acid residue 160 (of 557 total residues) with a UGA stop codon (Panel C). The variant results in the truncation of the mRNA message within exon 2 (of 9 total exons) (Panel D). This variant is predicted to result in a severely truncated protein or, more likely, no protein at all (i.e., a null variant) from nonsense-mediated decay of the mRNA message, which is generally triggered by a premature stop codon more than 50 base pairs upstream of the 3' (downstream) end of the penultimate exon.

The patient's initial presentation to the emergency department (when he was 16 years of age) with hyperglycemia and a BMI of 18.8 could easily be mistaken for type 1 diabetes, the most common type of pediatric diabetes. However, the following features detected at that time were less suggestive of type 1 diabetes: the negative tests for GAD65, IA-2, and insulin autoantibodies; the detectable blood level of C peptide; the absence of autoimmune conditions in the patient history; and the absence of autoimmune conditions in the family history.

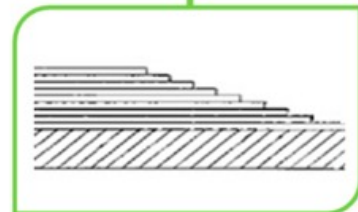
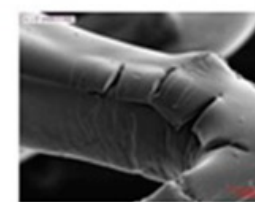
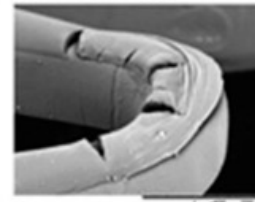
The patient's initial presentation with diabetes was more consistent with MODY, the most common type of monogenic diabetes. MODY is characterized by primary pancreatic beta-cell dysfunction that is diagnosed during adolescence or early adulthood. This patient had features that were specifically consistent with *HNF1B*-related MODY, which accounts for less than 5% of cases of MODY. As compared with the more common subtypes of MODY (related to *GCK*, *HNF1A*, or *HNF4A*), MODY related to *HNF1B* (previously known as MODY5) has an increased likelihood of the following features: extrapancreatic manifestations, including morphologic abnormalities of the kidneys and chronic kidney disease at the time of diabetes diagnosis; wide variation in the age at diabetes onset; de novo mutations and the absence of a strong family history of diabetes; pancreatic anomalies, including exocrine dysfunction; and reduced insulin sensitivity. Although some patients with *HNF1B*-related MODY may have well-controlled blood glucose levels with the use of noninsulin medications for a period after diagnosis, the vast majority of patients with *HNF1B*-related MODY eventually receive insulin treatment. When this patient was initially evaluated in the diabetes clinic, he had been receiving treatment with a basal–bolus insulin regimen since the time of diabetes diagnosis, almost 4 years earlier. The blood glycosylated hemoglobin level was 9.0%. A C-peptide level obtained almost 4 years earlier was 1.9 ng per milliliter. The presence of a detectable C-peptide level in this patient indicated that his diabetes could potentially be treated with a noninsulin agent. Data that support the use of a specific agent and data that compare outcomes for such agents with those for basal–bolus insulin therapy are limited. We opted to obtain a repeat C-peptide level before considering additional treatment options. I also encouraged more consistent use of basal insulin, because the patient reported that he often missed his basal dose.

The Ultimaster Biodegradable-Polymer Sirolimus-Eluting Stent: An Updated Review of Clinical Evidence

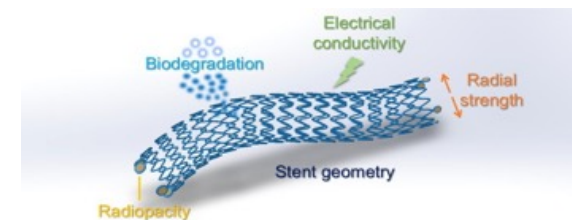


No drug polymer coating on parts of the stent that experience the most physical stress

Prevents the damage that can occur with other stent coatings:



Cross-sectional illustration of **Gradient Coating**, made by a slope with the coating multi-layers



Long-term outcomes with biodegradable polymer sirolimus-eluting stents versus durable polymer everolimus-eluting stents in ST-segment elevation myocardial infarction: 5-year follow-up of the BIOSTEMI randomised superiority trial

Summary

Background Biodegradable polymer sirolimus-eluting stents improve early stent-related clinical outcomes compared to durable polymer everolimus-eluting stents in patients with ST-segment elevation myocardial infarction (STEMI) undergoing primary percutaneous coronary intervention. The long-term advantages of biodegradable polymer sirolimus-eluting stents after complete degradation of its polymer coating in patients with STEMI remains however uncertain.

Methods BIOSTEMI Extended Survival (BIOSTEMI ES) was an investigator-initiated, follow-up extension study of the BIOSTEMI prospective, multicentre, single-blind, randomised superiority trial that compared biodegradable polymer sirolimus-eluting stents with durable polymer everolimus-eluting stents in patients with STEMI undergoing primary percutaneous coronary intervention at ten hospitals in Switzerland. All individuals who had provided written informed consent for participation in the BIOSTEMI trial were eligible for this follow-up study. The primary endpoint was target lesion failure, defined as a composite of cardiac death, target vessel myocardial re-infarction, or clinically indicated target lesion revascularisation, at 5 years. Superiority of biodegradable polymer sirolimus-eluting stents over durable polymer everolimus-eluting stents was declared if the Bayesian posterior probability for a rate ratio (RR) of less than 1 was greater than 0.975. Analyses were performed according to the intention-to-treat principle. The study was registered with ClinicalTrials.gov, NCT05484310.

Findings Between April 26, 2016, and March 9, 2018, 1300 patients with STEMI (1622 lesions) were randomly allocated in a 1:1 ratio to treatment with biodegradable polymer sirolimus-eluting stents (649 patients, 816 lesions) or durable polymer everolimus-eluting stents (651 patients, 806 lesions). At 5 years, the primary composite endpoint of target lesion failure occurred in 50 (8%) patients treated with biodegradable polymer sirolimus-eluting stents and in 72 (11%) patients treated with durable polymer everolimus-eluting stents (difference of -3%; RR 0.70, 95% Bayesian credible interval 0.51–0.95; Bayesian posterior probability for superiority 0.988).

Interpretation In patients undergoing primary percutaneous coronary intervention for STEMI, biodegradable polymer sirolimus-eluting stents were superior to durable polymer everolimus-eluting stents with respect to target lesion failure at 5 years of follow-up. The difference was driven by a numerically lower risk for ischaemia-driven target lesion revascularisation.

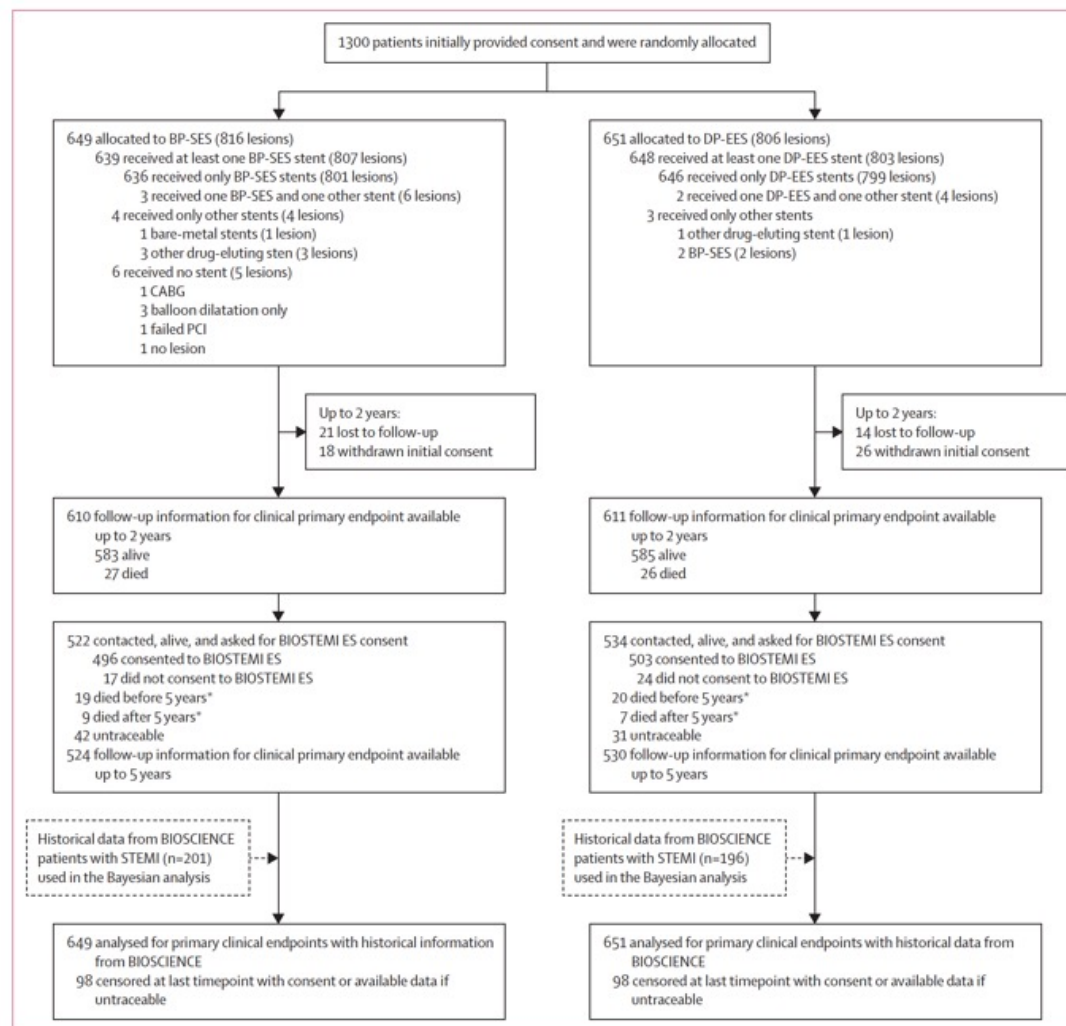


Figure 1: Participant flowchart

BIOSTEMI ES=BIOSTEMI Extended Survival. BP-SES=biodegradable polymer sirolimus-eluting stents. CABG=coronary artery bypass grafting. DP-EES=durable polymer everolimus-eluting stents. PCI=percutaneous coronary intervention. *Deceased patients who provided informed consent for BIOSTEMI were included in the BIOSTEMI ES analysis, because they were exempted from an additional BIOSTEMI ES consent.

	Total (n=1012)	BP-SES group (n=503)	DP-EES group (n=509)	p value
Aspirin	894 (88%)	451 (90%)	443 (87%)	0.20
Clopidogrel	49 (5%)	23 (5%)	26 (5%)	0.77
Prasugrel	10 (1%)	5 (1%)	5 (1%)	1.00
Ticagrelor	25 (2%)	13 (3%)	12 (2%)	0.84
Any SAPT	35 (3%)	18 (4%)	17 (3%)	0.87
Any DAPT	55 (5%)	29 (6%)	26 (5%)	0.68
Oral anticoagulation	18 (2%)	10 (2%)	8 (2%)	0.64
Direct oral anticoagulants	94 (9%)	40 (8%)	54 (11%)	0.16
Any anticoagulant treatment	112 (11%)	50 (10%)	62 (12%)	0.27
Statin	844 (83%)	413 (82%)	431 (85%)	0.31
PCSK9 inhibitor	25 (2%)	11 (2%)	14 (3%)	0.69
Other lipid-lowering drug	305 (30%)	157 (31%)	148 (29%)	0.49
ACE inhibitor	463 (46%)	221 (44%)	242 (48%)	0.26
β blocker	579 (57%)	291 (58%)	288 (57%)	0.70

Values are n (%). Column totals show patients with available data; medication information at 5 years was not available for 146 patients in the BP-SES group and 142 patients in the DP-EES group. BP-SES=biodegradable polymer sirolimus-eluting stent. DP-EES=durable polymer everolimus-eluting stent. SAPT=single antiplatelet therapy. DAPT=dual antiplatelet therapy. ACE=angiotensin-converting enzyme. PCSK9=proprotein convertase subtilisin/kexin type 9.

Table 1: Medication at 5 years of follow-up

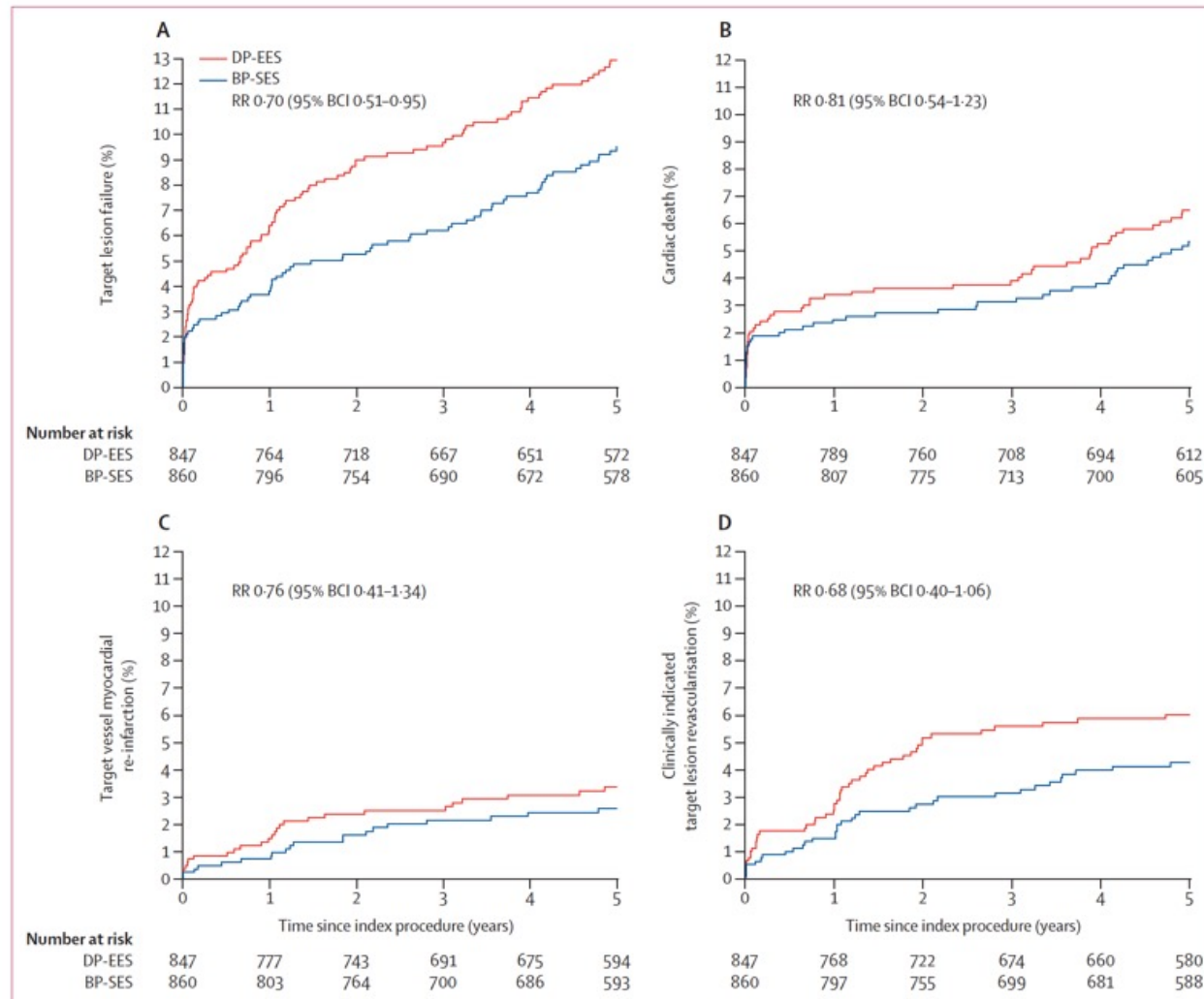


Figure 2: Time-to-event curves for the primary endpoint and individual components of the primary endpoint at 5 years

(A) Target lesion failure. (B) Cardiac death. (C) Target vessel myocardial re-infarction. (D) Clinically indicated target lesion revascularisation. BCI=Bayesian credible interval. BP-SES=biodegradable polymer sirolimus-eluting stents. DP-EES=durable polymer everolimus-eluting stents. RR=rate ratio.

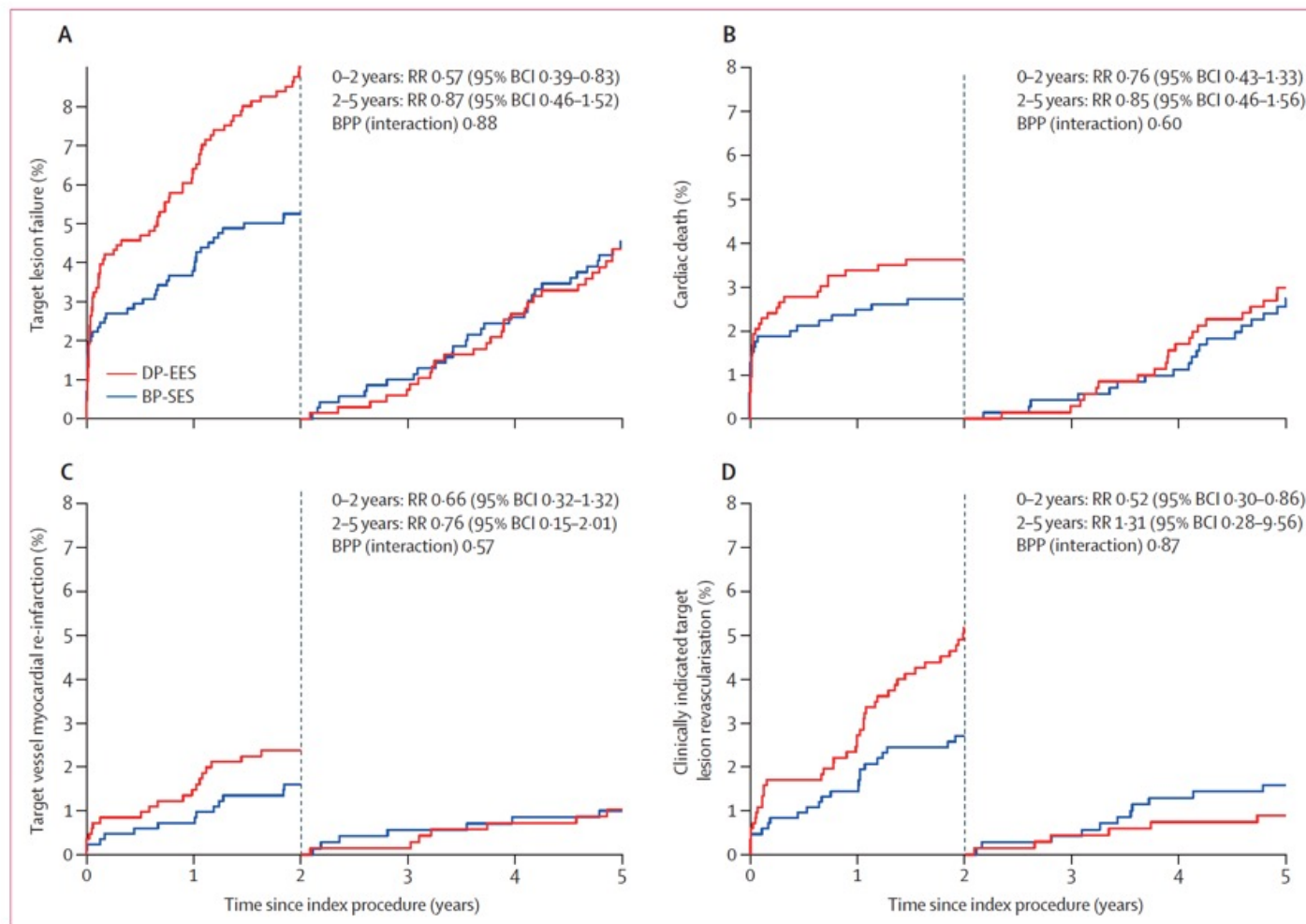


Figure 3: Time-to-event curves for the primary endpoint and individual components of the primary endpoint with a landmark set at 2 years

(A) Target lesion failure. (B) Cardiac death. (C) Target vessel myocardial re-infarction. (D) Clinically indicated target lesion revascularisation. BCI=Bayesian credible interval. BP-SES=biodegradable polymer sirolimus-eluting stents. BPP=Bayesian posterior probability. DP-EES, durable polymer everolimus-eluting stents. RR=rate ratio.

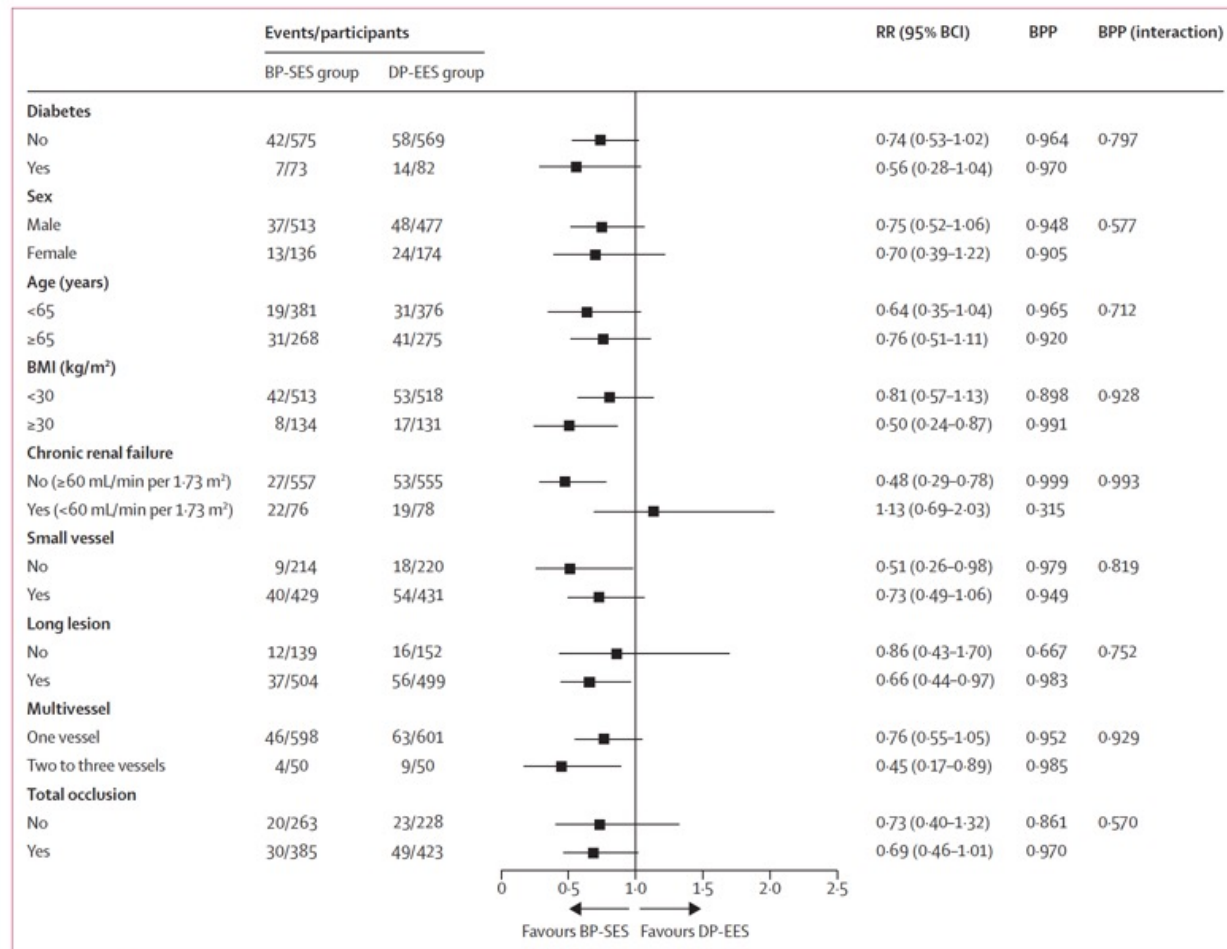


Figure 4: Stratified analyses of the primary endpoint at 5 years across major patient subgroups

Prespecified subgroups were diabetes and multivessel disease. Bayesian log Poisson models were used to estimate RRs and BCIs. BPP is calculated as the BPP of an RR of less than 1.0 within each subgroup. BPP for interaction is calculated as the BPP of a difference between the two subgroups. Small vessels were defined as stent diameter in any lesion of 3.0 mm or less. Long lesions were defined as total stent length in any lesion of at least 20 mm. Chronic renal failure was defined as creatinine eGFR of less than 60 mL/min per 1.73 m² using the Modification of Diet in Renal Disease formula. BCI=Bayesian credible interval. BP-SES=biodegradable polymer sirolimus-eluting stents. BPP=Bayesian posterior probability. DP-EES, durable polymer everolimus-eluting stents. eGFR=estimated glomerular filtration rate. RR=rate ratio.

Research in context

Evidence before this study

Newer-generation drug-eluting stents with durable or biodegradable polymer coatings improve long-term stent-related and patient-oriented clinical outcomes compared with early-generation drug-eluting stents in patients with ST-segment elevation myocardial infarction (STEMI) and are the current standard of care. In the BIOSTEMI randomised trial, newer-generation thin-strut biodegradable polymer sirolimus-eluting stents significantly improved early clinical outcomes compared with contemporary second-generation durable polymer everolimus-eluting stents in patients with STEMI, but the long-term effectiveness of biodegradable polymer sirolimus-eluting stents after complete degradation of the polymer coating in this setting remains uncertain.

We searched PubMed, Embase, and Cochrane Central Register of Controlled Trials databases from database inception to Sept 11, 2023, with no language restriction for randomised trials comparing newer-generation drug-eluting stents in patients with STEMI treated with primary percutaneous coronary intervention. Using the search terms “drug-eluting stent and acute myocardial infarction” and “drug-eluting stent and ST-segment elevation myocardial infarction”, BIOSTEMI was the only head-to-head randomised trial found that was assessing the incremental benefits of different drug-eluting stent designs in patients with STEMI. The available evidence shows improved early device-oriented clinical outcomes after primary percutaneous coronary

intervention with newer-generation biodegradable polymer sirolimus-eluting stents compared with durable polymer everolimus-eluting stents in patients with STEMI.

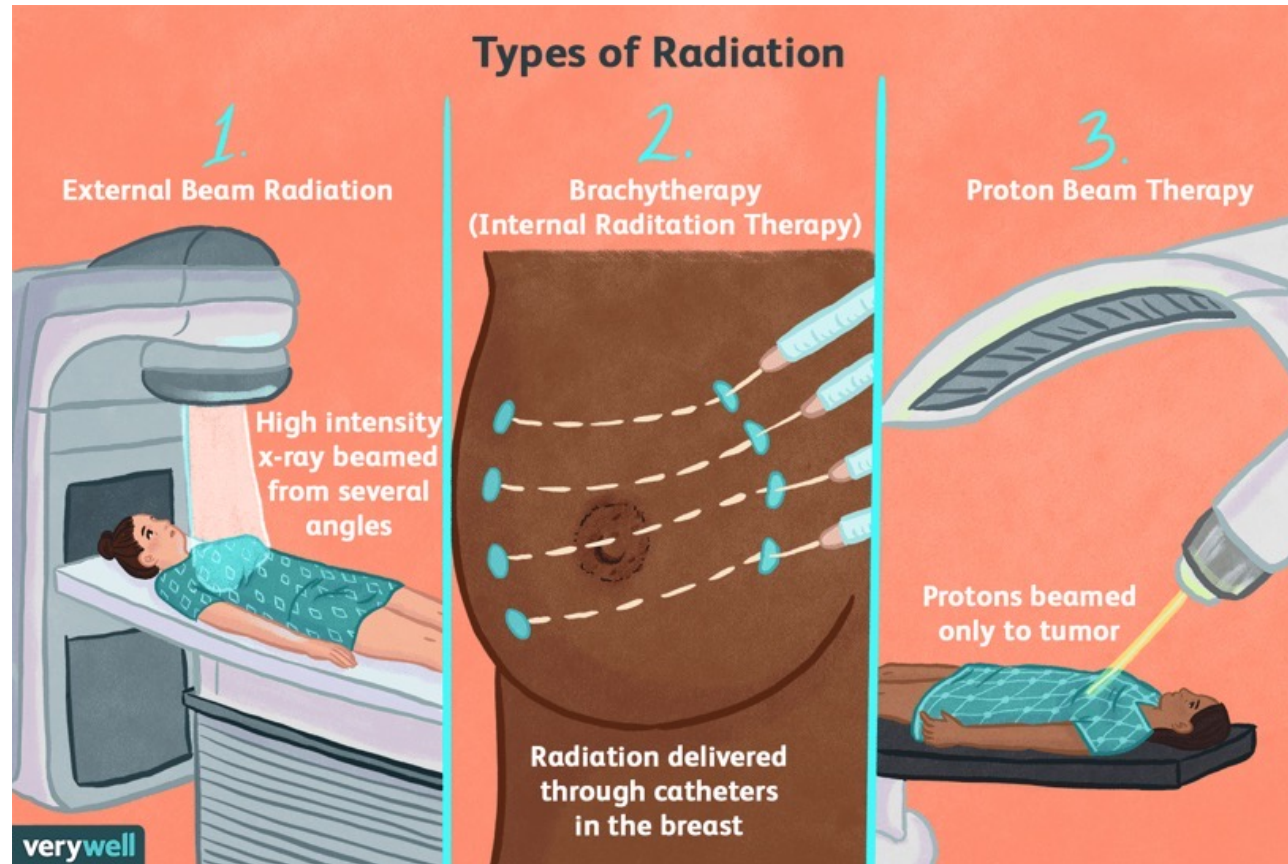
Added value of this study

To our knowledge, the BIOSTEMI Extended Survival (BIOSTEMI ES) study is the first head-to-head randomised comparison with long-term follow-up between two newer-generation drug-eluting stents for the treatment of patients with STEMI. BIOSTEMI ES is an investigator-initiated superiority trial showing that biodegradable polymer sirolimus-eluting stents are associated with a lower risk of target lesion failure at 5 years of follow-up compared with durable polymer everolimus-eluting stents among patients with STEMI, a difference driven by lower rates of ischaemia-driven repeat revascularisations. In addition, the study shows the absence of a late catch-up phenomenon with newer-generation biodegradable polymer drug-eluting stents in patients with STEMI.

Implications of all the available evidence

Newer-generation drug-eluting stents combining thin-strut metallic stent platforms with biodegradable polymer coatings improve both early and long-term clinical outcomes compared with durable polymer drug-eluting stents among patients undergoing primary percutaneous coronary intervention for STEMI.

Radiation Therapy for Breast Cancer



Radiotherapy to regional nodes in early breast cancer: an individual patient data meta-analysis of 14 324 women in 16 trials

Summary

Background Radiotherapy has become much better targeted since the 1980s, improving both safety and efficacy. In breast cancer, radiotherapy to regional lymph nodes aims to reduce risks of recurrence and death. Its effects have been studied in randomised trials, some before the 1980s and some after. We aimed to assess the effects of regional node radiotherapy in these two eras.

Methods In this meta-analysis of individual patient data, we sought data from all randomised trials of regional lymph node radiotherapy versus no regional lymph node radiotherapy in women with early breast cancer (including one study that irradiated lymph nodes only if the cancer was right-sided). Trials were identified through the EBCTCG's regular systematic searches of databases including MEDLINE, Embase, the Cochrane Library, and meeting abstracts. Trials were eligible if they began before Jan 1, 2009. The only systematic difference between treatment groups was in regional node radiotherapy (to the internal mammary chain, supraclavicular fossa, or axilla, or any combinations of these). Primary outcomes were recurrence at any site, breast cancer mortality, non-breast-cancer mortality, and all-cause mortality. Data were supplied by trialists and standardised into a format suitable for analysis. A summary of the formatted data was returned to trialists for verification. Log-rank analyses yielded first-event rate ratios (RRs) and confidence intervals.

Findings We found 17 eligible trials, 16 of which had available data (for 14 324 participants), and one of which (henceforth excluded), had unavailable data (for 165 participants). In the eight newer trials (12 167 patients), which started during 1989–2008, regional node radiotherapy significantly reduced recurrence (rate ratio 0·88, 95% CI 0·81–0·95; $p=0\cdot0008$). The main effect was on distant recurrence as few regional node recurrences were reported. Radiotherapy significantly reduced breast cancer mortality (RR 0·87, 95% CI 0·80–0·94; $p=0\cdot0010$), with no significant effect on non-breast-cancer mortality (0·97, 0·84–1·11; $p=0\cdot63$), leading to significantly reduced all-cause mortality (0·90, 0·84–0·96; $p=0\cdot0022$). In an illustrative calculation, estimated absolute reductions in 15-year breast cancer mortality were 1·6% for women with no positive axillary nodes, 2·7% for those with one to three positive axillary nodes, and 4·5% for those with four or more positive axillary nodes. In the eight older trials (2157 patients), which started during 1961–78, regional node radiotherapy had little effect on breast cancer mortality (RR 1·04, 95% CI 0·91–1·20; $p=0\cdot55$), but significantly increased non-breast-cancer mortality (1·42, 1·18–1·71; $p=0\cdot00023$), with risk mainly after year 20, and all-cause mortality (1·17, 1·04–1·31; $p=0\cdot0067$).

Interpretation Regional node radiotherapy significantly reduced breast cancer mortality and all-cause mortality in trials done after the 1980s, but not in older trials. These contrasting findings could reflect radiotherapy improvements since the 1980s.

	Number of trials	Number of women	Number of deaths	Woman-years since diagnosis					Women given systemic therapy, %		
				Median follow-up (IQR)	Total ('000s)	Distribution by years ('000s)			Chemo-therapy*	ER+ and endocrine therapy	Any
						<10	10 to <20	≥20			
Older trials (1961–78)†											
IMC, SCF, and axilla‡	7	1940	1424	29.3 (16.3–41.8)	23.9	13.5	6.5	3.9	22.6%	0.0%	22.6%
IMC
SCF and axilla§	1	217	117	9.9 (9.5–10.0)	1.5	1.5	0.0	0.0	0.0%	0.0%	0.0%
Subtotal	8	2157	1541	25.6 (12.4–41.7)	25.4	15.0	6.5	3.9	20.3%	0.0%	20.3%
Newer trials (1989 onwards)†											
IMC, SCF, axilla‡	2	5836	1446	13.5 (10.1–16.2)	66.7	50.6	16.1	0.0	66.0%	60.4%	89.2%
IMC¶	4	5420	2041	14.3 (11.2–15.8)	58.6	43.6	13.8	1.3	58.8%	60.9%	91.9%
SCF and axilla§	2	911	107	5.4 (3.2–11.4)	6.8	5.2	1.5	0.1	55.9%	65.1%	92.5%
Subtotal	8	12 167	3594	13.7 (9.9–16.0)	132.1	99.3	31.4	1.4	62.0%	61.0%	90.7%
All trials											
IMC, SCF, and axilla‡	9	7776	2870	14.1 (10.4–17.4)	90.6	64.1	22.6	4.0	55.2%	45.3%	72.6%
IMC	4	5420	2041	14.3 (11.2–15.8)	58.6	43.6	13.8	1.3	58.8%	60.9%	91.9%
SCF and axilla§	3	1128	224	6.3 (3.6–11.2)	8.2	6.6	1.5	0.1	45.1%	52.6%	74.7%
All	16	14 324	5135	14.0 (10.0–16.4)	157.5	114.3	37.9	5.4	55.7%	51.8%	80.1%

Treatment to the breast and chest wall was the same in both groups and might have included radiotherapy. IMC=internal mammary chain. SCF=supraclavicular fossa (level medial 3/4). Axilla=nodes in levels 1–3. ER=oestrogen receptor. *In women who received chemotherapy, the type given was anthracycline (no taxane) in 2079 (26.0%) of 7986 women, taxane-containing in 1254 (15.7%) women, and unknown or other in 4653 (58.3%) women. In the newer trials, chemotherapy was received by 7548 (62.0%) of 12 167 women and endocrine therapy by 7421 (61.0%) women. †Data were available for 16 trials, start dates from 1961 to 2008, and unavailable for one trial including 165 women, starting in 1985 (appendix pp 17–20). ‡IMC, SCF, and axilla: two trials were IMC and SCF radiotherapy versus no radiotherapy to these nodal regions (4060 women), and seven were IMC, SCF, and axilla radiotherapy versus no radiotherapy to these nodal regions (3716 women). §SCF and axilla: one trial was axilla radiotherapy versus no radiotherapy to this nodal region (435 women), one trial was SCF radiotherapy versus no radiotherapy to this nodal region (476 women), and one trial was SCF and axilla radiotherapy versus no radiotherapy to these nodal regions (217 women). ¶IMC: all four trials were IMC radiotherapy versus no radiotherapy to this nodal region (5420 women) including a study in which nodal radiotherapy was allocated by laterality. Patients with right breast cancers received IMC radiotherapy, and patients with left breast cancers did not.

Table 1: Availability of data from trials beginning before 2009 and comparing radiotherapy versus no radiotherapy to the regional nodes

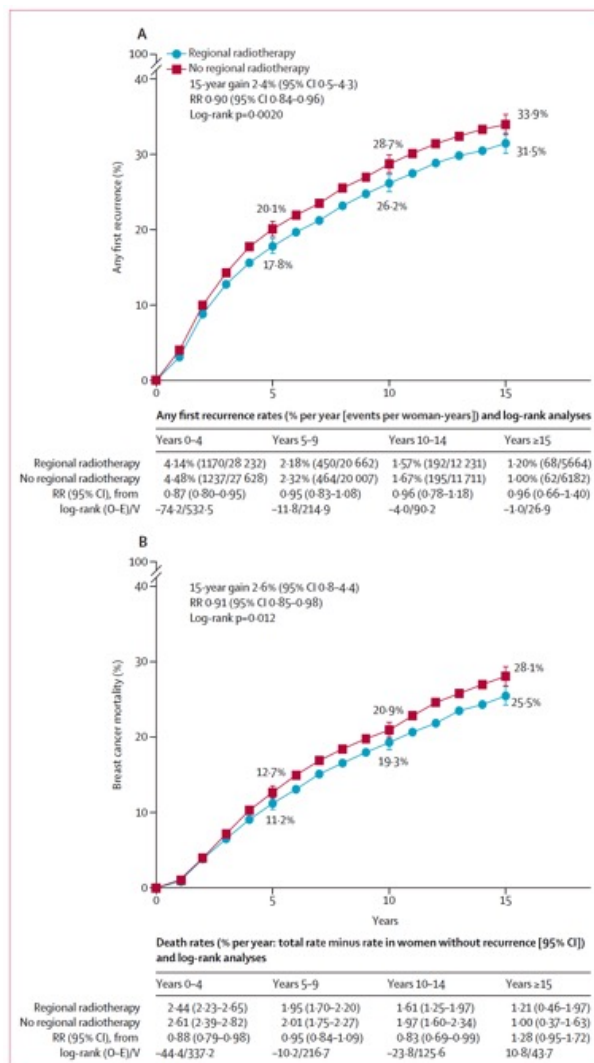


Figure 1: Effect of regional node radiotherapy on (A) any recurrence and (B) breast cancer mortality in 12 990 women in 15 trials
2157 women in eight older trials and 10 833 women in seven newer trials. One newer trial of 1334 women that reported only all-cause mortality was excluded. RR=rate ratio.

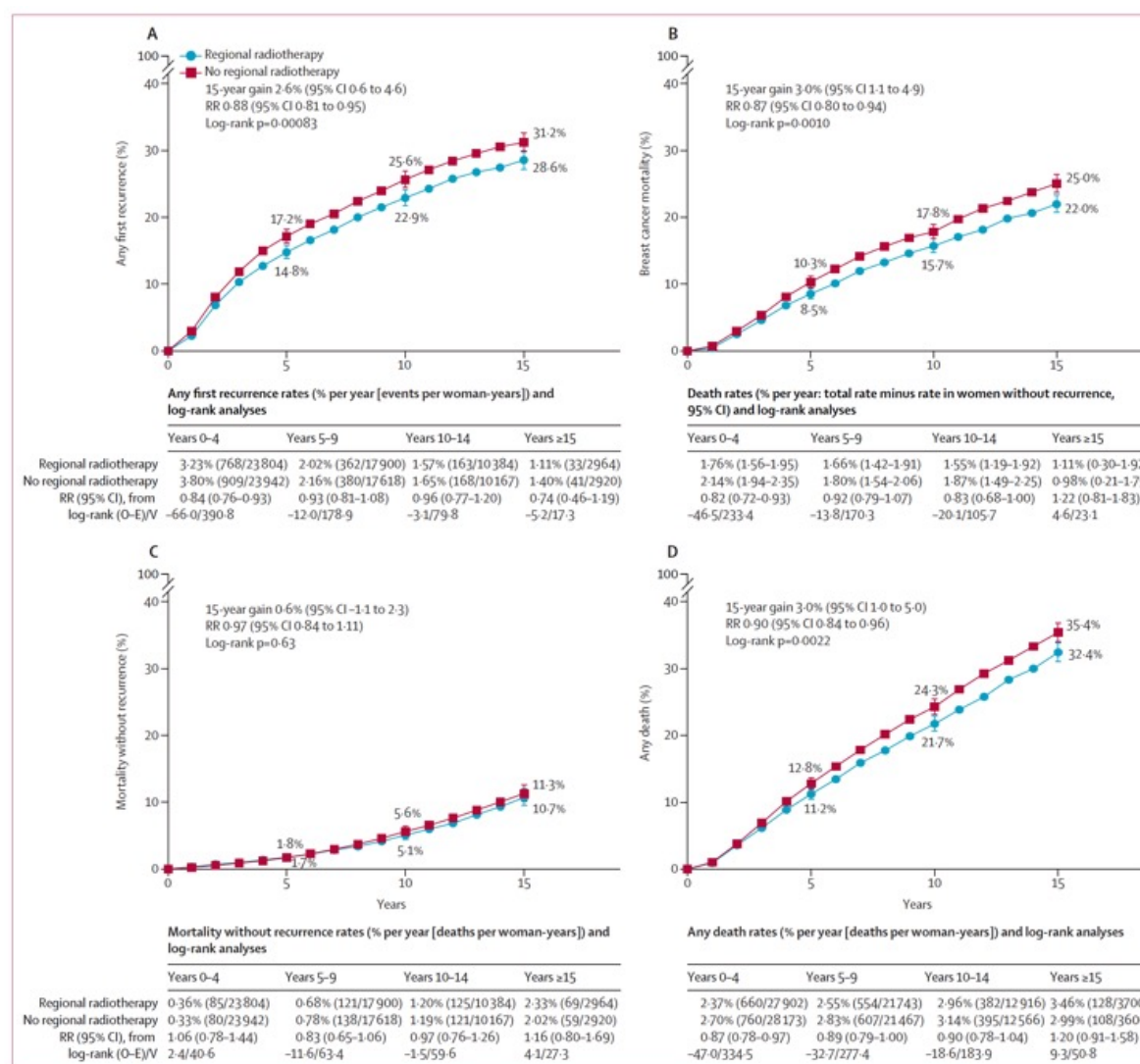


Figure 2: Effect of regional node radiotherapy in the eight newer trials on (A) any recurrence, (B) breast cancer mortality, (C) non-breast-cancer mortality, and (D) any death
One newer trial of 1334 women that reported only all-cause mortality is included only in graph D. RR=rate ratio.

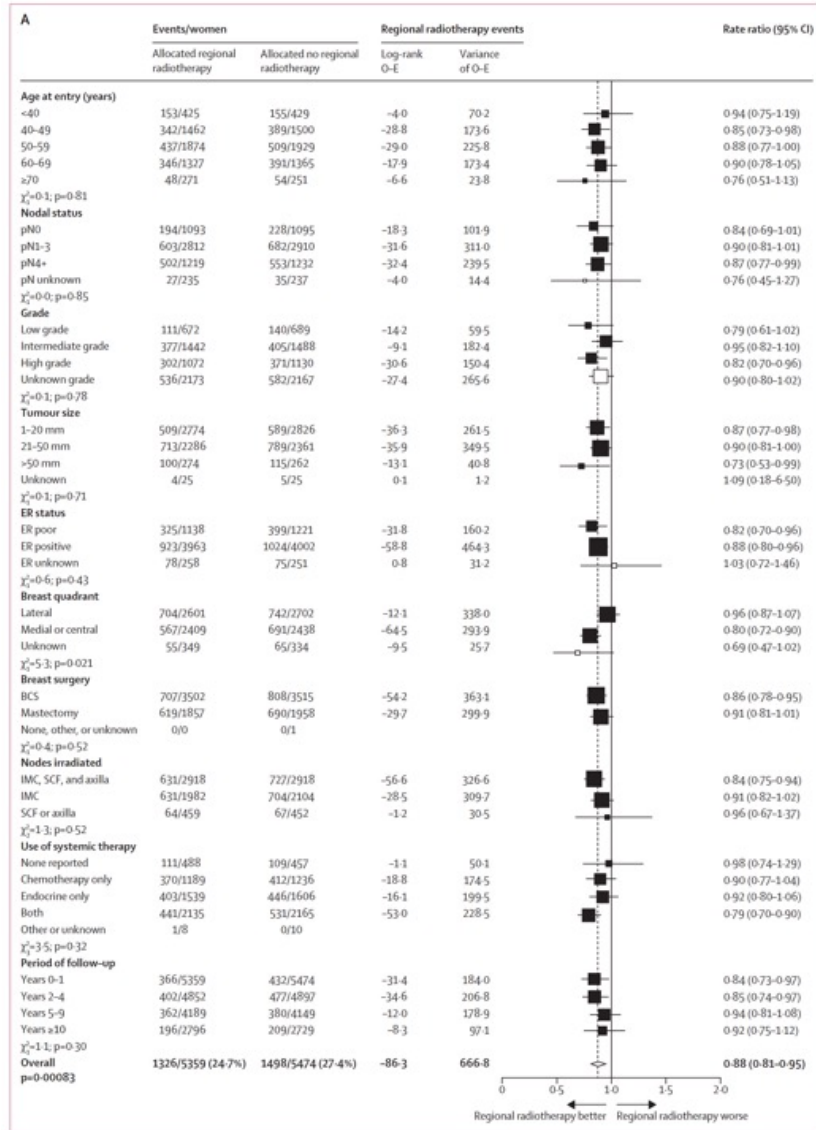
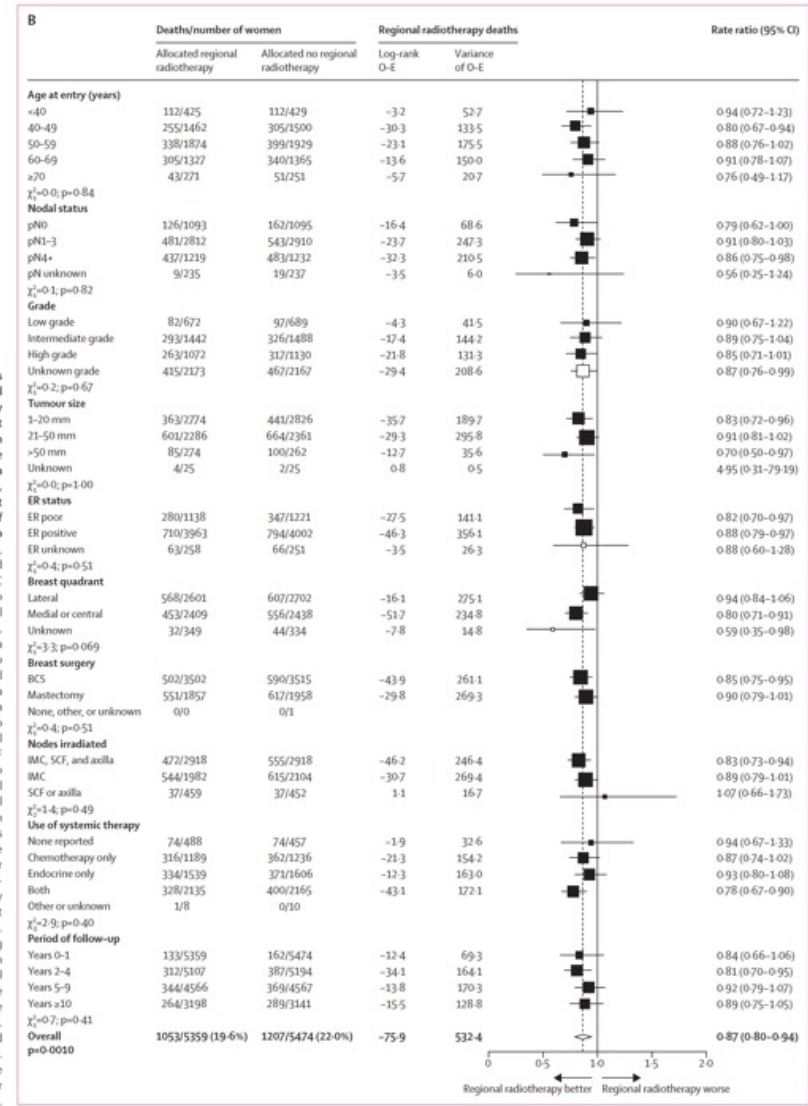


Figure 3: Subgroup analyses for event rate ratios and 95% CIs for (A) any recurrence and (B) breast cancer mortality in 10 833 women in the seven newer trials with data on recurrence by patient, tumour, and treatment factors, and period of follow-up

Internal mammary chain, supraclavicular fossa, and axilla included one trial of IMC and SCF versus no radiotherapy to those nodal regions and one trial of IMC, SCF radiotherapy, and axilla radiotherapy versus no radiotherapy to these nodal regions. SCF and axilla included one trial of axilla radiotherapy versus no radiotherapy to this nodal region, and one trial of SCF radiotherapy versus no radiotherapy to this nodal region. In graph B, the total numbers of deaths with recurrence are cited (regardless of the causes of death), but the analyses are of breast cancer mortality, allowing (by log-rank subtraction) for any mortality from non-breast cancer causes after recurrence.

BCS=breast conserving surgery; ER=estrogen receptor; IMC=internal mammary chain; N0=node negative; N1-3=one to three involved axillary lymph nodes; N4+=four or more involved axillary lymph nodes; pN=pathological lymph node status; SCF=supraclavicular fossa.



	Regional radiotherapy	No regional radiotherapy	Gain from regional radiotherapy
Any recurrence			
pN0	19.0%	21.3%	2.3%
pN1–3	25.6%	28.5%	2.9%
pN4+	46.8%	51.1%	4.3%
Breast cancer mortality			
pN0	10.9%	12.5%	1.6%
pN1–3	20.3%	23.0%	2.7%
pN4+	40.5%	45.0%	4.5%

Data are 15-year cumulative risks. The overall rate ratios (RRs) for any recurrence (RR=0.88; figure 3) and breast cancer mortality (0.87; figure 3) were applied to annual rates of any recurrence and breast cancer mortality in the trials, averaged over treatment groups (there was no significant heterogeneity in the proportional reductions [RRs] for any recurrence and breast cancer mortality). pN0=pathologically node negative. pN1–3=one to three involved axillary lymph nodes. pN4+=four or more involved axillary lymph nodes.

Table 2: Absolute effect of regional node radiotherapy on 15-year risk of any recurrence and breast cancer mortality by nodal status in 10 833 women in the seven newer trials with data on recurrence

Research in context

Evidence before this study

Previous Early Breast Cancer Trialists' Collaborative Group (EBCTCG) meta-analyses have shown that radiotherapy after breast-conserving surgery, or after mastectomy in node-positive disease, reduces breast cancer recurrence and mortality. Some of those trials irradiated just the breast or chest wall, but others also irradiated some of the regional lymph nodes, and it is not known how much of the protective effect was due to irradiation of the nodes. The separate effects of irradiating regional lymph nodes after surgery have been assessed in individual trials. The EBCTCG's ongoing searches of bibliographic databases including MEDLINE, Embase, the Cochrane Library and relevant meeting abstracts identified 17 trials which started before 2009 and compared radiotherapy to regional lymph nodes versus no radiotherapy to regional lymph nodes, with randomisation, or allocation by tumour laterality, but did not identify any individual patient data meta-analyses.

Added value of this study

This collaborative meta-analysis collated, checked, and analysed individual patient data on 14 324 women in 16 trials that started during 1961–2008 and assessed the effects of irradiating the internal mammary chain, supraclavicular fossa, and axillary lymph nodes. The trials were done during the past six decades. During this time, there were major changes in breast cancer radiotherapy, and these are reflected by our findings. Eight trials, which started during 1961–78 assessed older radiotherapy techniques and did not usually involve radiotherapy to the chest wall in node-positive disease. Radiotherapy in these trials did not reduce breast cancer mortality. Eight trials, which started during 1989–2008

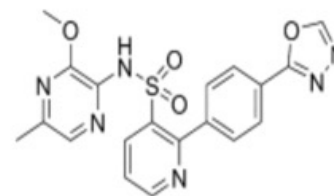
assessed more tailored radiotherapy. Most of these newer trials assessed the addition of regional node irradiation to chest wall or breast radiotherapy in node-positive disease. In analyses of data on 12 167 women, regional node radiotherapy significantly reduced breast cancer recurrence, breast cancer mortality, and all-cause mortality. With 15 years of follow-up, no increase was seen in non-breast-cancer mortality. This meta-analysis provides more precise estimates of the effects of regional node radiotherapy than the individual trials. Absolute improvements in breast cancer recurrence and mortality from regional node radiotherapy in the 1990s–2000s were greatest for women with the highest breast cancer recurrence and mortality risks. The absolute reductions in 15-year breast cancer mortality were 1–2% for women with no positive axillary lymph nodes, 2–3% for those with one to three positive nodes, and 4–5% for those with four or more positive nodes.

Implications of all the available evidence

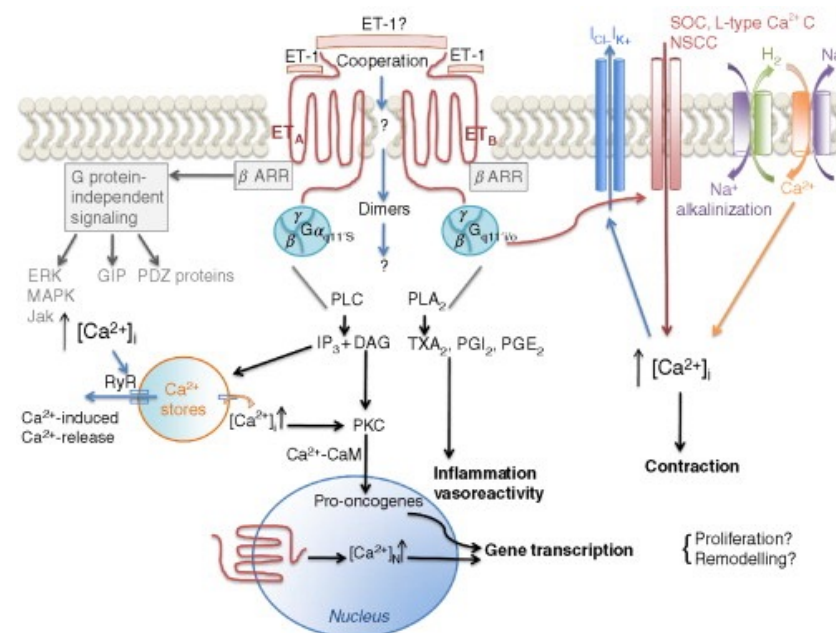
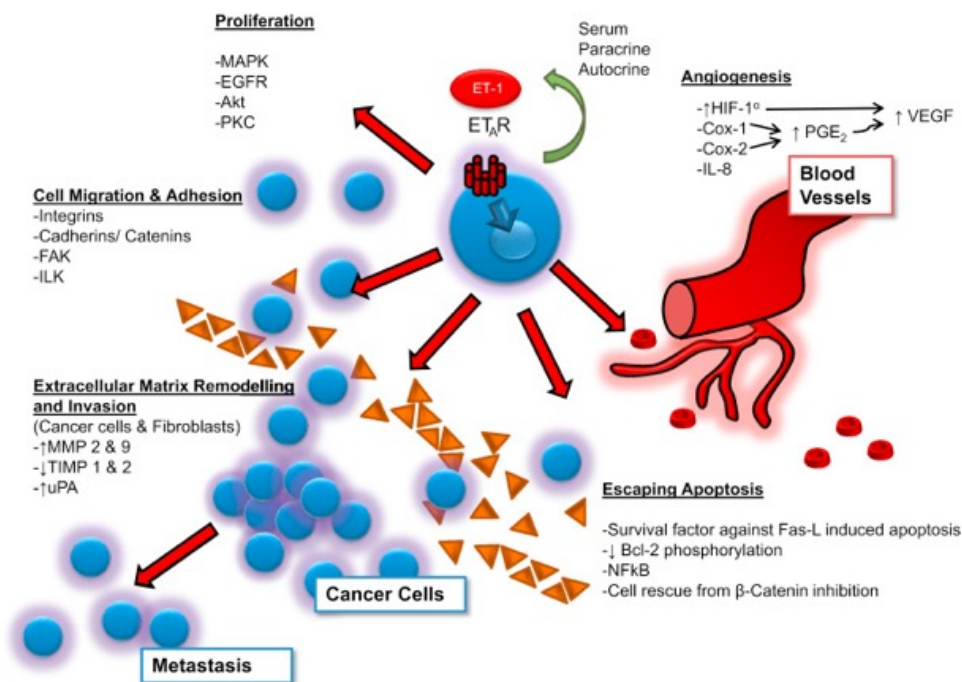
Our results show the benefits of irradiating the regional lymph nodes in women who also receive effective local and systemic therapies. For women being considered for radiotherapy today, the proportional benefits of regional node radiotherapy could be greater than those in the newer trials due to further improvements in radiotherapy. The absolute breast cancer mortality benefits could be somewhat lower than in the trials due to reductions in population breast cancer death rates. Our findings have implications for policy and for patients. Implementation of regional node radiotherapy could improve breast cancer survival at little or no additional cost. Clinicians and patients can use this information to estimate survival gains from regional node radiotherapy in shared decision making.

Zibotentan

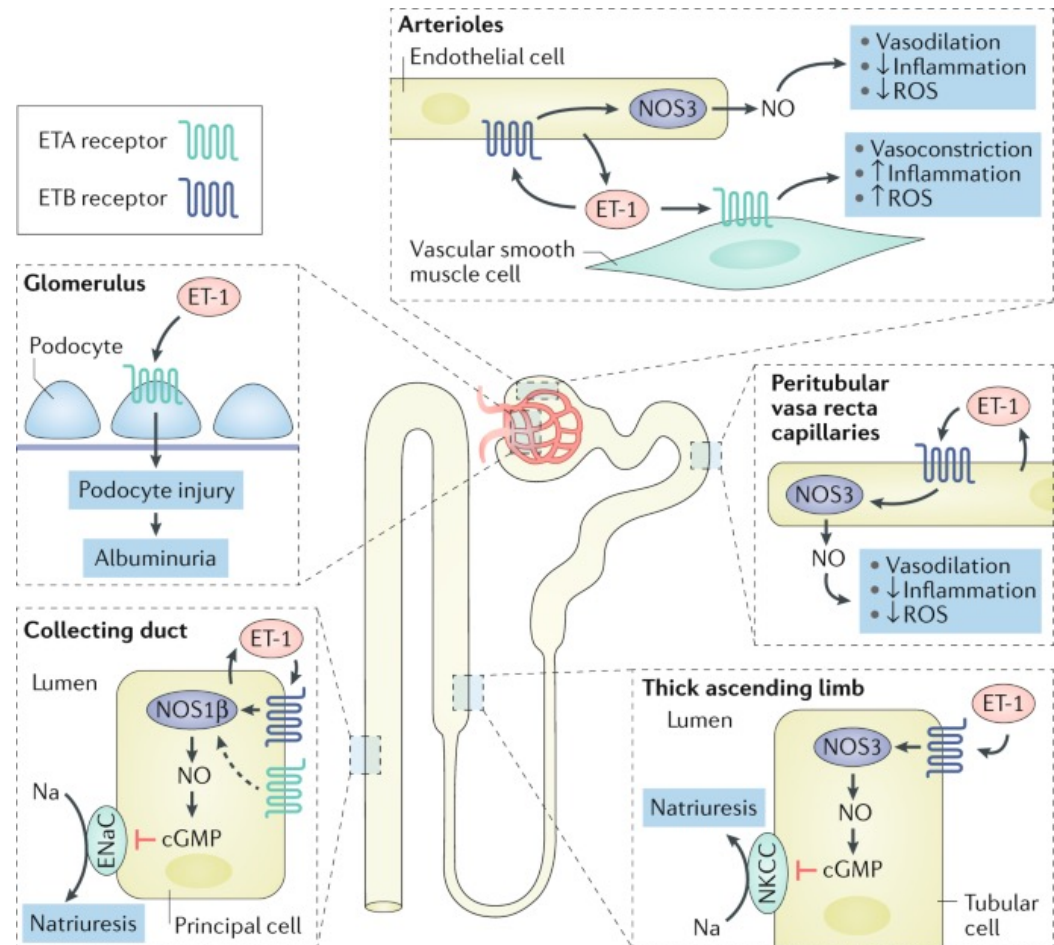
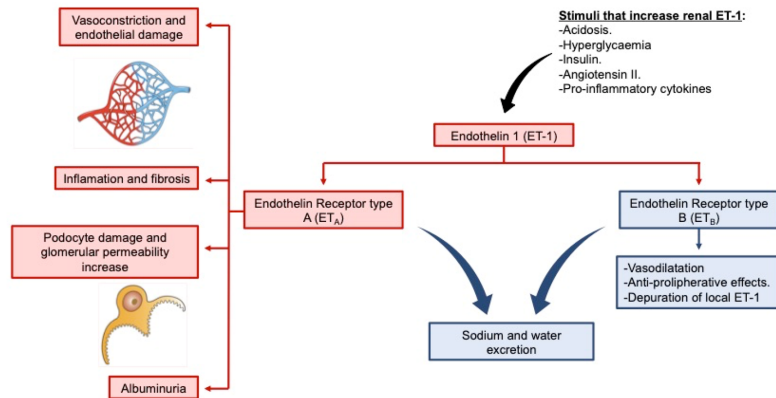
Zibotentan and atrasentan, two oral endothelin-A antagonists that showed increased PFS in two different phase II placebo-controlled clinical trials failed to confirm overall survival benefit in subsequent phase III trials in the pre-chemotherapy and post-chemotherapy settings.



Zibotentan, 25
Zeneca



Fluid retention and edema have been identified as major side effects of endothelin receptor antagonists.



Zibotentan in combination with dapagliflozin compared with dapagliflozin in patients with chronic kidney disease (ZENITH-CKD): a multicentre, randomised, active-controlled, phase 2b, clinical trial

Summary

Background In patients with chronic kidney disease, SGLT2 inhibitors and endothelin A receptor antagonists (ERAs) can reduce albuminuria and glomerular filtration rate (GFR) decline. We assessed the albuminuria-lowering efficacy and safety of the ERA zibotentan combined with the SGLT2 inhibitor dapagliflozin.

Methods ZENITH-CKD was a multicentre, randomised, double-blind, active-controlled clinical trial, done in 170 clinical practice sites in 18 countries. Adults (≥ 18 to ≤ 90 years) with an estimated GFR (eGFR) of 20 mL/min per 1.73 m² or greater and a urinary albumin-to-creatinine ratio (UACR) of 150–5000 mg/g were randomly assigned (2:1:2) to 12 weeks of daily treatment with zibotentan 1.5 mg plus dapagliflozin 10 mg, zibotentan 0.25 mg plus dapagliflozin 10 mg, or dapagliflozin 10 mg plus placebo, as adjunct to angiotensin-converting enzyme inhibitors or angiotensin receptor blockers if tolerated. The primary endpoint was a change from baseline in log-transformed UACR (zibotentan 1.5 mg plus dapagliflozin vs dapagliflozin plus placebo) at week 12. Fluid retention was an event of special interest, defined as an increase in bodyweight of at least 3% (at least 2.5% must have been from total body water) from baseline or an increase of at least 100% in B-type natriuretic peptide (BNP) and either a BNP concentration greater than 200 pg/mL if without atrial fibrillation or BNP greater than 400 pg/mL if with atrial fibrillation. This trial is registered with ClinicalTrials.gov, NCT04724837, and is completed.

Findings Between April 28, 2021, and Jan 17, 2023, we assessed 1492 participants for eligibility. For the main analysis, we randomly assigned 449 (30%) participants, 447 (99%) of whom (mean age 62.8 years [SD 12.1], 138 [31%] female, 309 [69%] male, 305 [68%] White, mean eGFR 46.7 mL/min per 1.73 m² [SD 22.4], and median UACR 565.5 mg/g [IQR 243.0–1212.6]) received treatment with zibotentan 1.5 mg plus dapagliflozin (n=179 [40%]), zibotentan 0.25 mg plus dapagliflozin (n=91 [20%]), or dapagliflozin plus placebo (n=177 [40%]). Zibotentan 1.5 mg plus dapagliflozin and zibotentan 0.25 mg plus dapagliflozin reduced UACR versus dapagliflozin plus placebo throughout the treatment period of the study. At week 12, the difference in UACR versus dapagliflozin plus placebo was –33.7% (90% CI –42.5 to –23.5; $p < 0.0001$) for zibotentan 1.5 mg plus dapagliflozin and –27.0% (90% CI –38.4 to –13.6; $p = 0.0022$) for zibotentan 0.25 mg plus dapagliflozin. Fluid-retention events were observed in 33 (18%) of 179 participants in the zibotentan 1.5 mg plus dapagliflozin group, eight (9%) of 91 in the zibotentan 0.25 mg plus dapagliflozin group, and 14 (8%) of 177 in the dapagliflozin plus placebo group.

Interpretation Zibotentan combined with dapagliflozin reduced albuminuria with an acceptable tolerability and safety profile and is an option to reduce chronic kidney disease progression in patients already receiving currently recommended therapy.

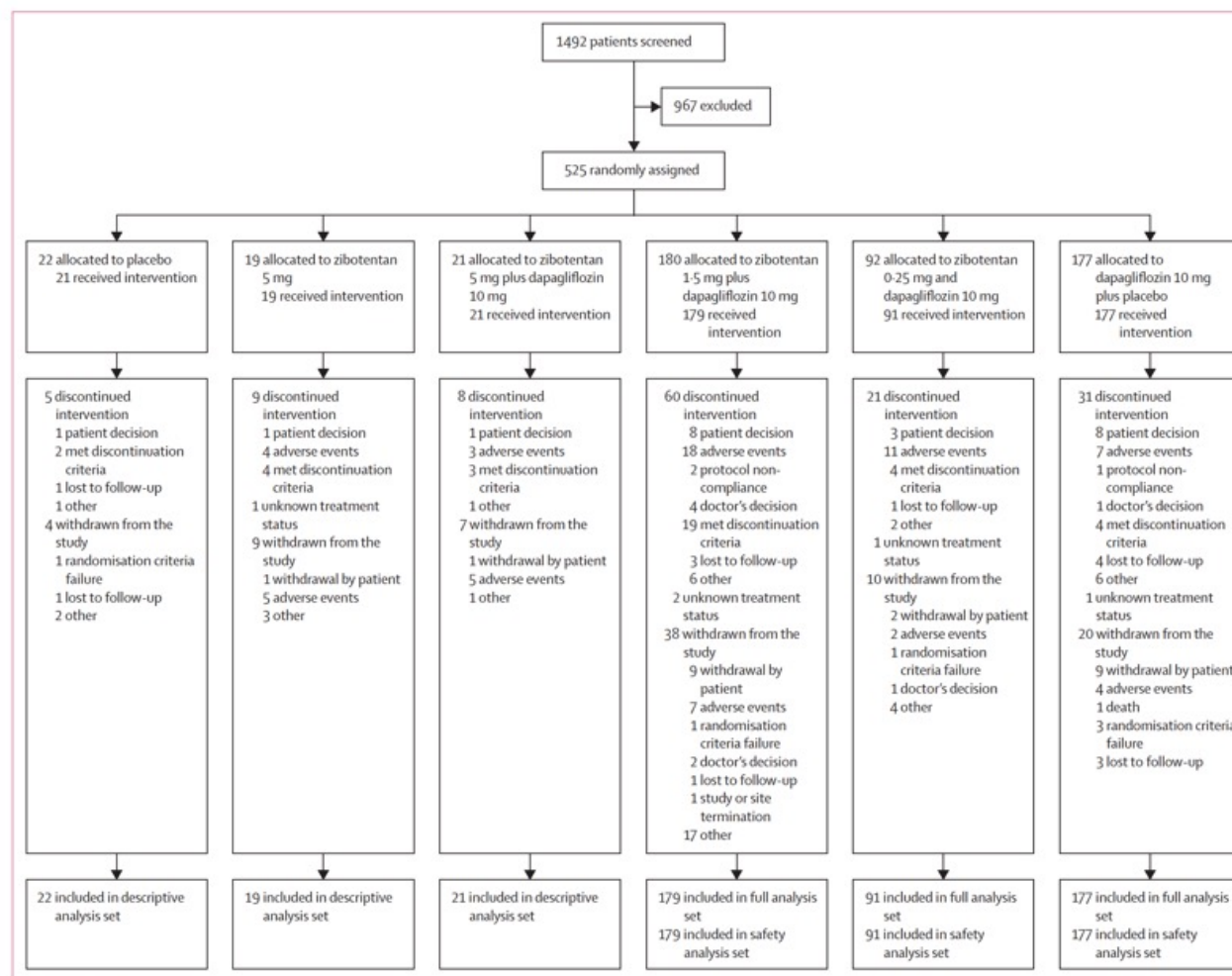


Figure 1: Trial profile

Placebo, zibotentan 5 mg, and zibotentan 5 mg plus dapagliflozin 10 mg groups were discontinued. Participants randomly assigned to dapagliflozin 10 mg/day during part A are not shown.

	Dapagliflozin 10 mg plus placebo (n=177)	Zibotentan 0.25 mg plus dapagliflozin 10 mg (n=91)	Zibotentan 1.5 mg plus dapagliflozin 10 mg (n=179)
Age, years	63.6 (11.60)	61.3 (12.72)	62.7 (12.33)
Sex			
Female	55 (31%)	28 (31%)	55 (31%)
Male	122 (69%)	63 (69%)	124 (69%)
Race			
White	125 (71%)	56 (62%)	124 (69%)
Black or African American	22 (12%)	7 (8%)	17 (9%)
Asian	26 (15%)	18 (20%)	26 (15%)
Other	4 (2%)	10 (11%)	10 (6%)
Weight, kg	85.5 (18.2)	83.8 (16.5)	85.9 (16.9)
BMI, kg/m ²	30.2 (5.4)	29.6 (5.0)	30.1 (5.0)
Current nicotine user	25 (14%)	12 (13%)	22 (12%)
Blood pressure, mm Hg			
Systolic	137.6 (17.6)	136.5 (17.8)	136.4 (16.1)
Diastolic	79.9 (9.8)	79.6 (10.5)	78.9 (9.4)
eGFR, mL/min per 1.73 m ²	45.2 (20.7)	48.4 (23.5)	47.4 (23.4)
eGFR ≥60	32 (18%)	22 (24%)	45 (25%)
eGFR 45 to <60	41 (23%)	19 (21%)	27 (15%)
eGFR 30 to <45	62 (35%)	28 (31%)	61 (34%)
eGFR <30	42 (24%)	22 (24%)	46 (26%)
Haemoglobin, g/L	132.0 (16.7)	131.7 (16.5)	130.3 (16.2)
Serum potassium, mmol/L	4.60 (0.46)	4.64 (0.48)	4.64 (0.52)
Median UACR	577.0 (279.5–1150.6)	526.7 (212.1–1287.0)	566.8 (235.6–1202.7)
UACR >1000, mg/g	58 (33%)	32 (35%)	55 (31%)
Type 2 diabetes	105 (59%)	52 (57%)	104 (58%)
Chronic kidney disease cause			
Cystic kidney disease	1 (<1%)	0	3 (2%)
Type 2 diabetes and chronic kidney disease	93 (53%)	44 (48%)	88 (49%)
Ischaemic or hypertensive nephropathy	32 (18%)	20 (22%)	30 (17%)
Chronic glomerulonephritis	20 (11%)	10 (11%)	25 (14%)
IgA nephropathy	7 (4%)	4 (4%)	8 (4%)
Other	13 (7%)	6 (7%)	17 (9%)
Unknown	13 (7%)	11 (12%)	19 (11%)
Other	17 (10%)	6 (7%)	14 (8%)
Family history of premature cardiovascular disease	38 (21%)	12 (13%)	38 (21%)
Heart failure	17 (10%)	3 (3%)	11 (6%)
Previous medication			
ACE inhibitor	56 (32%)	33 (36%)	58 (32%)
ARB	98 (55%)	48 (53%)	96 (54%)
Diuretic	75 (42%)	36 (40%)	61 (34%)
Calcium-channel blocker	91 (51%)	47 (52%)	88 (49%)
β blocker	56 (32%)	41 (45%)	67 (37%)
Statin	125 (71%)	60 (66%)	130 (73%)

Data are n (%), mean (SD), or median (IQR). ACE=angiotensin-converting enzyme. ARB=angiotensin receptor blocker. eGFR=estimated glomerular filtration rate. UACR=urinary albumin-to-creatinine ratio.

Table 1: Baseline demographic and clinical characteristics

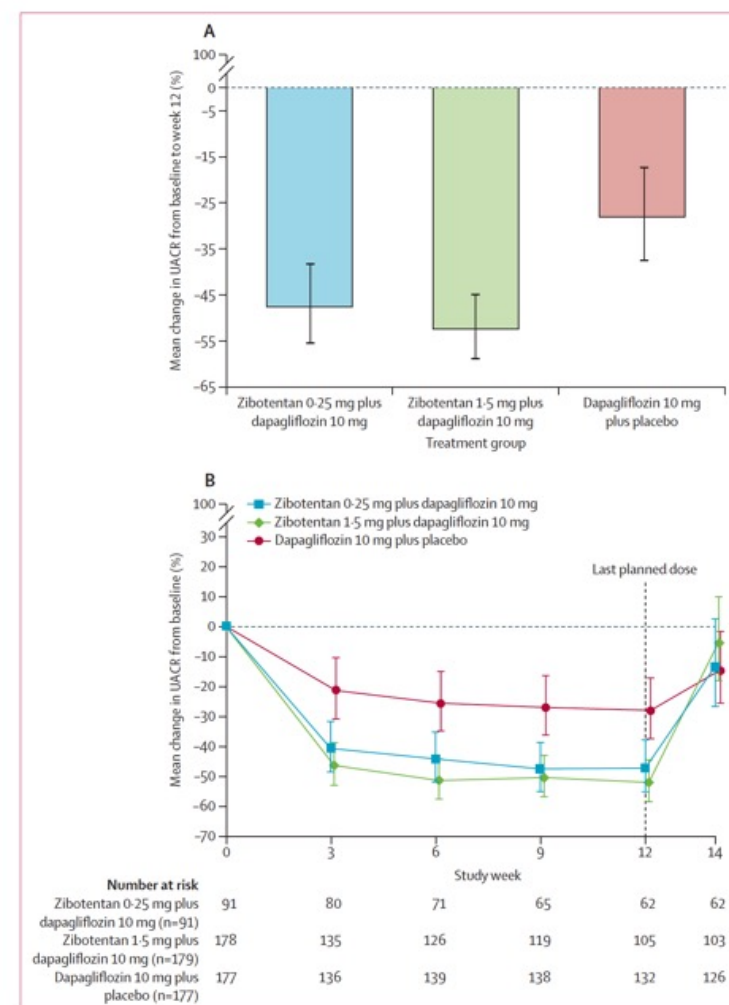


Figure 2: Mean change in UACR

(A) Bar graph of the percentage mean change in UACR from baseline to week 12 in the dapagliflozin 10 mg plus placebo, zibotentan 1.5 mg plus dapagliflozin 10 mg, and zibotentan 0.25 mg plus dapagliflozin 10 mg groups. (B) UACR trajectory over time in the three treatment groups. Vertical bars indicate the 90% CIs of the mean at given timepoints. UACR=urinary albumin-to-creatinine ratio.

SBP

DPB

eGFR

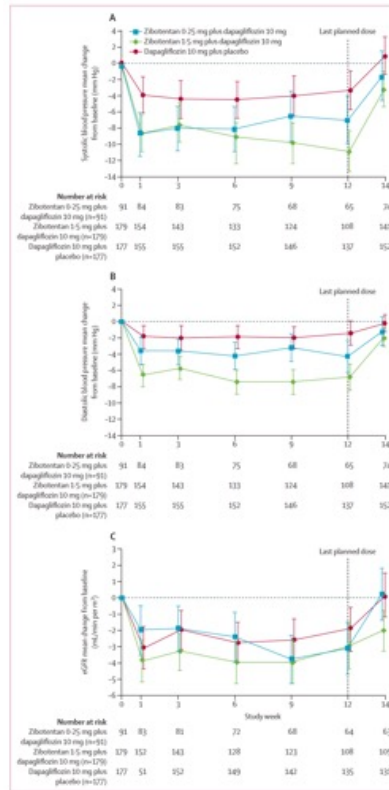


Figure 3: Mean change from baseline in systolic blood pressure, diastolic blood pressure, and eGFR
 (A) Mean change from baseline in systolic blood pressure in the three treatment groups. (B) Mean change from baseline in diastolic blood pressure in the three treatment groups. (C) Mean eGFR change from baseline in the three treatment groups. Vertical bars indicate the 90% CIs of the mean at given timepoints. eGFR=estimated glomerular filtration rate.

ICF

BWT

ECF

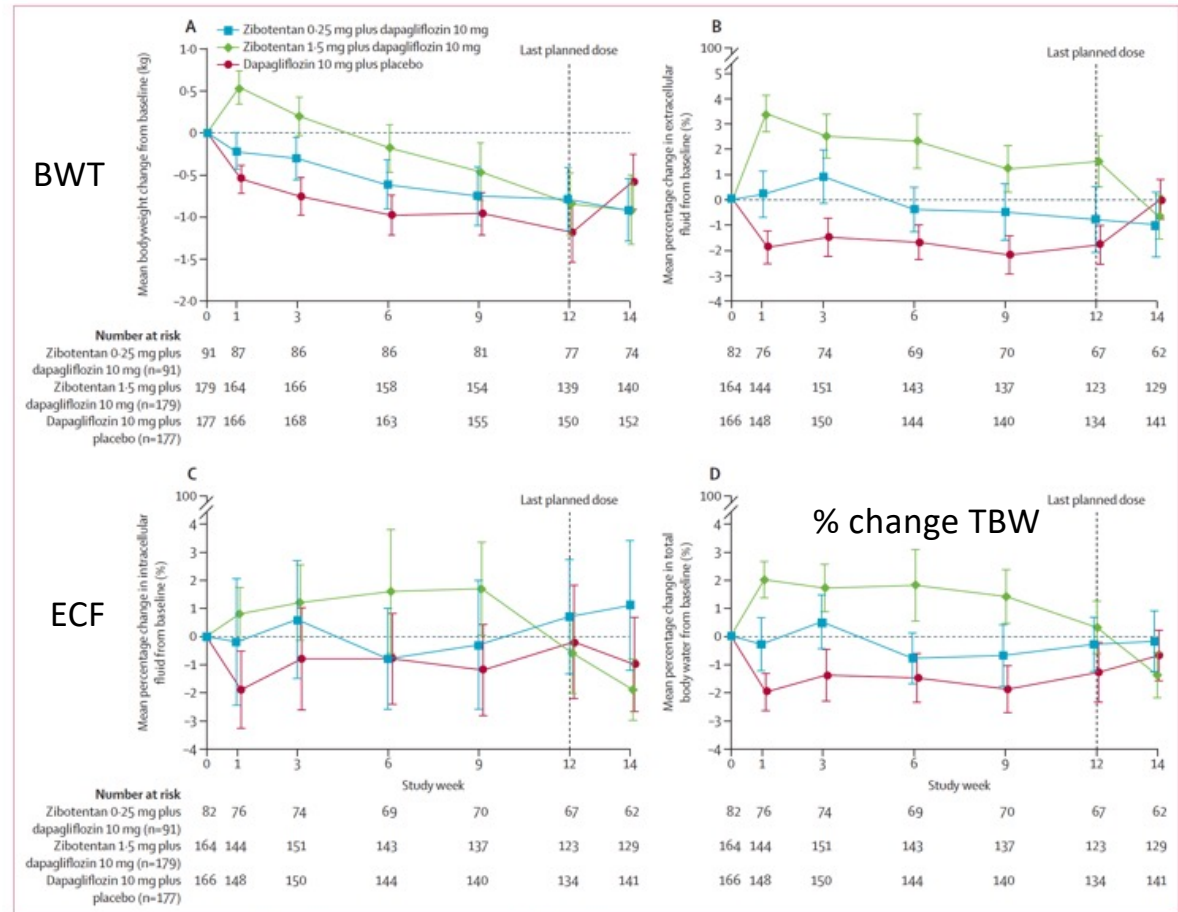


Figure 4: Mean change from baseline in bodyweight, extracellular fluid, intracellular fluid, and total body water
 (A) Mean bodyweight change from baseline. (B) Mean percentage change in extracellular fluid. (C) Mean percentage change in intracellular fluid. (D) Mean percentage change in total body water from baseline. Vertical bars indicate the 90% CIs of the mean at given timepoints.

	Dapagliflozin 10 mg plus placebo (n=177)	Zibotentan 0.25 mg plus dapagliflozin 10 mg (n=91)	Zibotentan 1.5 mg plus dapagliflozin 10 mg (n=179)
Any adverse event	66 (37%)	45 (49%)	85 (47%)
Adverse events leading to drug discontinuation*	7 (4%)	11 (12%)	22 (12%)
BNP increase	1 (<1%)	2 (2%)	6 (3%)
Fluid retention	1 (<1%)	1 (1%)	4 (2%)
Peripheral oedema	0	1 (1%)	3 (2%)
Hypotension	1 (<1%)	1 (1%)	1 (<1%)
Serious adverse events	4 (2%)	2 (2%)	9 (5%)
Adverse events of clinical interest			
Headache	2 (1%)	6 (7%)	8 (4%)
Metabolic acidosis	2 (1%)	4 (4%)	7 (4%)
BNP increase	1 (<1%)	2 (2%)	9 (5%)
Hypertension	1 (<1%)	5 (5%)	0
Fluid retention	1 (<1%)	1 (1%)	5 (3%)
Peripheral oedema	1 (<1%)	4 (4%)	7 (4%)
Death	1 (<1%)	0	0

Data are number of patients (%). All adverse events and serious adverse events were reported by participating investigators and collected without further adjudication. BNP=B-type natriuretic peptide. *Only adverse events leading to drug discontinuation that occurred in more than two participants are reported. One case reported as an adverse event in the zibotentan 0.25 mg plus dapagliflozin 10 mg group was classified as an adverse event on the basis of a follow-up echocardiogram showing a reduction in ejection fraction from 52% to 28%. This patient's baseline electrocardiogram was left bundle branch block; a within-study silent myocardial infarction cannot be excluded as the cause of reduction in ejection fraction.

Table 2: Number of participants with adverse events (safety analysis set)

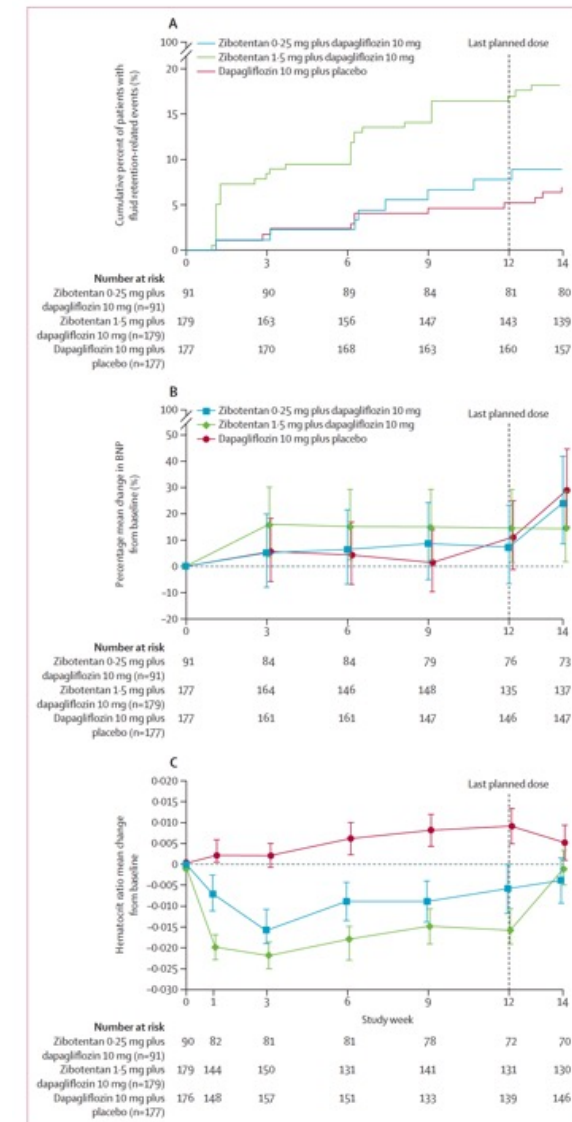
Figure 5: Kaplan-Meier curves of fluid retention and change from baseline in BNP and haematocrit ratio

(A) Kaplan-Meier curve of fluid retention. (B) Percentage mean change in BNP from baseline. (C) Mean haematocrit ratio change from baseline over time. Vertical bars indicate the 90% CIs of the mean at given timepoints. BNP=B-type natriuretic peptide.

Fluid Retention Events

BNP

HCT



Research in context

Evidence before this study

We searched PubMed for randomised controlled trials published between Jan 1, 2010, and Feb 1, 2023, with the terms “chronic kidney disease” AND “albuminuria” AND “endothelin receptor antagonist” AND “randomized controlled trial”.

Clinical-practice guidelines recommend renin-angiotensin-system inhibitors and SGLT2 inhibitors to slow the progression of kidney function decline in patients with chronic kidney disease. Despite these guideline-recommended therapies, progressive loss of kidney function occurs in many patients and is associated with persistently high albuminuria. Novel albuminuria lowering therapies might further slow chronic kidney disease progression. Increased expression of endothelin-1 might contribute to the progression of chronic kidney disease through several pathophysiological effects, including injury to the vasculature, podocytes, tubulointerstitium, and mesangium. In the SONAR trial, the endothelin receptor antagonist atrasentan slowed decline of kidney function in adults with type 2 diabetes. In people with immunoglobulin A nephropathy or focal segmental glomerulosclerosis, the dual endothelin angiotensin receptor antagonist sparsentan reduced proteinuria. High doses of non-selective endothelin receptor antagonists increase risk of fluid retention, which can lead to heart failure. Because SGLT2 inhibitors exert natriuretic and diuretic effects, combining an SGLT2 inhibitor with a selective endothelin receptor antagonist holds promise to augment nephroprotection while potentially mitigating fluid retention. Zibotentan is a highly selective endothelin receptor antagonist originally developed for the treatment of prostate cancer. We aimed to characterise the effects of zibotentan plus dapagliflozin versus dapagliflozin plus placebo on albuminuria and fluid retention to select the appropriate zibotentan dose for further investigation in clinical outcome trials.

Added value of this study

ZENITH-CKD, an international, randomised, double-blind, active-controlled clinical trial, is the first prospective study of a fixed-dose combination of an endothelin receptor antagonist (zibotentan) with an SGLT2 inhibitor (dapagliflozin) on top of maximum tolerated renin-angiotensin-system inhibition (if tolerated) in adults with chronic kidney disease. The primary albuminuria efficacy endpoint showed that 12-week treatment with low doses of 0.25 mg/day and 1.5 mg/day zibotentan in combination with dapagliflozin 10 mg/day led to meaningful and statistically significant reductions in albuminuria versus dapagliflozin 10 mg/day plus placebo. The reduction in albuminuria was greater for zibotentan and dapagliflozin compared with dapagliflozin plus placebo from the first post-randomisation assessment at week 3 until week 12. The albuminuria levels returned to baseline values 2 weeks after discontinuation of study medication. No clinically meaningful changes in B-type natriuretic peptide, bodyweight, or total body water, as proxies for fluid retention, were observed during 12 weeks of treatment with zibotentan 0.25 mg plus dapagliflozin, whereas modest increases were observed in these parameters with zibotentan 1.5 mg plus dapagliflozin compared with dapagliflozin plus placebo.

Implications of all the available evidence

The ZENITH-CKD trial showed the safety and efficacy of combining a low dose of the selective endothelin receptor antagonist zibotentan with dapagliflozin in adults with chronic kidney disease. The results showed a robust and clinically meaningful reduction in albuminuria and an acceptable safety profile. These findings support the conduct and inform the design of a long-term phase 3 clinical trial to show the efficacy and safety of zibotentan plus dapagliflozin in reducing the risk of kidney failure in patients with chronic kidney disease and increased albuminuria.

Difficulty diagnosing oral cancer: seeking an early specialist opinion is key

A 95-year-old woman attended our oral medicine department reporting a painful white plaque on the left margin of her tongue. The patient had been seen by her dentist 8 months earlier, who concluded that the small, nodular, white patch (figure), opposite a broken tooth, had been caused by trauma; he polished the broken tooth and arranged no follow-up appointments. However, 8 months later, the patient went back to her dentist because of persistent pain; the white patch had progressed, and the dentist referred her to us.

The patient had a history of hypertension treated with candesartan; she reported no tobacco use or alcohol consumption.

On examination, she was generally well; in her mouth the original white plaque had developed an ulcerated lichenoid appearance, and three new plaques were present on her tongue (figure). Regional lymph nodes in the neck were not palpable. Two biopsies were taken and each examined at three levels: the first showed squamous cell carcinomatous proliferation—essentially in situ, locally ulcerated, with focal budding of the basal layer and micro-infiltrative subepithelial small clumps or squamous epithelial cells (figure); the second biopsy found an acanthotic leukokeratotic mucosa with sparse subepithelial lymphocytic inflammation, and a few apoptotic bodies (figure). Well differentiated micro-invasive squamous cell carcinoma of the tongue was diagnosed. The second biopsy also showed lichenoid inflammation.

The patient had a partial glossectomy and a sentinel lymph node biopsy which showed no signs of metastasis; no adjuvant treatment was indicated. At her last follow-up 1 year after surgery, the patient was in clinical remission.

Late diagnosis of oral cancers—as with many malignancies—results in poorer prognosis. Notably, oral traumatic lesions typically resolve within 4 weeks once the causative agent is removed.

All new oral white and red patches, whether they appear malignant or not, should be monitored and investigated. Importantly, any plaque, patch, ulcer, lump, or anything that appears atypical needs to be explored and the aetiology found; many head and neck cancers present initially with lesions in the oral cavity. The persistence of pain and any persistent or progressive lesion should be biopsied to avoid missing an oral squamous cell carcinoma or misdiagnosing a lesion that appears to be benign. The National Institute for Health and Care Excellence (NICE), in the UK, guidelines recommend that any non-healing oral ulcer or a lump on the tongue should be referred to a specialist so that patients with a suspected cancer are seen within 2 weeks.

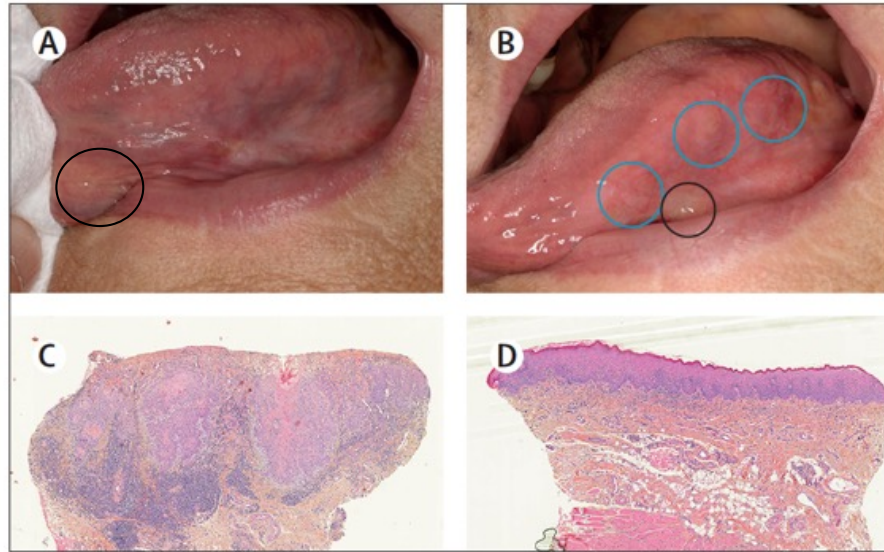


Figure: Difficulty diagnosing oral cancer: seeking an early specialist opinion is key

(A) Photograph shows small nodular white plaque on the left margin of the tongue at time of initial presentation. (B) Photograph shows original white plaque with an ulcerated lichenoid appearance (circled in black), and new lingual plaques (circled in blue). (C) Histopathological examination of biopsy samples shows squamous cell carcinomatous proliferation—essentially in situ—locally ulcerated, with focal budding of the basal layer and micro-infiltrative subepithelial small clumps of cells (C); and an acanthotic leukokeratotic mucosa with sparse subepithelial lymphocytic inflammation, and a few apoptotic bodies (D); haematoxylin and eosin stain. Original magnification x10.

Rheumatoid arthritis

Rheumatoid arthritis is a chronic, systemic, autoimmune inflammatory disease that mainly affects the joints and periarticular soft tissues. In this Seminar, we provide an overview of the main aspects of rheumatoid arthritis. Epidemiology and advances in the understanding of rheumatoid arthritis pathogenesis will be reviewed. We will discuss the clinical manifestations of rheumatoid arthritis, classification criteria, and the value of imaging in the diagnosis of the disease. The advent of new medications and the accumulated scientific evidence demand continuous updating regarding the diagnosis and management, including therapy, of rheumatoid arthritis. An increasing number of patients are now able to reach disease remission. This major improvement in the outcome of patients with rheumatoid arthritis has been determined by a combination of different factors (eg, early diagnosis, window of opportunity, treat-to-target strategy, advent of targeted disease-modifying antirheumatic drugs, and combination therapy). We will discuss the updated recommendations of the two most influential societies for rheumatology worldwide (ie, the American College of Rheumatology and European Alliance of Associations for Rheumatology) for the management of rheumatoid arthritis. Furthermore, controversies (ie, the role of glucocorticoids in the management of rheumatoid arthritis and safety profile of Janus kinase inhibitors) and outstanding research questions, including precision medicine approach, prevention, and cure of rheumatoid arthritis will be highlighted.

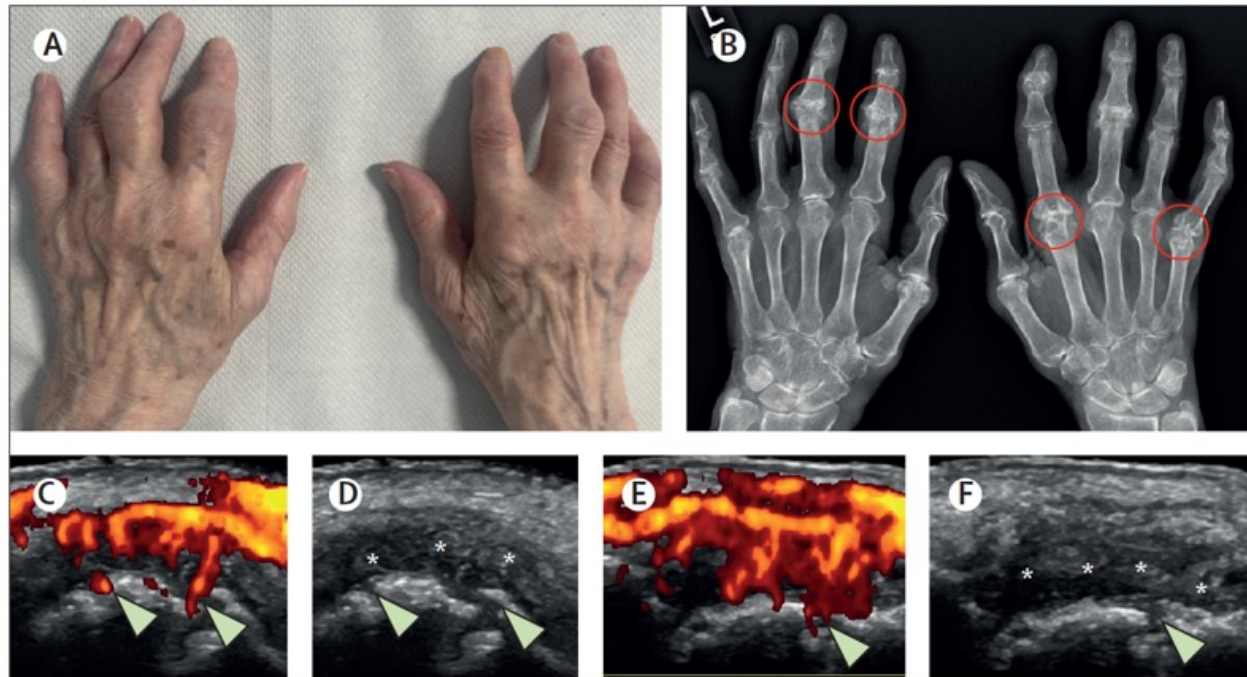


Figure 1: Long-standing rheumatoid arthritis

(A) Polyarticular synovitis and joint deformities are shown in the hands of a patient with long-standing rheumatoid arthritis (ie, >20 years disease duration). (B) X-rays show diffuse structural damage (ie, severe cartilage loss and bone erosions in multiple metacarpophalangeal and proximal interphalangeal joints bilaterally), with complete loss of normal joint architecture (ie, ulnar deviation, joint subluxation, and multiple bone erosions) in the metacarpophalangeal and proximal interphalangeal joints (red circles). A longitudinal ultrasonography scan of the medial aspect of the second right metacarpophalangeal joint (C, D) and second left metacarpophalangeal joint (E, F) shows diffuse synovial hypertrophy (asterisks) and large bone erosions (arrows) in the metacarpal head filled with power doppler signal (intrasynovial red spots), indicating active synovitis (ie, bone erosions).

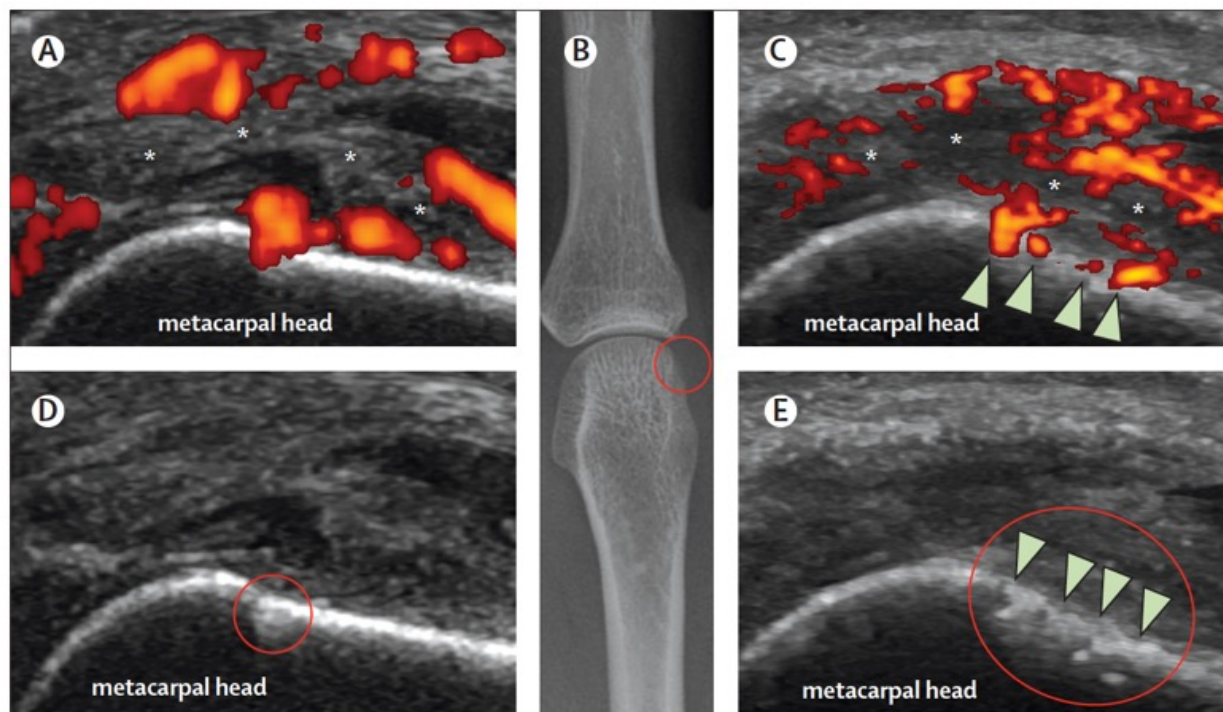


Figure 2: Conventional radiography and ultrasonography findings in early rheumatoid arthritis

Longitudinal ultrasonography (A, C-E) and x-rays (B) of the right third metacarpophalangeal joint in a patient with early rheumatoid arthritis (ie, disease duration of 16 weeks). The ultrasonography images, which were done with a 15 MHz (A, D) and 18 MHz (C, E) probe, show synovial hypertrophy (A, C; asterisks) and diffuse power doppler signal (D, E; red circles), indicating active inflammation. High-frequency probes (ie, 18 MHz probe) provide a detailed morphological evaluation of the superficial structures. In this patient, loss of sharpness of the bony cortex, suggestive for a pre-erosive change, can be seen (E; arrows). The presence of highly vascularised synovial hypertrophy (C, E; asterisks and red circles) is visible in close contact with the bone surface (C; arrows). No abnormality was reported in the x-rays of this patient (D).

	Target	Route of administration (dose)	Adverse events	Management of rheumatoid arthritis
Glucocorticoids	Genomic and non-genomic pathways	Oral, intramuscular, intravenous, intra-articular (dose depends on route of administration and clinical indication)	Depending on dose and duration of therapy; diabetes, hypertension, infections, gastrointestinal diseases, skin atrophy, psychiatric, osteoporosis, and ophthalmological diseases (eg, cataract and glaucoma)	Bridging therapy when DMARD therapy is initiated or switched and treating flares; in some patients is sometimes used as a long-term maintenance therapy (similar to a DMARD)
Conventional synthetic DMARDs	--	--	--	First-line therapy in patients who are naive to DMARDs
Methotrexate	Unknown	Oral, subcutaneous, intramuscular (10–25 mg/week)	Gastrointestinal, increased liver enzymes, bone marrow suppression, stomatitis, hair loss, teratogenicity, and interstitial pneumonitis	First choice among conventional synthetic DMARDs
Sulfasalazine	Unknown	Oral (2–3 g/day)	Gastrointestinal, skin rash, temporary oligospermia, and drug-induced systemic lupus erythematosus	Combination therapy with methotrexate (or monotherapy if methotrexate is contraindicated)
Leflunomide	Dihydroorotate dehydrogenase	Oral (20 mg/day)	Gastrointestinal, increased liver enzymes, leukopenia, hypertension, and teratogenicity	Monotherapy if methotrexate is contraindicated (combination therapy with methotrexate uncommon)
Hydroxychloroquine	Unknown	Oral (200–400 mg/day)	Gastrointestinal, skin rash, and retinopathy	Combination therapy with methotrexate (or monotherapy if methotrexate is contraindicated in patients with low disease activity)
Targeted synthetic DMARDs (ie, JAK inhibitors)	--	--	Gastrointestinal, infections, colonic perforation, increased creatinine kinase concentrations, tuberculosis or herpes zoster reactivation, cytopenia, increased risk of venous thromboembolism, and lipid abnormalities	In patients who have had at least one conventional synthetic DMARD, after at least one TNF inhibitor (ACR), or as first-line therapy (EULAR) in selected populations*; might have some advantages in monotherapy compared with other biological DMARDs
Tofacitinib	JAK 1,2,3	Oral (10 mg/day)	Possible increased risk of major adverse cardiovascular event and neoplasm (especially in smokers and people older than 65 years)	--
Baricitinib	JAK 1,2	Oral (2–4 mg/day)	--	--
Upatacitinib	JAK 1,2†	Oral (15 mg/day)	--	--
Filgotinib	JAK 1	Oral (200 mg/day)	--	--
Biological DMARDs	--	--	--	First-line therapy in patients who have had at least one unsuccessful conventional synthetic DMARD
TNF inhibitors	--	--	Infections, tuberculosis reactivation, cytopenia, drug-induced systemic lupus erythematosus, non-melanoma skin cancer, demyelinating syndromes, congestive heart failure, and infusion or injection-related reactions	Commonly used as first-line therapy among biological DMARDs
Adalimumab	TNF	Subcutaneous (40 mg every 2 weeks)	--	--
Etanercept	TNF	Subcutaneous (50 mg/week)	--	--
Golimumab	TNF	Intravenous (2 mg/kg at week 0, 4, and every 8 weeks); subcutaneous (50 mg every 4 weeks)	--	--
Certolizumab pegol	TNF	Subcutaneous (400 mg at week 0, 2, and 4, then 200 mg every 2 weeks)	--	--
Infliximab	TNF	Intravenous (3 mg/kg at week 0, 2, and 6, and every 8 weeks); subcutaneous (120 mg every 2 weeks)	--	--

(Table continues on next page)

	Target	Route of administration (dose)	Adverse events	Management of rheumatoid arthritis
(Continued from previous page)				
Anti-B cell	In patients, who have had at least one conventional synthetic DMARD, usually after TNF inhibitors; ACR suggests use after inadequate response to TNF inhibitors or in patients with history of lymphoproliferative disorder
Rituximab	CD20	Intravenous (1–2 g every 6 months)	Infusion reactions, reduced response to vaccines, infections, hepatitis B reactivation, and progressive multifocal leukoencephalopathy	..
Anti T-cell co-stimulation	First-line therapy in patients who have had at least one unsuccessful biological or conventional synthetic DMARD
Abatacept	CD80–CD86 co-stimulation	Intravenous (500–1000 mg, depending on weight, at week 0, 2, and 4 and then every 4 weeks); subcutaneous (125 mg/week)	Infections, infusion or injection site reaction, reduced response to vaccines, tuberculosis reactivation, and leukopenia	..
Anti-IL-6	Infections, colonic perforation, lipid abnormalities, cytopenia, liver enzyme elevations, and infusion or injection-related reactions	First-line therapy in patients who have had at least one conventional synthetic DMARD; might have some advantages compared with biological DMARDs in monotherapy
Tocilizumab	IL-6 receptor	Intravenous (4–8 mg/kg every 4 weeks, max 800 mg); subcutaneous (162 mg/week)
Sarilumab	IL-6 receptor	Subcutaneous (150–200 mg every 2 weeks)
<p>Anakinra is approved for the treatment of rheumatoid arthritis in the USA and Europe; however, clinical trials showed modest therapeutic effects in rheumatoid arthritis, and it is not mentioned in EULAR and ACR recommendations. ACR=American College of Rheumatology. DMARD=disease-modifying antirheumatic drug. EULAR=European Alliance of Associations for Rheumatology. JAK=Janus kinase. TNF=tumour necrosis factor. *Risk factors for cardiovascular events and malignancies to consider before prescribing a JAK inhibitor: age older than 65 years, previous or current smoking, diabetes, obesity, hypertension, current or previous malignancy (other than non-melanoma skin cancer), and risk factors for thromboembolic events (eg, history of myocardial infarction or heart failure, history of blood clots or inherited disorders of coagulation, combined contraceptives or hormonal replacement therapy, immobility, and undergoing major surgery). †Various assays showed different specificities for JAK 2 inhibition.</p>				
<p>Table: Main characteristics of glucocorticoids, conventional synthetic DMARDs, biological DMARDs, and targeted synthetic DMARDs, which are approved for the treatment of rheumatoid arthritis in the USA and Europe</p>				

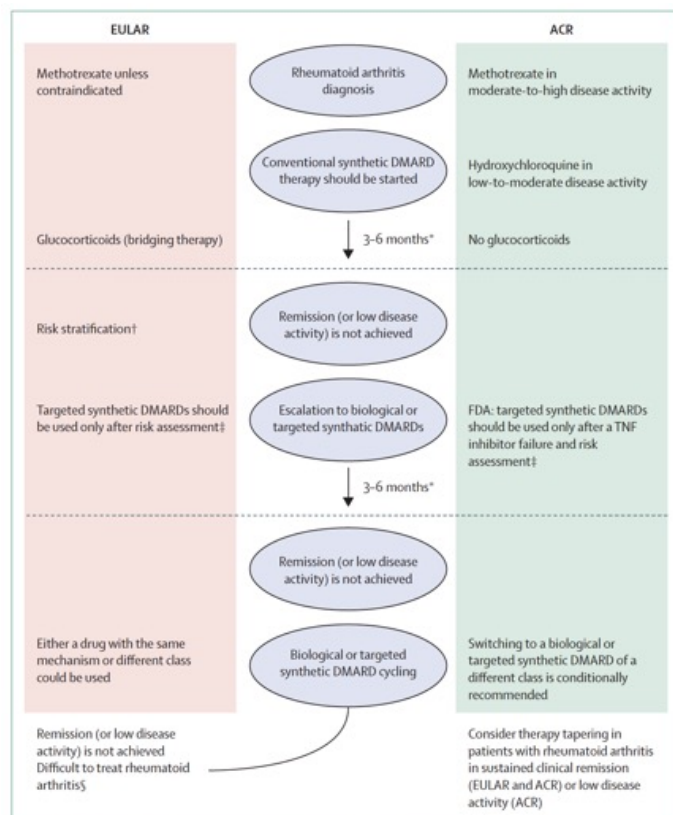


Figure 3: The therapeutic management of rheumatoid arthritis according to ACR and EULAR guidelines and recommendations
 ACR=American College of Rheumatology. DMARD=disease-modifying antirheumatic drugs. EULAR=European Alliance of Associations for Rheumatology. FDA=US Food and Drug Administration. TNF=tumour necrosis factor.
 *Treatment target is remission (according to the ACR and EULAR definition) or low disease activity at 6 months. According to EULAR, therapy should be adapted if 50% improvement is not reached at 3 months. †In the presence of poor prognostic factors (eg, autoantibodies, high disease activity, bone erosion, and two ineffective conventional synthetic DMARDs), a biological or targeted synthetic DMARD should be added. Otherwise, another conventional synthetic DMARD should be considered. ‡Risk factors for cardiovascular events and malignancies to consider before prescribing a Janus kinase inhibitor are age older than 65 years, previous or current smoking, diabetes, obesity, hypertension, current or previous malignancy (other than non-melanoma skin cancer), and risk factors for thromboembolic events (eg, history of myocardial infarction or heart failure, history of blood clots or inherited disorders of coagulation, combined contraceptives or hormonal replacement therapy, immobility, and undergoing major surgery). §In patients with difficult-to-treat rheumatoid arthritis, after two or more ineffective biological or targeted synthetic DMARDs (particularly TNF inhibitors), a biological or targeted synthetic DMARD with a different target (ie, mechanism of action) should be considered.



Figure 4: Patients with difficult-to-treat rheumatoid arthritis and different sonographic scenarios
 Photographs of two patients with difficult-to-treat rheumatoid arthritis (A, B) and associated ultrasonography scenarios (C, D). Both patients had at least one ineffective conventional synthetic DMARD, at least two ineffective biological DMARDs with different mechanisms of action, a DAS-28 C-reactive protein of more than 3.2, and reduced quality of life related to rheumatoid arthritis disease activity at the time of the clinical visit. The patients were not on glucocorticoids. The metacarpophalangeal joints (A, B; red circles) were swollen and painful on clinical examination. In both patients, intra-articular synovial hypertrophy could be seen on ultrasonography (C, D; asterisks). Although there is evidence of diffuse power doppler signal (C; red areas) indicating active inflammation in one patient, the ultrasonography features of the second patient suggest advanced structural damage (D; arrowheads), mainly involving the metacarpal head (ie, joint subluxation and multiple bone erosions). In addition, no power doppler signal is detectable (D) but an area of joint effusion (D; white dots), together with the bony deformity involving the metacarpal head, could cause the clinical swelling. The presence of power doppler signal could indicate a persistent inflammatory process, which would be useful to identify persistent inflammatory refractory rheumatoid arthritis. Alternatively, chronic joint damage rather than active inflammation could explain the clinical signs and symptoms of the patient (D; non-inflammatory refractory rheumatoid arthritis). However, further studies are needed to define the prognostic value and implications of the different ultrasonography abnormalities in the population with difficult-to-treat rheumatoid arthritis. DAS-28=Disease Activity Score using 28 joints. DMARD=disease-modifying antirheumatic drug.

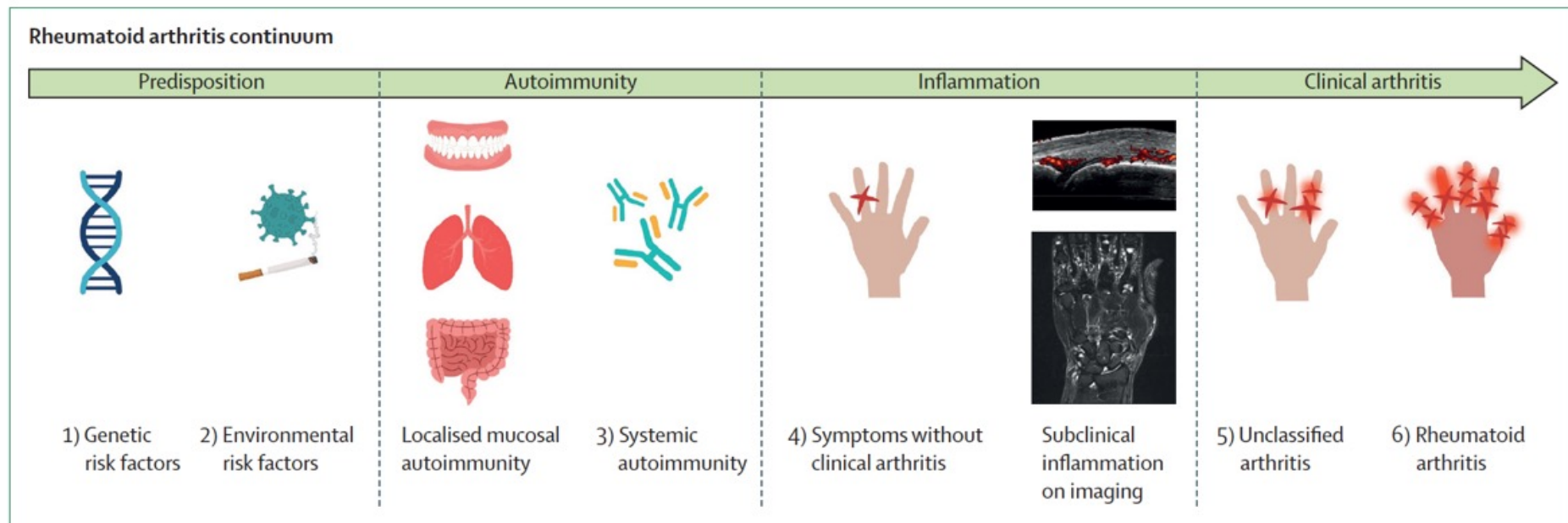


Figure 5: The rheumatoid arthritis continuum: an overview of the rheumatoid arthritis preclinical phase

Six stages along the rheumatoid arthritis continuum were defined in 2012 by the European Alliance of Associations for Rheumatology Committee on Investigative Rheumatology: (1) genetic risk factors for rheumatoid arthritis, (2) environmental risk factors for rheumatoid arthritis, (3) systemic autoimmunity associated with rheumatoid arthritis, (4) musculoskeletal symptoms without clinical arthritis, (5) unclassified arthritis, and (6) rheumatoid arthritis.¹²³ The phases do not necessarily occur in all patients (ie, seronegative rheumatoid arthritis) or in the same order in all patients. Increasing evidence suggests that systemic autoimmunity is preceded by a phase of mucosal dysbiosis with localised production of antibodies related to rheumatoid arthritis, mainly in the oral, lung, or gut mucosa (ie, localised mucosal autoimmunity). In addition, several studies have shown that a large proportion of patients with rheumatoid arthritis go through a stage of subclinical synovitis on imaging (eg, ultrasonography or MRI), which is, in people at high risk, associated with a substantial increase in the risk of progression to inflammatory arthritis (ie, subclinical inflammation on imaging).

Conclusions

The management and outcomes of patients with rheumatoid arthritis have drastically improved in the last two decades. The recommendations for managing rheumatoid arthritis are changing rapidly, due to newly developed therapies and evolving scientific evidence. In this Seminar, the new ACR and EULAR recommendations are discussed, the controversies regarding the use of glucocorticoids and the uncertainty around JAK inhibitors have been highlighted, and the approaches to tapering therapy in patients who are in remission have been outlined. There is a clear need for reliable biomarkers for diagnosis, prognosis, and especially for response to therapy due to a proportion of patients not responding to multiple biological or targeted synthetic DMARDs. New areas of research have been illustrated, including difficult-to-treat rheumatoid arthritis, precision medicine, and attempts to delay or prevent arthritis.

CAR T-cell therapy in autoimmune diseases

Despite the tremendous progress in the clinical management of autoimmune diseases, many patients do not respond to the currently used treatments. Autoreactive B cells play a key role in the pathogenesis of autoimmune diseases, such as systemic lupus erythematosus, rheumatoid arthritis, and multiple sclerosis. B-cell-depleting monoclonal antibodies, such as rituximab, have poor therapeutic efficacy in autoimmune diseases, mainly due to the persistence of autoreactive B cells in lymphatic organs and inflamed tissues. The adoptive transfer of T cells engineered to target tumour cells via chimeric antigen receptors (CARs) has emerged as an effective treatment modality in B-cell malignancies. In the last 2 years treatment with autologous CAR T cells directed against the CD19 antigen has been introduced in therapy of autoimmune disease. CD19 CAR T cells induced a rapid and sustained depletion of circulating B cells, as well as in a complete clinical and serological remission of refractory systemic lupus erythematosus and dermatomyositis. In this paper, we discuss the evolving strategies for targeting autoreactive B cells via CAR T cells, which might be used for targeted therapy in autoimmune diseases.

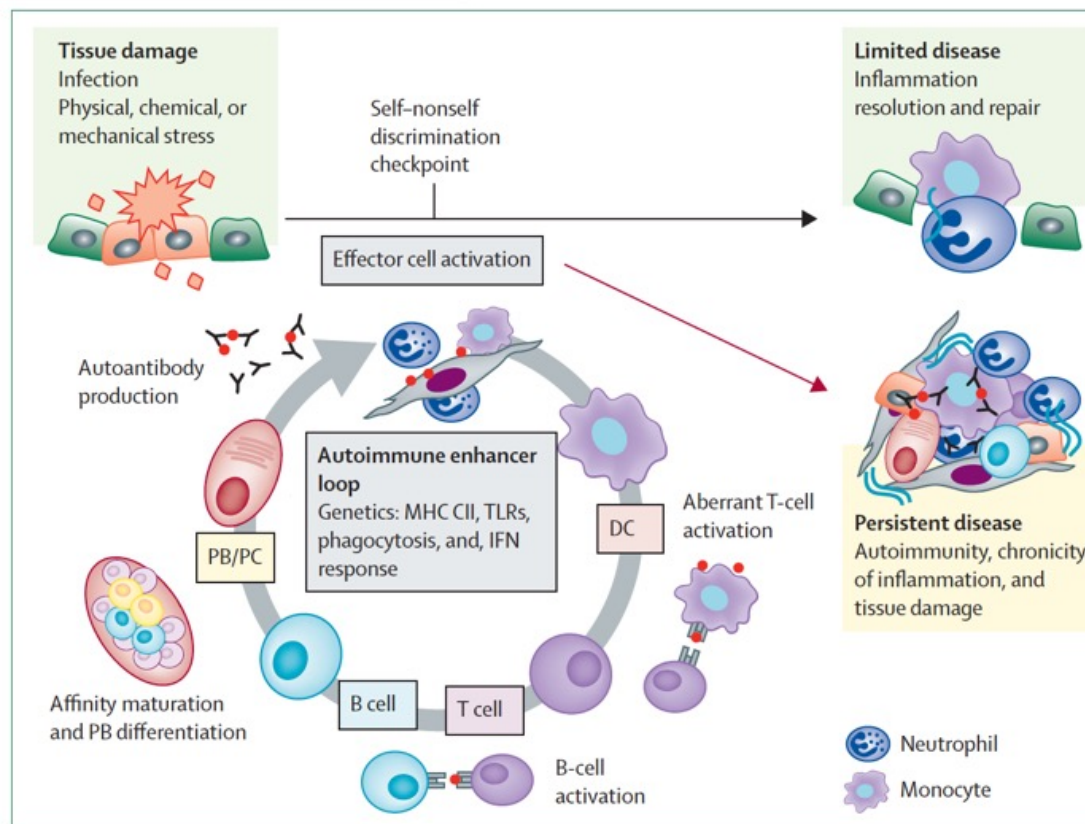


Figure 1: Autoimmune loop of triggering chronic inflammation and tissue damage

Tissue damage leads to a fast but time-limited inflammatory response that is orchestrated by neutrophils and monocytes (effector cell activation). The inflammatory response usually resolves and results in a tissue repair process. In case of sensitisation to self, an autoimmune loop starts that is characterised by auto-antigen presentation by dendritic cells, auto-reactive T-cell activation, affinity maturation of B cells, and plasmablast-mediated autoantibody production. Autoantibodies cause sustained activation of effector cells and tissue damage. This autoimmune loop, once initiated, leads to persistence of the autoimmune disease. Conventional treatments mitigate this loop but do not break it. PB/PC=plasmablast or plasma cell. DC=dendritic cell. MHC CII=major histocompatibility class II complex. TLRs=toll-like receptors IFN=interferon.

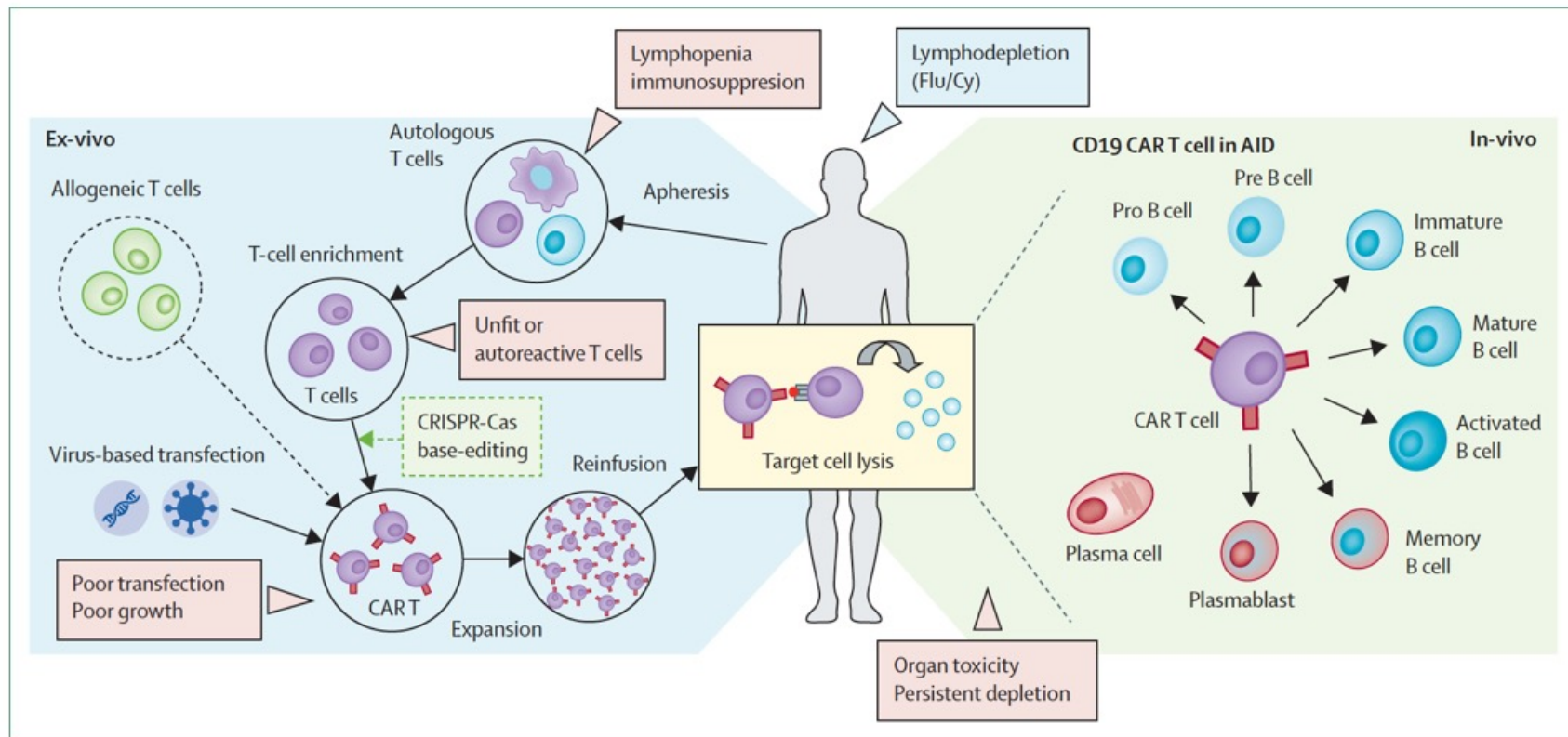


Figure 2: Principle of treatment with autologous CART T cells

Leukocytes are collected from the patients' peripheral blood by apheresis. To ensure an immediate access to the cell product and avoid possible dysfunctions of the donor T cells (eg, chemotherapy-induced toxicity, or autoreactive clones), allogeneic off-the-shelf concepts are currently being developed. Next, lymphocytes are transduced with a lentiviral vector encoding the CAR followed by an in-vitro expansion. Virus-free approaches currently being explored include CRISPR-Cas gene editing and base-editing. In autoimmune disease, CARs against B cells are used, which target the B-cell-specific surface molecule CD19. After expansion and a preparatory lymphodepleting chemotherapy, usually with the use of a combination of Flu and Cy, CART T cells are reinfused into the patients, where they further expand and eliminate all CD19-expressing B cells. CD19 negative cells (among them the long-lived plasma cells in the bone marrow) are spared from CART T-cell-mediated cytotoxicity. AID=autoimmune disease. CAR=chimeric antigen receptor. Cy=Cyclophosphamide. Flu=Fludarabine.


B-cell lineage differentiation 								
Tumour cells antigen	Pro B cell	Prä B cell	Imm B B cell	Mature B cell	Memory B cell	Plasma blast	Plasma cell	Target
CD19								B cell
CD20								Bcell
CD22								B cell
BCMA								PC
CD38								PC
CD138								PC

Figure 3: Surface antigen expression of the B-cell lineage

B-cell lineage differentiation from early-stage (left) to late-stage cells (right).

Expression of respective markers is indicated by the coloured rectangle.

BCMA=B-cell maturation antigen. Imm=immature. PC=plasma cell

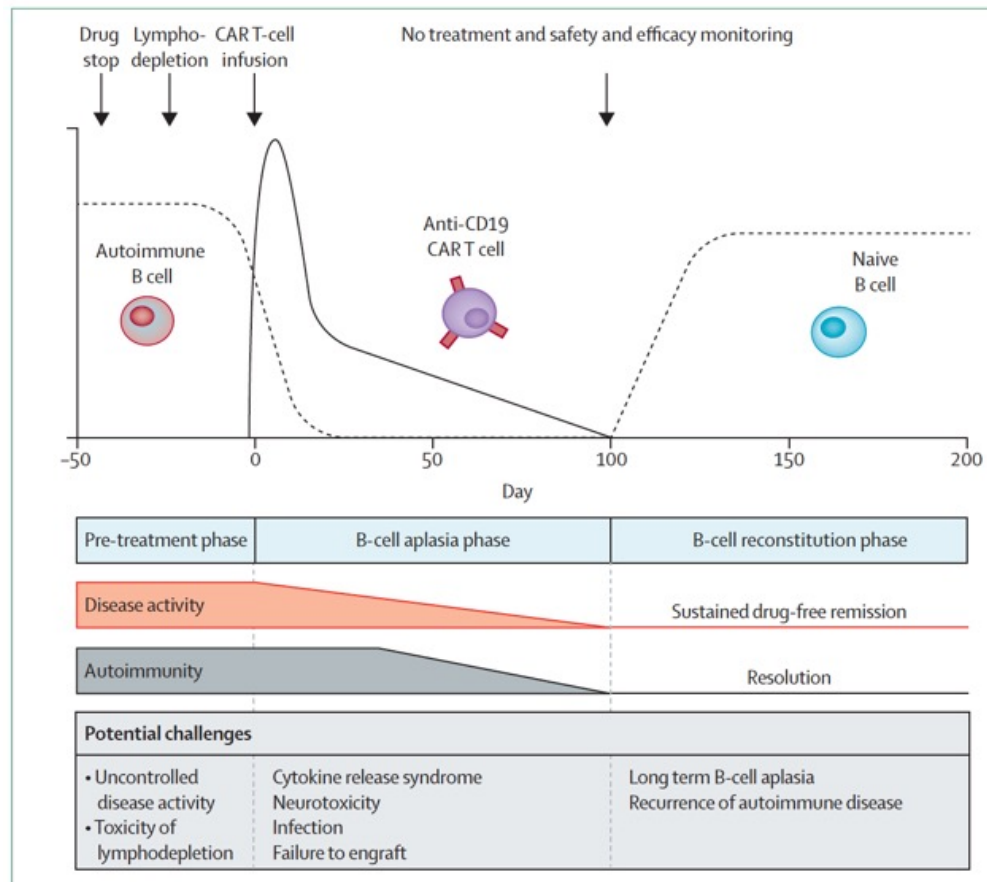


Figure 4: Phases and challenges of treatment with autologous CART cells in autoimmune diseases

The pre-treatment phase consists of cessation of immunosuppressive treatment, leukapheresis, and lymphodepleting chemotherapy (conditioning), before CART cells are infused. This phase is followed by B-cell aplasia, which is characterised by expansion of CART T cells. B cells then recur, and the B-cell pool is reconstituted. During aplasia disease activity (clinical, laboratory, and imaging signs of inflammation) decreases, autoimmunity (autoantibodies) resolves, and a phase of drug-free remission follows. The length of drug-free remission is unknown, but it is possible for some patients to be fully cured of their disease. Potential challenges of CART T-cell therapy are summarised with respect to the different phases of treatment.

Conclusions

CAR T cells have been successfully introduced into the treatment of autoimmune diseases.⁹² This approach is unique not only because it is based on complex manufacturing of a personalised genetically modified autologous cell product, but also because it is conceptualised as a single-shot intervention to induce long-standing drug-free remission; this ambitious approach could herald a new era of autoimmune disease treatment, transforming the current principle of long-term immunosuppression into a strategy that induces an immune reset with no need for further treatment. Further studies addressing the potential of CAR T-cells' applications for treatment of autoimmune diseases are underway and will shed more light on the potential of this treatment approach.

Question of the Week

Which one of the following management approaches is most appropriate for a 65-year-old woman with a bicuspid aortic valve and a dilated ascending aorta (5.6 cm in diameter; reference, <3.5 cm)?

- ☐ Annual monitoring with transesophageal echocardiography
- ☐ Beta-blocker therapy and continued observation
- ☐ Endovascular repair
- ☐ Annual monitoring with CT of the chest
- ☒ Surgical repair

SUBMIT



Your answer is correct.

Annual monitoring with transesophageal echocardiography
Beta-blocker therapy and continued observation
Endovascular repair
Annual monitoring with CT of the chest

✓ Surgical repair

Key Learning Point

[View Case Presentation >](#)

The most appropriate management approach for a patient with a bicuspid aortic valve who has an ascending aortic aneurysm >5.5 cm in diameter is surgical repair of the aneurysm.

Detailed Feedback

Thoracic aortic aneurysms are usually asymptomatic until an acute, often catastrophic complication occurs (e.g., a dissection or rupture). In most patients, an ascending aortic aneurysm should be repaired surgically when it exceeds 5.5 cm in diameter or enlarges more than 0.5 cm per year. However, it should be repaired earlier (at 4.0 to 5.0 cm in diameter, depending on the condition) in patients with genetically mediated causes of aortic aneurysm (e.g., Marfan syndrome, Turner syndrome) because dissection or rupture may occur in these individuals with minimal aortic dilatation.

Endovascular repair for thoracic aortic aneurysms is not routinely recommended unless the patient is at prohibitive surgical risk.

When surgical repair is not yet indicated, annual imaging of the thoracic aorta (with CT, MRI, or, in some cases, transesophageal echocardiography) is recommended.

Beta-blocker therapy is used to slow the progression of aortic aneurysm dilation, but continued observation on beta-blocker therapy is not appropriate once surgical repair is indicated.



A fluctuating solution to the dolomite problem

Episodes of dissolution and crystal growth stoke the formation of a common carbonate mineral

By Juan Manuel García-Ruiz

Featured

The impressive massif of the Dolomite Mountains in Northern Italy was formed almost entirely of $\text{CaMg}(\text{CO}_3)_2$, a calcium-magnesium carbonate mineral discovered in 1791 by the French naturalist Déodat de Dolomieu (¹), who gave name to both the mineral—dolomite—and to the impressive Alpine rocky landscape considered by the architect Le Corbusier as “the most beautiful architectural work in the world” (²). Although abundant in ancient sedimentary rock, its rarity in modern environments has puzzled geologists for more than a century. Indeed, tackling this mystery in laboratories has proven formidable, hindering the study of this mineral—the so-called “dolomite problem.” On page 915 of this issue, Kim *et al.* (³) demonstrate that cycles of saturation conditions promote dolomite crystal growth in the laboratory. This discovery opens the door to investigating the geochemical process that influenced massive dolomite formation in the natural world.

Editor’s summary

Dolomite, a calcium magnesium carbonate, is one of the major minerals in carbonate rocks. However, growing the mineral under laboratory conditions has proven very difficult, resulting in the so-called “dolomite problem.” Kim *et al.* may have solved this problem by identifying the need to cycle the solution between under-saturated and supersaturated conditions (see the Perspective by García-Ruiz). Cycling speeds up crystal growth 10 million times and may be imperative for making large amounts of dolomite. This observation is consistent with where we see dolomite formation in nature: in coastal and evaporative environments. —Brent Grocholski

MINERALOGY

Dissolution enables dolomite crystal growth near ambient conditions

Crystals grow in supersaturated solutions. A mysterious counterexample is dolomite $\text{CaMg}(\text{CO}_3)_2$, a geologically abundant sedimentary mineral that does not readily grow at ambient conditions, not even under highly supersaturated solutions. Using atomistic simulations, we show that dolomite initially precipitates a cation-disordered surface, where high surface strains inhibit further crystal growth. However, mild undersaturation will preferentially dissolve these disordered regions, enabling increased order upon reprecipitation. Our simulations predict that frequent cycling of a solution between supersaturation and undersaturation can accelerate dolomite growth by up to seven orders of magnitude. We validated our theory with in situ liquid cell transmission electron microscopy, directly observing bulk dolomite growth after pulses of dissolution. This mechanism explains why modern dolomite is primarily found in natural environments with pH or salinity fluctuations. More generally, it reveals that the growth and ripening of defect-free crystals can be facilitated by deliberate periods of mild dissolution.

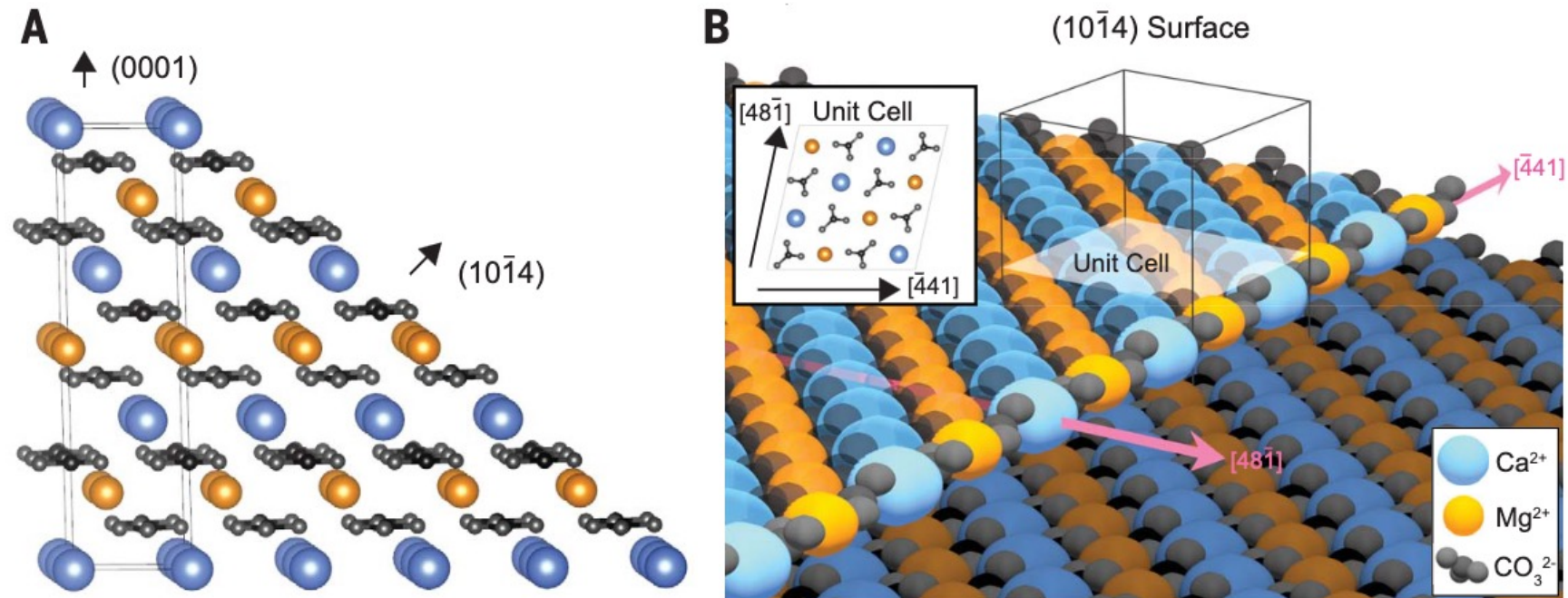
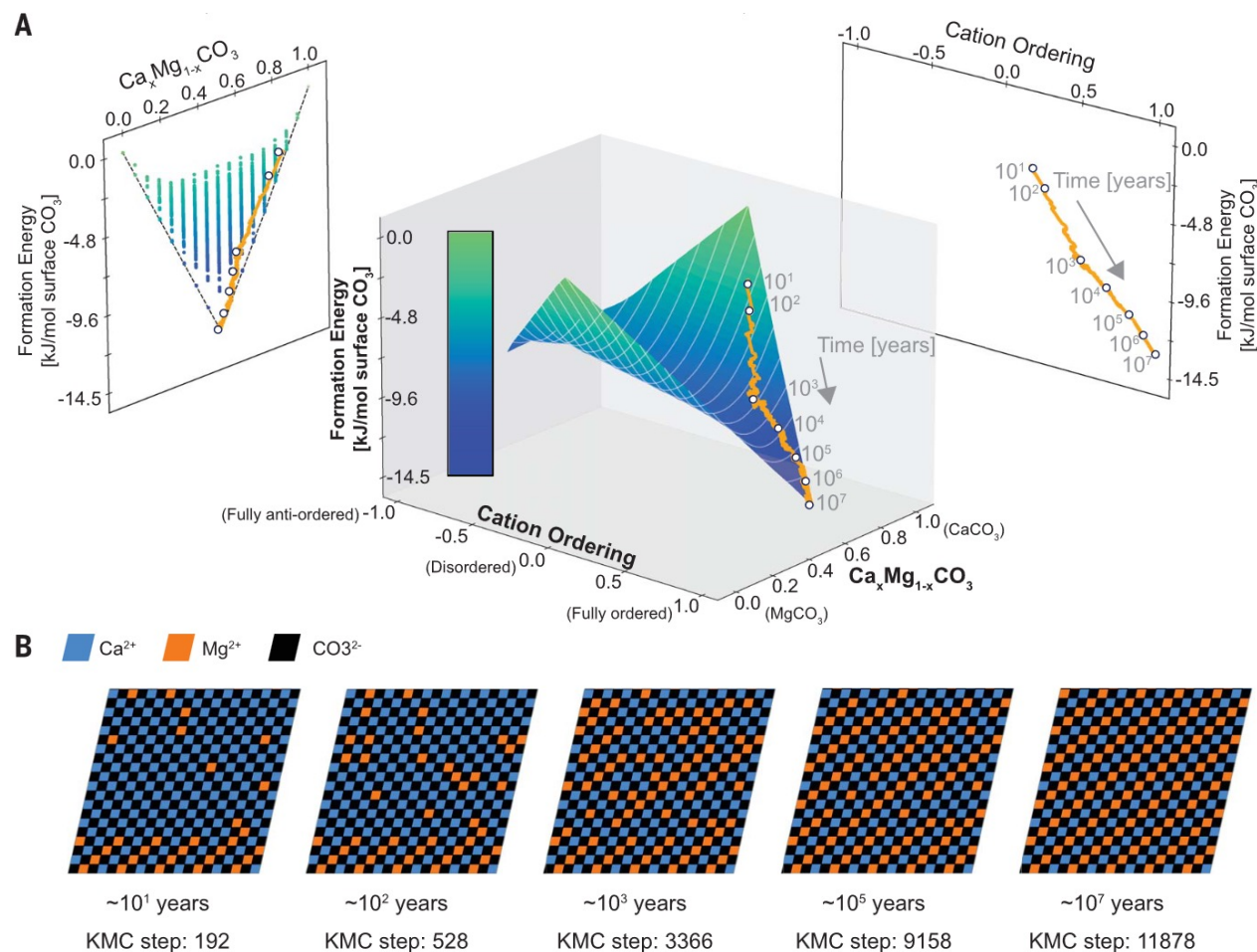


Fig. 1. Dolomite crystal structure and growth surface. (A) The orientation of the (10 $\bar{1}$ 4) growth surface with respect to the conventional unit cell. (B) [441] step edge on the (10 $\bar{1}$ 4) growth surface of the ordered dolomite crystal. (Inset) Top view of the (10 $\bar{1}$ 4) surface unit cell. In ordered dolomite, Ca²⁺ and Mg²⁺ demonstrate alternating order along this [441] step edge.

Fig. 2. Dolomite step-edge growth and ordering through dissolution-reprecipitation under constant supersaturation as simulated with kinetic Monte Carlo.

(A) Surface formation energy is plotted versus composition and cation ordering. The lowest energy configuration for a given composition and ordering is plotted as the blue-green surface. The coordinate for ordered dolomite is at $\text{Ca}_{0.5}\text{Mg}_{0.5}\text{CO}_3$ composition, +1.0 ordering, and surface formation energy of $\Delta E = -13.27$ kJ/(mol surface CO_3). The orange trace is the KMC simulated progression of dolomite surface evolution from a Ca-rich initial carbonate to an ordered dolomite layer over the course of 10^7 years under constant supersaturation. Two-dimensional projections of the energy surface are also shown. **(B)** The atomic configuration of the evolving surface at five different KMC steps. The initially disordered dolomite surface evolves to complete order within $\sim 10^7$ years.



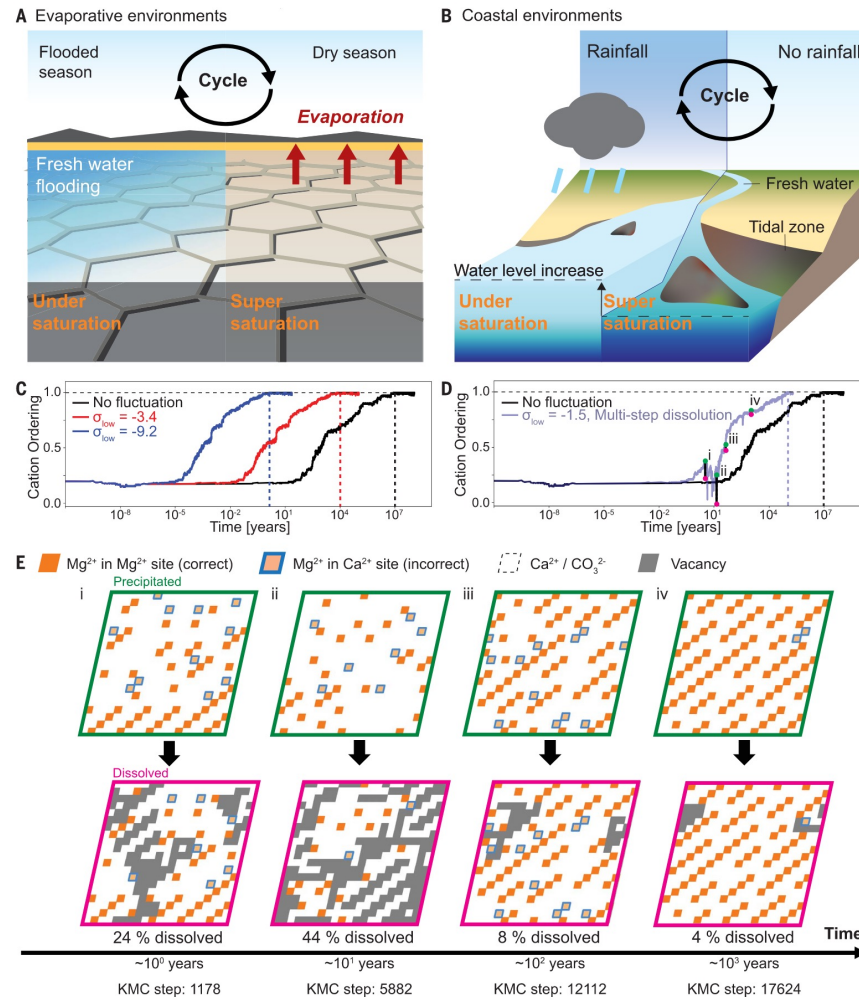


Fig. 3. The role of supersaturation fluctuations in accelerating dissolution-precipitation processes in dolomite ordering. (A and B) Although rare, modern dolomite deposits are observed where salinity fluctuations are common, such as (A) evaporative and (B) coastal environments. (C and D) We simulated the salinity fluctuation by means of (C) step-regulated supersaturation fluctuation, in which supersaturation is inverted every step,

and (D) time-regulated KMC simulation, in which supersaturation is inverted after a time limit (fig. S17) (24). Under supersaturation fluctuations, the cation ordering process is accelerated by orders of magnitude compared with ordering under constant supersaturation. (E) Snapshots of surface structures from time-regulated supersaturation fluctuations at $\sigma = -1.5$, with corresponding times marked in (D).

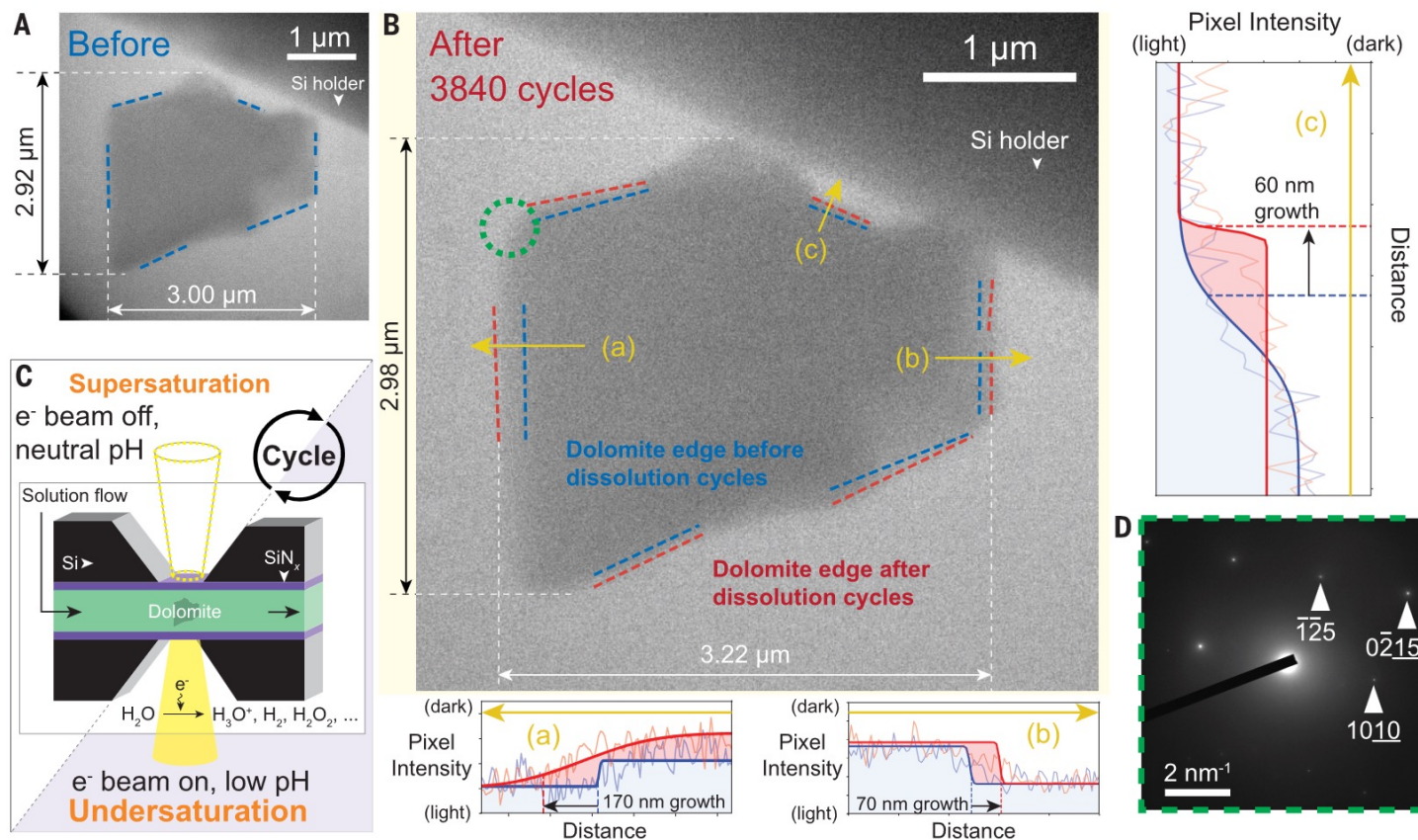


Fig. 4. In situ liquid cell TEM images of dolomite crystal growth. (A) Dolomite crystal before beam-induced dissolution cycles. (B) Crystal after 3840 dissolution cycles. The blue dashed lines (before dissolution cycles) and the red dashed lines (after dissolution cycles) indicate the crystal edges quantified with image contrast analysis (24). The blue dashed lines in (A) are identical to the ones in (B). The blue and red dashed lines show that the crystal grows in all

directions after 3840 dissolution cycles. The growth rate ranges from 8 to 30 nm per 1000 cycles, depending on the direction. (C) Schematic of the in situ liquid cell TEM experiment. (D) Electron diffraction pattern measured from the area indicated with a green dashed circle in (B). Diffraction spots shown by white triangles have been assigned as ordered dolomite (JCPDS 36-426).